Sandpile behaviour in Mexico clay soils

Assessing the application of sandpiles as alternative to PVDs

J.C.A.J. Vork

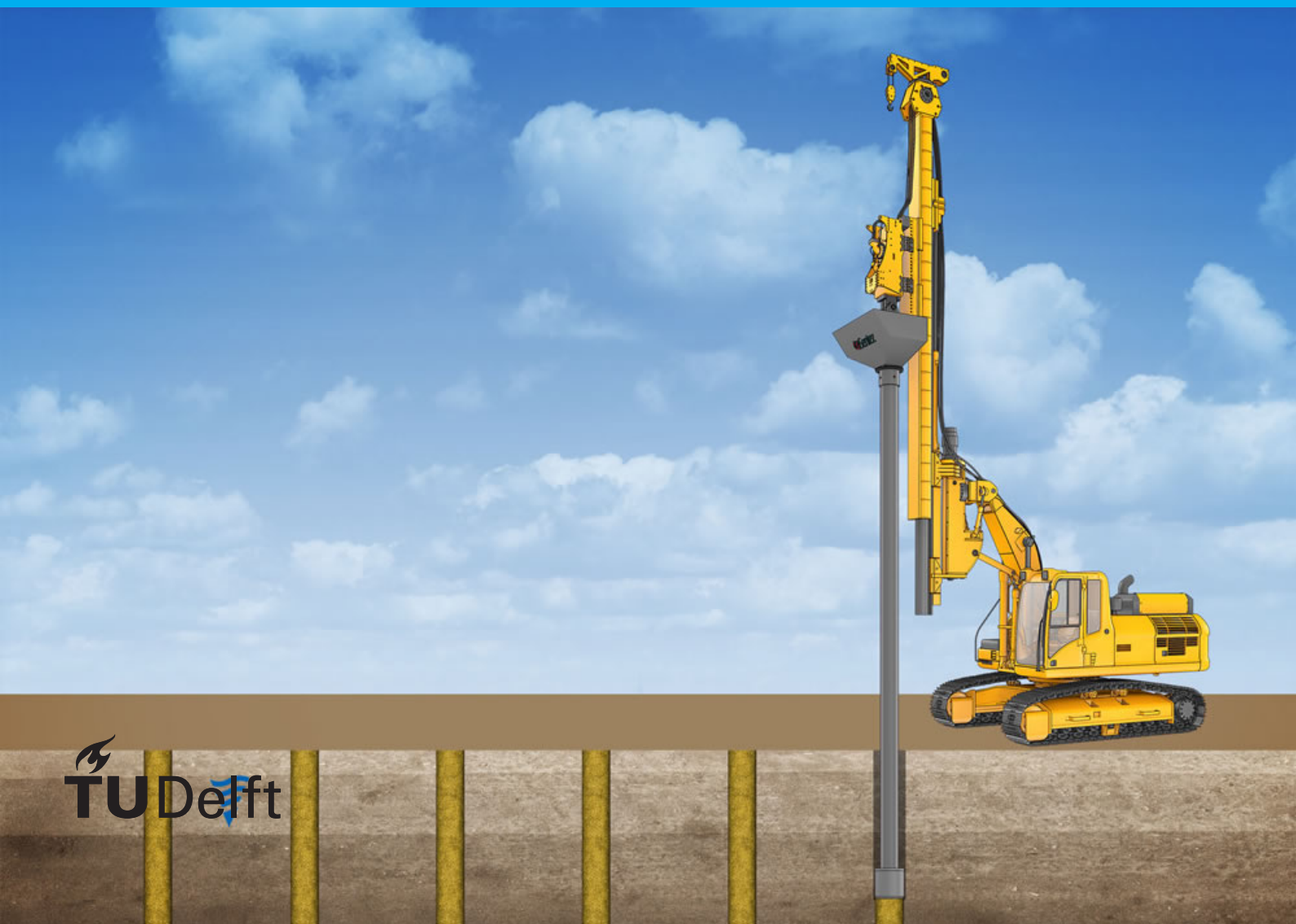

TU Delft

Sandpile behaviour in Mexico clay soils

Assessing the application of sandpiles as alternative to PVDs

by

J.C.A.J. Vork

to obtain the degree of Master of Science
at the Delft University of Technology,

Student number:	4079728	
Project duration:	March 22, 2017 – November 27, 2017	
Thesis committee	Prof. dr. ir. T. Heimovaara,	TU Delft, chair
	Dr. ir. W. Broere,	TU Delft, supervisor
	Ing. M. de Kant,	Royal HaskoningDHV
	Ir. C. Kasbergen,	TU Delft

An electronic version of this thesis is available at `http://repository.tudelft.nl/`.

TU Delft

Abstract

The construction of the new airport of Mexico City (NAICM) is challenging, as the subsoil at the site is very weak. The airport, which is under construction at the moment, is located on top of thick layers of Mexico Clay soils. These clayey layers consist of a mixture of both clay particles and pyroclastic volcanic materials. These unique soils are characterised by a high water content and compressibility. Upon loading, the soft soils will settle as a result of the consolidation process. This consolidation is defined as the dissipation of excess pore water as a result of an increase in stress. The rate of consolidation is governed by the hydraulic conductivity of the soil, which is in general very low in soft soils, and the drainage path. In order to speed up this time consuming process, vertical permeable elements can be installed in the soil. Upon installation of these elements, a reduction in drainage path is realised. This reduction in drainage path allows faster dissipation of excess pore water pressure, hence reducing the consolidation time. Due to the conditions at the site, the design of the runways is challenging. The differential- and residual settlements need to be within strict boundaries in order to keep the runways operational. Prior to the design of the runways, trial embankments have been constructed in order to measure the performance of different soil improvement techniques at this specific site. Based upon this field test results, prefabricated vertical drains (PVDs) were selected as the most efficient soil improvement technique. Besides the PVD trial, the sandpile trial also showed promising results. The PVDs and sandpiles both decrease the drainage path length inside the soft soil layers. The main difference is the relative high stiffness of the sandpiles, the stiffness of the PVDs is negligible. By installing stiff elements in the soft soil, the loads applied on the top of the soils are transferred to deeper and stiffer soils. Hence, the total settlements of the top soft soil layers are reduced. The sandpiles could therefore be feasible alternative to PVDs, applied at locations in which the total settlement needs to be limited.

The investigation into the behaviour of sandpiles in Mexico Clay soils is performed in multiple stages. First, analytical models are used for gaining knowledge about the expected sandpile behaviour. In the second stage the FEM software Plaxis 2D is used for the numerical modelling of the sandpiles, using an axisymmetric model setup. The model is constructed in multiple steps, with increasing complexity. The first models simulate the material behaviour with the Mohr-Coulomb model, in the advanced models the Soft Soil Creep and Hardening Soil models are used. The final numerical model is verified by the measurement data obtained from the field trials. After fitting the numerical model to the field data, the verified model is used in the sandpile sensitivity analysis. In this analysis the sensitivity of the material properties and geometry of the sandpile on the performance are researched. The residual settlements or performance, which is defined as the difference in settlement after construction and over a period of 8 years, is affected by the length, radius and centre to centre (ctc) distance of the sandpile. Adjusting the pile stiffness has minimal effect on the performance of the sandpile. An optimum in performance is found by varying both the pile radius and ctc distance. A combination of a small pile diameter with a small ctc distance results in the best performance. When comparing the performance of both sandpile and PVD, the PVD is found to be more effective in terms of performance. The additional stiffness of the sandpile is not reducing the total settlements, on the contrary, the self-weight of the piles increases the total settlements by providing an additional load to the soft soil layers located underneath the pile tip. In conclusion the sandpiles have no additional benefit over the use of PVDs, therefore the application of sandpiles at the NAICM site is not a feasible alternative to the use of PVDs.

Acknowledgements

I would like to express my gratitude to my graduation committee. Thanks to my supervisor from Royal HaskoningDHV, Martin de Kant, for introducing me to the research topic and providing guidance and support. I am grateful to Dr. Wout Broere for providing feedback throughout the study and support during the numerical modelling with Plaxis 2D. I am also grateful to Prof. Timo Heimovaara for being the chair of my committee and for sharing his contagious enthusiasm for scientific research. A special thanks goes to my external supervisor Ir. Cor Kasbergen for always providing detailed feedback during the different stages of the research and for being closely involved during the whole process. Finally, I would like thank my family and friends for your enduring encouragement.

J.C.A.J. Vork
Delft, November 2017

Nomenclature

Abbreviations

NAICM	Nuevo Aeropuerto Internacional de la Ciudad de México
PVD	prefabricated vertical drain
FE	finite element
FEM	finite element method
FR-EE	Fernando Romero EntreprisE
NACO	Netherlands Airport Consultants
CPT	cone penetration test
CPTU	cone penetration test with water pressure meters
SPT	standard penetration test
MC	Mohr-Coloumb
HS	Hardening Soil
SSC	Soft Soil Creep
DC	dessicated crust
FAS	upper compressible clay formation
CD	capa dura, sandy silt to silty sand formation
FAI	lower clay formation
SES	stratified formation
FAP	deep clay formation
SEI	second stratified formation
POP	pre-overburden pressure
OCR	overconsolidation ratio
NC	normal consolidation
TPDV	trial embankment with surcharge and vertical drains
TDA	trial embankment with sandpiles
TDP	trial embankment with surcharge and prefabricated vertical drains
PC	pressure cell
PZ	piëzometer
ctc	centre to centre distance
NC	normal consolidated

Soil parameters

p, p'	$[kN/m^2]$	total, effective isotropic stress
q	$[kN/m^2]$	deviatoric stress
u	$[kN/m^2]$	pore water pressure
U	$[-]$	degree of consolidation
Q	$[m^3/s]$	discharge
A	$[m^2]$	area
i	$[-]$	gradient
σ, σ'	$[kg/m^3]$	total, effective stress
τ, c_u, S_u	$[kN/m^2]$	shear strength
ρ	$[kN/m^3]$	material density
γ	$[kN/m^3]$	unit weight
e	$[-]$	void ratio
E	$[kN/m^2]$	Young's modulus
E_{oed}, E_m	$[kN/m^2]$	oedemetric stiffness

E_{ur}	$[kN/m^2]$	unloading/reloading stiffness
G	$[kN/m^2]$	shear modulus
c	$[kN/m^2]$	cohesion
C_c, C_r, C_α	$[-]$	compression, reloading and creep indices
ν	$[-]$	Poisson's ratio
ϕ	$[^o]$	friction angle
ψ	$[^o]$	dilatancy angle
k	$[m/s]$	hydraulic conductivity
g	$[m/s^2]$	gravitational acceleration
α	$[-]$	displacement parameter
β	$[-]$	displacement parameter
ϵ	$[-]$	strain rate
λ	$[-]$	Lamé constant
$\lambda*$	$[-]$	modified compression index
κ	$[m/s]$	permeability independent of fluid
$\kappa*$	$[-]$	modified swelling index
$\mu*$	$[-]$	modified creep index
ξ	$[-]$	stress ratio parameter
m_v	$[-]$	coefficient of compressibility
m	$[-]$	power used in Hardening Soil material model
c_k	$[-]$	change of permeability
R_f	$[-]$	ratio of failure
K	$[-]$	earth pressure coefficient, bulk modulus
s_f	$[-]$	smear factor

Subscripts

$sat, unsat$	saturated, unsaturated
u	undrained
$0, i$	initial
f	final
avr	average
c, r, α	compression, reloading, creep
ur, oed	unloading/reloading, oedometer
t, y	tensile, yield
v, h, r	vertical, horizontal, radial
in, out	inflow, outflow
w, s, c	water, soil, column
d, e	drain, influence zone
i, j	radial element number, vertical element number
ac, p	active, passive

Superscripts

z, r	depth, radius
e, p	elastic, plastic
$*$	modified
ref	reference
$\overline{u}$	average (pore pressure)

List of Figures

List of Tables

Contents

1

Introduction

The new airport of Mexico City, the NAICM (Nuevo Aeropuerto Internacional de la Ciudad de México), is currently under construction. The engineering and design of this airport is challenging, as the subsoil at the site is very weak. The airport is located on top of thick layers of Mexico Clay soils. These clayey layers consist of a mixture of both clay particles and pyroclastic volcanic materials. These unique soils are characterised by a high water content and compressibility. Due to the conditions at the site, the design of the runways and taxiways require extra attention. The differential- and residual settlements need to be within strict boundaries to keep the runways operational. Upon loading, the soft soils will settle as a result of the consolidation process. This consolidation is defined as the dissipation of excess pore water as a result of an increase in stress. The rate of consolidation is governed by the hydraulic conductivity of the soil, which is in general very low in soft soils, and the drainage path. In order to accelerate the consolidation rate the soil can be treated with soil improvement methods. The improvement methods can have different working principles, i.e. reducing stresses in soft soils by transferring surface loads towards stronger deeper soil layers or providing a drainage path through which pore water can dissipate faster. Having multiple different improvement techniques available means that depending on the desired behaviour of the soil, an optimal improvement method can be chosen to facilitate this behaviour. In this study the soil improvement methods considered are sandpiles, prefabricated vertical drains (PVDs) and rigid inclusions.

Although mostly prefabricated vertical drains (PVDs) are used for shortening the drainage path of soft soils, sandpiles are still commonly used all over the world as soil improvement method. In delta areas where thick layers of soft soils are present, sandpiles are often applied. Upon installation, these compression elements possess high compressive strength and stiffness. The columnar inclusion therefore carries a substantially greater proportion of applied loads with significantly smaller deformation compared to the surrounding soft clay [13]. Besides the increase in stiffness the granular piles also have a high permeability. Installing the piles in a soft soil layers also contributes to reducing the drainage path, enhancing the consolidation rates of the adjacent soft soils.

Since the invention of PVDs, the use of sandpiles as soil reinforcement technique has strongly reduced. Similar to the sandpiles, the PVDs provide a shorter drainage path to the pore water trapped inside the soft soil layers. Although the PVDs do not provide an increase in stiffness of the soft soils, the application of PVDs is often preferred over the use of sandpiles. The main reason for this is the fast installation procedure combined with the low costs.

In order to predict the performance of different soil improvement methods, multiple trial embankments have been constructed at the site. Based upon the measured data obtained from these trials, the PVDs were selected as the best performing and most economic solution. Besides the PVD trial, the sandpile trial also showed promising results. The application of sandpiles as soil improvement techniques, as an alternative to PVDs, is investigated in this research.

1.1. Research objectives

The main research objective is to investigate the performance of sandpiles under specific soil conditions as found at the NAICM site. Therefore, the main research question is formulated as follows:

"How do sandpiles perform at the NAICM site, with respect to PVDs?"

In order to address the main research question, multiple sub-questions have been formulated. These questions are listed in order in which they investigated in this study, starting at the expectation based upon literature and analytical models towards the implementation of Finite Element Method (FEM) software using advanced material models. In this research the following 5 sub-questions are formulated:

1. What is the expected behaviour of the sandpiles at the NAICM site?
2. What material models can be used for modelling sandpiles in a FEM program?
3. How do the sandpile parameters affect the behaviour of the pile?
4. What sandpile configuration results in the best performance?
5. How can the numerical model be adjusted to model the PVD behaviour?

1.2. Reading guide

The research is structured into several parts, which are all listed and explained below.

Literature review

In the literature review the theory behind the main aspects of the research is provided. This includes a theorem about consolidation in 1D and 2D, drainage, sandpiles as soil improvement technique, installation of the piles and the material models available for simulating the behaviour of soils.

Modelling of the sandpile

In chapter 4 analytical formulas are used to predict the behaviour of the sandpiles at the NAICM site quantitatively. Based upon the results of the analytical models the simulated behaviour of the numerical models can be explained. The second part of the modelling is the numerical modelling of the sandpile in the FEM software Plaxis 2D, described in chapter 5.

Model verification

The models used for simulating the behaviour of the sandpiles are verified by the data obtained from the field tests performed at the NAICM site. By using the data from the trials the numerical model can be adjusted in order to match the observed behaviour. This part of the research is described in chapter 6.

Sandpile sensitivity analysis

The model verified in chapter 6 is used for analysing the sensitivity of the performance of the sandpiles to changes in the pile design. The results of the sensitivity analysis are discussed in chapter 7.

Discussion, conclusion and recommendation

In chapters 8 and 9 the results obtained from the previous chapters are discussed after which the research questions are answered. The study concludes with recommendations regarding future research, discussed in the last section of chapter 9.

2

Nuevo Aeropuerto Internacional de la Ciudad de México

In this chapter a brief introduction to the Nuevo Aeropuerto Internacional de la Ciudad de México (NAICM) project is provided, after which the site characteristics and soil properties derived from field tests and lab-testing are discussed. Besides field tests, a series of trial embankments have been constructed for measuring the ground response upon loading.

2.1. Introduction

A new airport will be built near Mexico City, replacing the Benito Juárez International Airport. The current airport is at full capacity and is unable to process the growing number of travellers. The construction of the new airport, the Nuevo Aeropuerto Internacional de la Ciudad de México (NAICM), started in 2015 and will be completed in 2020.

The project is divided into two parts, namely the design and construction of the terminal and the airside civil works. The terminal is designed by a collaboration of FR-EE (Fernando Romero EntreprisE) and Foster and Partners, the engineering works are performed by Arup. The engineering of the airside civil works is performed by TASANA, a collaboration of Tadco, Sacmag and Naco, the latter is a daughter company of Royal HaskoningDHV. The technical reports provided by TASANA are used as input in the analyses performed in this study.

Figure 2.1: Artist impressions of the NAICM terminal, with the distinctive X-shape [14].

The terminal is designed as an x-shaped building, which is not only considered efficient for extending the number of gates, it is also symbolic for the country's name, 'México'. The design includes a total of 6 runways, of which 3 will be completed in an early stage (2018) and the remaining 3 in 2020. The engineering of these runways is done by TASANA and is the main focus of this research. An impression of the x-shaped NAICM main terminal and runways as presented by Foster and Partners can be seen in figure 2.1.

2.1.1. Project location

The NAICM is located north-east of México City, at approximately 20 kilometres from the city centre. The location is bordered by the national roads 57D on the west and the 136D on the south. The 57D separates the build environment with the project location, which has not been used for construction before the project started. The project location of the NAICM in visualised in figure 2.2.

Figure 2.2: Location of the NAICM site next to Mexico City, indicated with the red box [15].

The design of the NAICM including the runways, terminals and service buildings is presented in appendix A. In this figure a total of two terminal buildings (T1 and T2) and six runways are visualised.

2.1.2. Project requirements

A complex project as an airport has many strict rules and requirements in order to ensure the safety and keep the airport operational. In this research the runways of the NAICM are the main focus, only the requirements regarding of runways are considered. When looking at settlements, two specific requirements have been highlighted. The first is regarding the total settlement of the runway. The connection between the aprons and the entrance of the runways is very sensitive to differences in settlement. In order to limit the amount of maintenance work during the life time of the airport, the settlements between aprons and runways needs to be limited.

Secondly, the settlement over the length of the runway need to be constrained. A large settlement difference (differential settlement) over the length of the runway can result in an unsafe situation during the departure or arrival of a plane. The amount of maintenance work and the time the runways are not operational can be limited by constraining the differential settlements at the runways. These constraints are only described qualitative, no quantification is prescribed. The aim is to limit the (differential) settlements as much as possible.

2.2. Geology

The NAICM site is described in terms of geology (section 2.2.1) and water extraction (section 2.2.2), which both contribute to the unique characteristics of the site.

2.2.1. Geology of Mexico City

The NAICM site is characterised by the presence of thick layers of very soft soil. The project is located at the former Texcoco lake, which once was the lowest point of the Valley of Mexico. The basin of this valley is situated at the centre of the volcanic belt that crosses the Mexican Republic from east to west and its subjected to major tectonic stresses and to volcanic eruptions[26]. The site was located in a lacustrine environment during long periods in which the deposition of large volumes of fly ash and other pyroclastic materials took place. These materials were driven into the lake by water flows running from the higher lands and by the winds. The formed clays and clayey silts are geologically very young and are notorious for their extremely high water content and compressibility [29].

The basin, at an altitude of 2,200 meters above sea level, is surrounded by mountains of over 5,000 meters above sea level. The sources of ground water recharge in the basin are largely derived from infiltrated precipi-

tation and snow melt in the surrounding mountains [28]. The Texcoco basin corresponds to a plateau underlaid by a highly compressible clay of lacustrine volcanic origin that covers alluvial and pyroclastic permeable material, which form the main aquifer of the region. Below these materials, igneous rocks are encountered that form a impervious barrier [26].

2.2.2. Water extraction

Since the beginning of the fourteenth century, the Aztec's extracted spring water from the Basin of Mexico down to the city situated on land reclaimed from the saline Lake Texcoco. Over the later centuries, a combination of increasing ground water extraction and artificial diversions to drain the valley resulted in the drying of many natural springs, shrinking of lakes and loss of pressure and subsequent consolidation of the lacustrian clay formation on which the city is built on [28]. The extraction of water from the semi-confined deep aquifers is exceeding the recharge of water, lowering the hydraulic head in the aquifer and the adjacent clay layers. This consolidation of the lacustrian clay (subsidence) is still continuing as the extraction of water from the deeper aquifers continues. The water pumped from the aquifers provides about two-third of the city's supply, thus it is unlikely that the water extraction will be stopped or even reduced in the future, given the trends of urban expansion observed over the last decades [29]. The subsidence of Mexico City is measured by the European Space Agency, the average settlement rate per month is presented in figure 2.3.

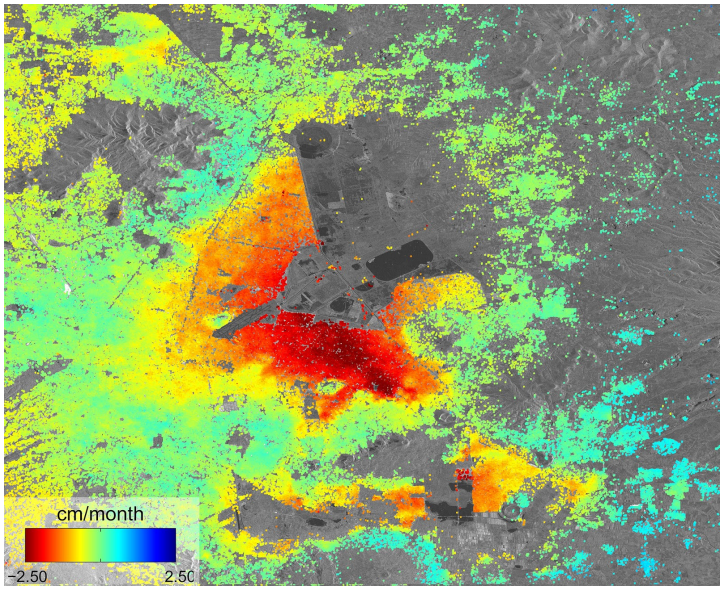

Figure 2.3: Subsidence of Mexico City between October and December 2014 [11].

The magnitude of the subsidence of Mexico City and the surrounding area is measured extensively over the last decades and is found to be 7-10 cm/year, at the location of newer wells it can exceed 30 cm/year. In figure 2.3 the subsidence per month are visualised, as measured by the European Space Agency.

2.3. Site characterisation

At the start of the NAICM project, the site has been extensively investigated in order to increase the knowledge about the subsurface. The performed test can be divided into two parts, first the field tests (section 2.3.1) and second the laboratory testing (section 2.3.2).

2.3.1. Field tests

The field tests performed can be divided into two groups. The first group is the field measurement group, including all the tests performed in order to analyse the soil properties at the site. The second group are the trial embankments, used for analysing the behaviour of the soil upon loading.

Field measurements

In order to map the geometry and properties of the subsurface of the NAICM site, field tests are performed at various locations along the NAICM site. The field tests include a large amount of cone penetrations tests

(CPT), CPT with water pressure meters (CPTU), SPTs, dilatometers, piezometers and boreholes. The data obtained is used for characterising the subsoil in terms of soil geometry, hydraulic head and soil properties. Note that for accurate determination of soil properties laboratory tests are mandatory, in combination with the in situ tests. The data obtained from the field test can be found in the report of UNAM [2].

Trial embankments

The trial embankments are located at the zona de estudio (study zone) indicated in figure 2.4. In this figure the future runways (Pista's) are indicated in red.

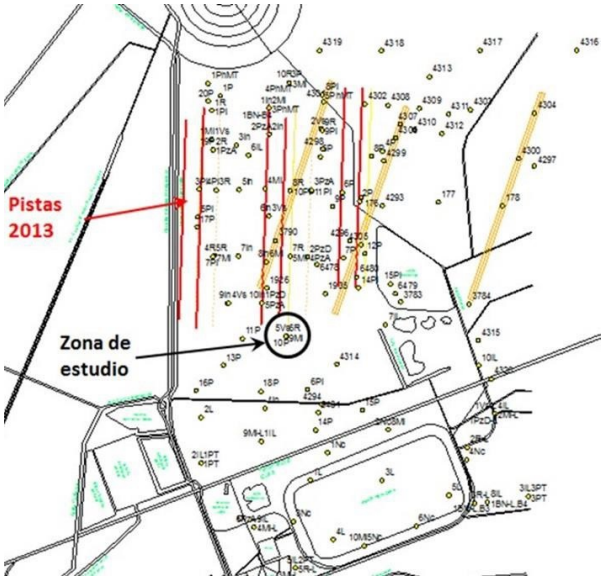

Figure 2.4: Location of the test area (Zona de estudio) at the NAICM site [2].

The trial embankments are installed in order to analyse the response of the subsoil upon loading. The embankments are installed on soils reinforced with different soil improvement techniques, including PVDs, sandpiles, rigid inclusions and prefab concrete piles. The response of the subsoil after installing the embankments is measured by changes in pore water pressure (piezometers), changes in applied pressure (pressure cells) and measured settlements at different locations of the embankment. The trial embankments are used for the verification of numerical models (see chapter 6). In Appendix B the results of the trial embankment positioned on top of the PVDs and sandpiles is elaborated in detail.

2.3.2. Laboratory testing

The soil property determination is done by laboratory tests including consolidated- and unconsolidated triaxial tests, oedometer tests and shear box tests. As mentioned before only performing field tests are not sufficient to accurately determine the soil properties of the soil layers identified. By performing laboratory tests, parameters including the undrained shear strength, the one-dimensional compression index, the undrained stiffness and the void ratios are determined. The downside of laboratory testing is that soil samples from the site are required. By taking the soil samples from the site the soil is disturbed by either the technique used for retrieving the samples and by the lack of confinement pressure once taken out of the natural environment. Secondly, the sample only provides information of the soil at the exact location of the sample itself, the soil nearby the sample might differ in properties. The results of all laboratory test can be found in the report of UNAM [2].

2.3.3. Soil properties and stratigraphy

Based upon the field tests and laboratory tests conducted, the stratigraphy of the soil is constructed. The stratigraphy of the soil at the location of the trial embankments is assessed and listed in table 2.1.

The test results can be found in the report of TASANA [34], the soil properties of the different soil layers are listed in table 2.2. The γ_{sat} is the saturated unit weight of the soil material, e_0 the initial void ratio and k_v the vertical hydraulic conductivity. The Cc, Cr and $C\alpha$ are the compression, reloading and creep indices,

Table 2.1: Geometry and hydraulic head of the soil layers identified at the trial location, conform TASANA [34].

Material name	**abbr.**	**Top [m]**	**Bottom [m]**	**Head top**	**Head bottom**
Desiccated crust	DC	0.00	0.70	Phreatic	Phreatic
Upper clay layer 1	FAS A	0.70	9.60	Phreatic	Phreatic
Upper clay layer 2	FAS B	9.60	23.40	Phreatic	Phreatic
Upper clay layer 3	FAS C	23.40	30.20	Phreatic	-4m
Silty sand layer	CD	30.20	31.30	-4m	-4m
Deep clay layer 1	FAI	31.30	44.10	-4m	-9m
Deep sand layer 1	SES	44.10	50.00	-9m	-9m
Deep clay layer 2	FAP	50.00	60.00	-9m	Linear
Deep sand layer 2	FEP	60.00	-	-50m	-50m

Table 2.2: Material properties of soil layer at the trial site [34].

Material	γ_{sat} [kN/m3]	e_0 [-]	Cc [-]	Cr [-]	$C\alpha$ [-]	k_v [m/s]	$c_k/(1+e_0)$ [-]	OCR [-]
DC	14.30	3.00	2.29	0.195	-	$1.0{\cdot}10^{-7}$	-	3.00
FAS A	12.10	7.60	5.86	0.312	0.030	$1.1{\cdot}10^{-9}$	0.26	1.56
FAS B	12.30	7.30	6.11	0.355	0.031	$1.1{\cdot}10^{-9}$	0.26	1.56
FAS C	12.80	6.20	6.03	0.313	0.032	$4.6{\cdot}10^{-8}$	0.26	1.40
CD	16.70	1.10	-	-	-	$6.5{\cdot}10^{-5}$	-	1.00
FAI	13.10	4.20	3.87	0.210	0.031	$2.6{\cdot}10^{-9}$	0.24	1.40
SES	17.00	2.50	-	-	-	$8.9{\cdot}10^{-5}$	-	1.00
FAP	13.50	2.50	2.44	0.160	-	$8.4{\cdot}10^{-11}$	0.21	1.00
FEP	18.00	1.25	-	-	-	$8.9{\cdot}10^{-5}$	-	1.00

respectively. The change in permeability is denoted by c_k and the OCR is the over consolidation ratio. The soil layers listed in the table above is only valid at the position of the trial embankments. Due to the nature of the deposits and the large area of the NAICM site, the geometry will vary over the site. As this report is mainly focused at the trial embankments, the values listed in table 2.2 are used in this research.

The properties of the soil layers indicate that the top 30 meter of the subsoil consists of soft clay layers (FAS A, B and C) with high initial void ratios. These are the clay layers containing fly ashes and other pyroclastic materials, as described at section 2.2.1. These top clay layers are positioned on top of the first drained layer, the Capa Dura (CD) layer. The hydraulic head of the CD layer is significant lower than those of the top clay layers, therefore the drains installed at the site are not allowed to reach into the CD layer.

Below the CD layer two deep clay layers are positioned (FAI & FAP), separated by a thick sand layer (SES). The FAP layer deserved extra attention as this layer has a very low permeability compared to the other layers and is bordering the aquifer (FEP layer) which is being used as a source of fresh water by Mexico City. Due to the extraction of water, the hydraulic head of the FAP layer is gradually reducing over time, causing the subsidence of the NAICM site. The subsidence rate of the NAICM site is 0.10m per year, conform the report of TASANA [34].

2.4. Proposed soil improvement methods

Prior to the design of the runways, different soil improvement methods have been tested at the NAICM site. The three methods considered in this research are the soil improvement with prefabricated vertical drains (PVDs), sandpiles and rigid inclusions. The methods all differ in the set of properties of the soil improved upon installation. PVDs provide a vertical drainage path, enabling the pore water trapped in the voids to dissipate faster from the soft soil adjacent to the drain. Installing sandpiles also provides vertical drainage to soft soil layers, but the sandpile also contributes to a higher stiffness of the improved soil. The higher stiffness reduces the total settlement of the improved soil. The last improvement technique analysed are the rigid inclusions, concrete cast-in-place piles, which do not provide drainage to the subsoil. The rigid inclusions

are primarily used to reduce the total settlement of the soil, by transferring the loads applied on the surface towards the deeper, often stiffer, soil layers. The three improvement methods considered in this research are visualised in figure 2.5.

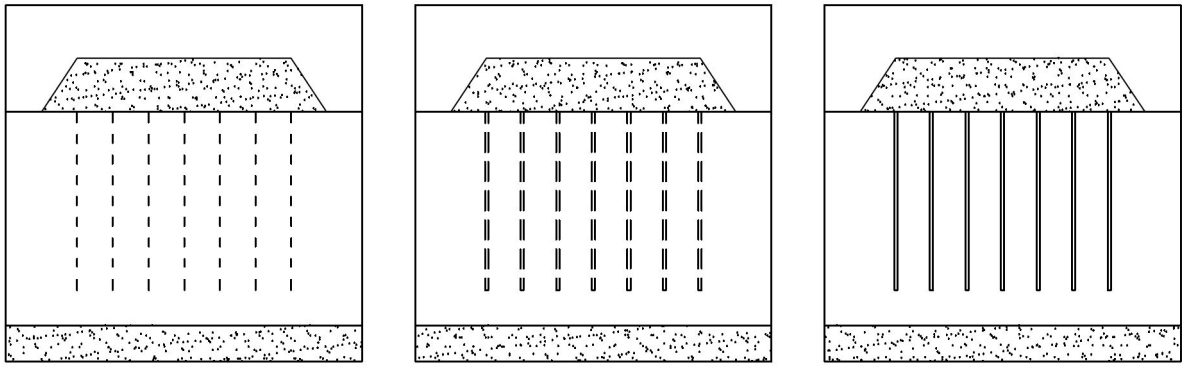

Figure 2.5: Embankment installed on soil improved with: prefabricated vertical drains (left), sandpiles (middle) an rigid inclusions (right).

Note that the improvement techniques visualised in figure 2.5 are not connected to the bottom sand layer, this is because of the critical improvement depth explained in section 2.4.4. In the subsections below the different improvement methods are briefly discussed.

2.4.1. Prefabricated Vertical Drains

Prefabricated vertical drains (PVDs) are rapidly increasing in popularity as one of the most cost-effective soft clay improvement techniques worldwide. With the installation of PVDs in a soft clay layer, the engineering properties the soil can be improved. When the PVDs are used in combination with preloading, a greater part of the surcharge weight can be contributed to effective stresses, hence increasing the efficiency of the surcharge. The PVDs consist of a perforated plastic core functioning as a drain, and a protective sleeve of fibrous material as a filter around the core. The typical size of band drains is usually in the order of 3-5mm x 100mm [19]. The PVDs provide a horizontal drainage path to the adjacent soft soil layers, reducing the time needed for pore water to dissipate from the voids in the soft soils. By installing the PVDs the consolidation time of soft soil layers can be reduced significantly.

The vertical drains are generally installed using one of two different methods, either dynamic or static. In the dynamic method a steel mandrel is driven into the ground using either a vibrating hammer or a conventional drop hammer. In the static method the mandrel is pushed into the soil by means of a static force. Although the dynamic method is quicker, it causes more disturbance of the surrounding soil during installation. It results in shear strain accompanied by an increase in total stress and pore water pressure, in addition to the displacement of the soil surrounding the vertical drain [19].

2.4.2. Rigid inclusions

Installing cast-in-situ concrete piles, also referred to as rigid inclusions, can be used for solving a foundation in a very soft soil deposit. The inclusions improve the mechanical characteristics of the soil, mainly the deformability and shear resistance. The difference between concrete piles and rigid inclusions is that the latter is not connected to a raft foundation, so there is no need for raft reinforcement at the connections, thus reducing the foundation costs [30] [8]. In short the main characteristics of rigid inclusions as soil reinforcement method is the reduction of surface settlements generated by the weight of a structure or by soil mass undergoing active consolidation processes. Furthermore the application of rigid inclusions increases of the subsoil's overall shear strength, increasing the bearing capacity of the treated soil mass.

The technique used in the NAICM field test for installing the cast in place rigid inclusions is using a drill for creating a circular hole in the soil until the desired depth. When the drill reaches the final depth, the propeller is removed. During the removal of the propeller, mortar is emptied in through the hollow shaft until it reached the upper level of the working platform. After the mortar has hardened, the tip of the now formed inclusion can be removed in order to have the top at the desired level.

2.4.3. Sandpiles

The third soil improvement method analysed are sandpiles, which combines the improvement principles of both the PVDs and the rigid inclusions. Similar to PVDs, the sandpiles function as a drain for pore water trapped in-between soil particles in soft soils. The relative high stiffness of the sandpiles contributes to the reinforcement of the soft soil adjacent to the piles, similar to the working principle of the rigid inclusion. Sandpiles installed in weak soils reinforce the soil and reduce the settlement of foundations and increase the bearing capacity of the soil, by increasing the shear resistance of the soil mass.

The main effects usually considered with respect to the untreated ground conditions are: improvement of bearing capacity, reduction of total and differential settlements, acceleration of consolidation, improvement of the stability of embankments and natural slopes and reduction of liquefaction potential [3] [7]. The inclusions consist of granular material compacted in long cylindrical holes. The granular material can be of the form of stone columns/granular piles, sand compaction piles and lime or cement columns, all with a higher stiffness and strength compared with the ambient soil. This research is primarily focused on the behaviour of sand piles; however, since the material properties and behaviour among granular materials are relative similar, research regarding the behaviour of stone columns is used as well [3] [18].

An important requirement for granular columns, including sandpiles, to drive sufficient load-carrying capacity is the lateral confinement provided by the surrounding soft soil. A single granular column installed in very soft clay with an undrained strength of less then 15 kPa, might fail through excessive bulging that occurs near the top. For shorter granular columns, general shear failure is more probable failure mechanism [17].

2.4.4. Critical improvement depth

The stratigraphy of the subsoil at the trial embankment site is described in section 2.3.2. The hydraulic head of each soil layers is listed in table 2.2. As can be observed in the table is an incline present in hydraulic head over the depth of the subsoil. The hydraulic head of the top clay layers (FAS) is constant over depth, at the phreatic surface. The underlaying Capa Dura (CD) has a hydraulic head of -4.0m. This difference in hydraulic head results in a requirement regarding the maximum depth of the soil improvement methods. This maximum or critical improvement depth ensures a safe boundary between the improvement technique and the CD layer, preventing a short circuit between the two. The prescribed minimum distance between the FAS layers and the CD layer is 3.0m. This results in a critical improvement depth of 27.0m below ground surface.

3

Theoretical Background

In this chapter the theoretical background of the analytical and numerical models are highlighted.

3.1. Introduction

This chapter gives an overview of the important theories applied in this research. The first section provides a brief description of the consolidation theorem in 1D, after which the 2D and 3D consolidation theorem are reviewed. In section 3.3 the drainage theorem is provided along with the effect of drainage on consolidation. Section 3.4 is focused on sandpiles, discussing the main features of this soil improvement technique. In section 3.5 the installation procedure of the sandpiles is mentioned, together with the installation effects. The final section of this chapter (section 3.6) provides the theoretical background of the material models used for the numerical models, which are the Mohr-Coulomb model, the Hardening Soil model and the Soft Soil Creep model.

3.2. Consolidation

In this section the consolidation theorem of soils is discussed. The first section is focused on the general principals of the consolidation theorem, after which in section 3.2.2 and 3.2.3 the general approached for estimating the degree of consolidation in 1D and afterwards in 2D and 3D are presented.

3.2.1. Consolidation theorem

When a saturated stratum of sandy soil is subjected to an increase in stress, the pore water pressure will be increased. This increase of pore pressure leads to the drainage of some water from the voids in the soil. In sandy soils the permeability is relatively high, therefore the dissipation of water will occur almost instantaneously. Therefore, the process of consolidation will occur quickly. As a result of water being drained from the soil, the soil particles will move closer to another and the volume of the soil will decrease. This decrease in soil volume results in a downwards movement of the surface, which is often referred to as settlement.

In the case of a saturated stratum of clayey soil subjected to an increase in stress, the dissipation of the excess pore pressure generated will occur much slower, as the relative permeability of clayey soils is low. This results in a longer period of time in which the settlement takes place. The process of excess pore-water pressure dissipating over time is what the consolidation theorem describes. In this report it is assumed that the consolidation of sandy soils is occurring instantaneously and the soil is incompressible, meaning that only the soft soils are prone to consolidation.

The following factors have effect on the rate of consolidation:

Permeability; An increase in permeability of the consolidating soils would lead to an increase in the discharge of water through the soil. The pore pressure will therefore dissipate more rapidly.

Compressibility; A soil with a higher compressibility leads to a bigger decrease in void space of the soil at a particular stress increase. This means that a greater volume of water must be expelled from the soil and this will require a longer time. This effect results in a lower rate of consolidation.

Layer thickness; When the thickness of the soil layer is increasing, the total head gradient during the stage of pore water expulsion is decreasing. It also means a greater volume of water that needs to dissipate from the pores, which both contribute to a lower rate of consolidation.

Boundary conditions; The presence of drained boundaries through which the water may be expelled will increase the rate of consolidation. Having drained boundaries on both sides of the layer will increase the rate of which excess pore water pressure dissipates with respect to a soft soil with only one drained boundary.

As stated above the presence of drained boundaries is improving the rate of consolidation considerably. An effective way of improving the consolidation rate is to install artificial drained boundaries inside the soil layer. In section 3.3 the effect of installing drainage systems is discussed.

3.2.2. Consolidation in 1D

The rate of consolidation of a soft soil over depth can be estimated with the theorem of Terzaghi [32]. With this theorem the excess pore water pressure in a soft soil layer can be calculated, both over depth and over time. The rate of water flow into the soil element is indicated with Q_{in} and the rate of water flow out the soil element is indicated with Q_{out}. The volume of the element will decrease during consolidation, therefore $Q_{out} > Q_{in}$. The ratio of flow in and out of the element is given with Darcy's equation:

$$Q_{in} = kiA = k\frac{\partial h}{\partial z}dxdy \tag{3.1}$$

where k is the hydraulic conductivity of the soil analysed, i is the gradient and A is the area of the flow path of the pore water. From the equation as presented by Darcy, the governing equation for 1 dimensional (1D) consolidation of soils was developed by Terzaghi [32]. In the derivation of the governing equation the change in water content is reducing the pore volume, which is linked to the change in pore water pressure. The governing equation for consolidation (1D) is presented in equation 3.2:

$$c_v\frac{\partial^2 u}{\partial z^2} = \frac{\partial u}{\partial t} \tag{3.2}$$

where c_v is the coefficient of consolidation, measuring the rate at which the consolidation process proceeds:

$$c_v = \frac{k}{\rho_w g m_v} \tag{3.3}$$

where m_v is the one dimensional compressibility. The effective stress (σ') due to an increase in pore water pressure can be calculated with $\sigma' = \sigma - (u_i + u)$ where u_i is the hydrostatic water pressure and u is the excess hydrostatic pore water pressure which varies with time.

There are several solutions of the equation for 1D consolidation for different boundary conditions. The solution for the case of a constant initial excess hydrostatic pore pressure (u) can be expressed as [33]:

$$\frac{u}{u_0} = \frac{4}{\pi}\sum_{j=1}^{\infty}\frac{(-1)^{j-1}}{2j-1}cos[(2j-1)\frac{\pi}{2}\frac{z}{h}]exp[-(2j-1)^2\frac{\pi^2}{4}T] \tag{3.4}$$

where u is the pore water pressure (excess hydrostatic) at particular depth (z) and time (t); u_0 is the initial value of hydrostatic pore pressures and T a dimensionless time factor:

$$T = \frac{c_v t}{h^2} \tag{3.5}$$

For time steps big enough, equation 3.4 can be simplified as follows:

$$\frac{c_v t}{h^2} >> 0.1 \quad : \quad \frac{u}{u_0} \approx \frac{4}{\pi}cos\left(\frac{\pi}{2}\frac{z}{h}\right)exp\left(-\frac{\pi^2}{4}\frac{c_v t}{h^2}\right) \tag{3.6}$$

where h is the thickness of a singly drained layer. The progress of consolidation can be indicated by a variable known as the degree of consolidation (U), which is defined as:

$$U(z,t) = 1 - \frac{u}{\Delta u} \tag{3.7}$$

The formula presented in equation 3.6 can be used for calculating the degree of consolidation of an one dimensional (z) consolidation problem. In a situation where multiple boundaries are drained, a different approach is required.

3.2.3. Consolidation in 2D and 3D

In the previous section the consolidation in one dimension (z) is discussed. However, when multiple boundaries of the soft soil layer are drained, the excess pore water pressure can dissipate in multiple directions instead of a single direction. By installing a vertical drain through the soft soil layer, the excess pore water can dissipate in both horizontal- and vertical direction. In this report consolidation in horizontal direction is only considered for the situation in which vertical drains are installed. These drains are linear elements positioned in a raster and penetrating the soft soil layer. For this configuration the soft soil layer can be divided into cylindrical cells. Since the cell with a drain in the middle is considered to be axisymmetric, each position in the cell can be indicated by cylindrical coordinates (r,z). The method proposed by Barron [4] is considering the consolidation of fine grained soils by drain wells in a axisymmetrical configuration.

In his derivation, Barron assumed that [4]:

1. Water in saturated soil is incompressible and at the moment of loading, excess pore water pressure carries all the vertical loads;
2. Soil mass only deforms vertically;
3. Each drain well has a circular influence zone;
4. Loads distribute uniformly over the compressible soil zone.

Based upon the assumption as listed above, the following differential equation for axisymmetric flow yields:

$$c_r \left(\frac{1}{r}\frac{\partial u}{\partial r} + \frac{\partial^2 u}{\partial r^2} \right) + c_v \frac{\partial^2 u}{\partial z^2} = \frac{\partial \overline{u}}{\partial t} \tag{3.8}$$

where c_r is the coefficient of consolidation in the radial direction; c_v is the coefficient of consolidation in the vertical direction; u is the excess pore water pressure at a certain location (r,z) in the soil; $\overline{u}$ is the excess pore water pressure at a depth z in the soil; r,z are the cylindrical coordinates with r is the radius and z is the depth and t is the time considered.

When comparing equation 3.8 with equation 3.2 as denoted by Terzaghi [32], it can be noticed that the part which describes the consolidation in vertical direction remains the same, while an extra component is added to account for the consolidation in radial direction.

By composing the total flow of water into the radial and vertical flows, equation 3.8 can be expressed in two equations as:

$$\frac{\partial u_z}{\partial t} = c_v \frac{\partial^2 u_z}{\partial z^2} \tag{3.9}$$

$$\frac{\partial \overline{u}}{\partial t} = c_v \left(\frac{\partial^2 u_r}{\partial r^2} + \frac{1}{r}\frac{\partial u_r}{\partial r} \right) \tag{3.10}$$

in which equation 3.9 is the same as Terzaghi's formula for one dimensional consolidation, but now denoted with a subscript z to indicate the vertical direction of the consolidation. In equation 3.10, u_r is the excess pore-water pressure due to radial flow only. Utilising the initial and boundary conditions, a solution for equation 3.10 can also be obtained as [16]:

$$u_r = \frac{4\overline{u}}{d_e^2 F(N)} \left[r_e^2 ln\left(\frac{r}{r_d}\right) - \frac{r^2 - r_c^2}{2} \right] \tag{3.11}$$

where $\overline{u} = u_0 e^{\lambda}$; $\lambda = -8T_r/F(N)$; u_0 = initial excess pore-water pressure; $F(N) = [N^2/N(N^2-1)]ln(N) - (3N^2-1)/(4N^2)$; $N = d_e/d_d$ which is the diameter ratio; $T_r = c_r t/d_e^2$ is the time factor in a radial flow; r_c and

r_e are the radii of a drain well and its influence zone, respectively; and d_d and d_e are the diameters of a drain well and its influence zone, respectively. The average rate (or degree) of consolidation in the radial direction can be obtained by:

$$U_r = 1 - e^{[-8/F(N)]T_r} \tag{3.12}$$

with the differential equation as proposed by Barron, the consolidation of a 2D or 3D (axisymmetrical) soil cell can be calculated.

Kjellman-Barron

The formula as presented by Barron (equation 3.11) has been adjusted by Kjellman [21] in order to calculate the average rate of consolidation in a 3D situation. The difference with the formulas corresponding to the Barron approach is that Kjellman is using the horizontal coefficient of consolidation for calculating the average horizontal degree of consolidation. Secondly, where Barron is using the radius of the drain and soil cell is Kjellman using the respective diameters. The formula presented by Kjellman is based upon the same assumptions as the Barron formulas. The time required for a soil to consolidate to a given degree of consolidation can be estimated by the following equation:

$$t = \frac{D^2}{8 * c_h}[ln\frac{D}{d} - 0.75]ln\frac{1}{1-U_h} \tag{3.13}$$

with c_h is the horizontal coefficient of consolidation, D is the zone of influence of the drain, d is the equivalent diameter of a drain and U_h is the average degree of consolidation for horizontal flow. By rearranging the term the average degree of consolidation at a given time can be calculated by the following formula [21]:

$$U_h = 1 - exp\left(\frac{-8c_h t}{D^2(ln\frac{D}{d} - 0.75)}\right) \tag{3.14}$$

by using equation 3.14 the horizontal average degree of consolidation (U_h) over time can be determined.

3.2.4. Change in permeability during consolidation

During consolidation the porosity of the soil is reducing. This reduction causes a decrease in permeability, as the reducing void volume allows less water to flow through. This effect of reducing permeability during consolidation induces a longer consolidation process, compared to the process calculated based on the initial permeability. Hence, for accurate simulations of the consolidation process it is important to know the magnitude of this change in permeability.

Besides the change in permeability the change in material stiffness is influencing the consolidation process. The increase in stresses in the soil particles increases the stiffness of the soil material. An increase in stiffness results in a acceleration of the consolidation process. The two phenomena, namely the change in permeability and the change in stiffness, have an opposite effect on the consolidation process.

For the change in permeability of a material the formula of Kozeny-Carman can be used:

$$\kappa = cd^2\frac{e^3}{1+e} \tag{3.15}$$

in which κ is the permeability of the material independent of the fluid, d is a measure of the particle size, c is a constant depending on the particle skeleton and e is the void ratio. As can be seen in equation 3.15 the permeability is changing with a change in void ratio. The relation between the change in void ratio and the change in permeability is based on theoretic grounds and is formulated as:

$$log\left(\frac{k}{k_0}\right) = \frac{\Delta e}{c_k} \tag{3.16}$$

in which c_k is a proportionality constant, ∂e the change in void ratio, k the permeability and k_0 the initial permeability of the soil material. The change in stiffness of the soil material during consolidation is captured in the one dimensional compression constant (m_v), which is related to the change in stresses and strains, as can be observed in formula 3.17:

$$m_v = \frac{\Delta\epsilon}{\Delta\sigma} \tag{3.17}$$

when only one dimensional compression is considered, the volumetric strain is equal to the vertical strain. The change in volumetric strain is related by the change in void ratio by:

$$e = e_0 + (1 + e_0)\Delta\epsilon_v \tag{3.18}$$

after combining the equation above the following relation between one dimensional compression constant (m_v) and change in void ratio can be derived:

$$\Delta e = e - e_0 = (1 + e_0)\, m_v \Delta\sigma \tag{3.19}$$

based upon one dimensional compression tests at different stress levels, it was proved that the stress dependent stiffness and the permeability were not changing at the same rate. The permeability reduces faster than the stiffness increases. When using the FE software Plaxis 2D, the change in permeability is updated at the beginning of each time step. In the analytical approach the change in permeability is not always taken into consideration. As the analytical models are often already implementing many assumptions in their simulations, it is assumed that when the change in void ratio is not included, the results are still useful as a first estimate of the soil behaviour.

3.3. Drainage

In section 3.3.1 the theorem of drainage of soft soils is discussed, after which in section 3.3.2 the application of prefabricated vertical drains is reviewed. In section 3.3.3 the use of granular inclusions as drains is briefly explained.

3.3.1. Drainage theorem

In section 3.2.1 a list of factors which are influencing the rate of consolidation is presented. One of them is the type of boundary conditions; the presence of drained boundaries through which the water may be expelled from the soft soil layer. In case there is not such a boundary present at the soil layer analysed, vertical permeable elements can be installed in order to facilitate these drained boundaries. The newly installed boundaries enables the excess pore water to dissipate not only vertically but also horizontally towards a permeable boundary. When the distance between the horizontal drains becomes smaller the drainage path becomes smaller as well. Therefore, installing vertical drains can contribute to an increase in consolidation rate of the soft soil layer.

The vertical permeable elements often used are prefabricated vertical drains (PVDs) and granular inclusions, including sand and stone columns. These soil improvement techniques both have a high permeability and act as a drainage path for the pore water. The main difference between the two is the drain stiffness. PVDs are considered to have no stiffness, where granular inclusions have a high stiffness compared to the soft soils. Both soil improvement techniques are elaborated in section 3.3.2 and section 3.3.3, respectively.

3.3.2. Prefabricated vertical drains

Prefabricated vertical drains (PVDs) are rapidly increasing in popularity as one of the most cost-effective soft clay improvement techniques worldwide. With the installation of PVDs in a soft clay layer, the engineering properties of the soil can be improved. When the PVDs are used in combination with preloading, a greater part of the ultimate settlement of the soft underlying strata is induced.

There are several types of PVDs available, including band shaped drains, Geodrains, Alidrain, and Mebradrain. The PVDs consist of a perforated plastic core functioning as a drain, and a protective sleeve of fibrous material as a filter around the core. The typical size of band drains is usually in the order of 3-5mm x 100mm [19]. The vertical drains are generally installed using one of two different methods, either dynamic or static. In the dynamic method a steel mandrel is driven into the ground using either a vibrating hammer or a conventional drop hammer. In the static method the mandrel is pushed into the soil by means of a static force. Although the dynamic method is quicker, it causes more disturbance of the surrounding soil during installation. The latter results in shear strain accompanied by an increase in total stress and pore water pressure, in addition to the displacement of the soil surrounding the vertical drain [19].

Effect drainage on consolidation

In order to estimate the effect of drainage on the consolidation process, an approach is suggested in which the drains have a high permeability but no stiffness. This approach is therefore valid when PVDs are considered.

The increase in consolidation rate of the soft soils by the installation of vertical drains can be analysed analytically. Depending on the configuration in which the drains are installed (square or triangular arrays), the zone of influence of each drain is either square or hexagonal. The drain and the zone of influence are modelled as a separate unit cell of equivalent circular shapes [23]. In figure 3.1 a drain in the zone of influence is visualised.

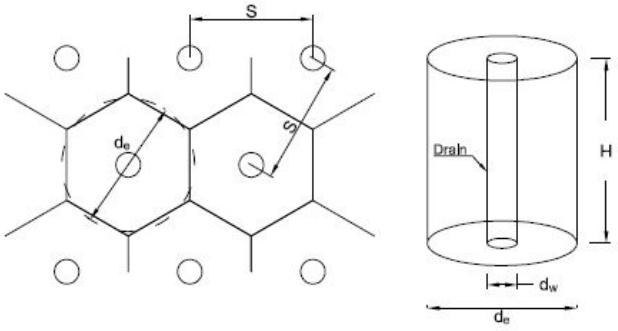

Figure 3.1: Schematised area of influence of vertical drain (left) and translation to a unit cell (right).

As can be observed in figure 3.1 the diameter of the zone of influence is not equal to the centre to centre distance between the drains. The influence area of soil surrounding the sandpile in all the different configurations can be closely approximated as an equivalent circle having the same total area [10]. In table 3.1 different drain configurations are listed with their equivalent influence area.

Table 3.1: Equivalent diameter zone of influence for different centre to centre distances (S) [3].

Configuration drains	**Equivalent diameter**
Triangular grid	$1.05 \cdot S$
Square grid	$1.13 \cdot S$
Hexagonal grid	$1.29 \cdot S$

In the analysis it is assumed that only radial flow is permitted and soil compression occurs in the vertical direction as a result of the lateral drainage. Under these conditions, the differential equation governing the radial consolidation in saturated soils is:

$$c_h \left(\frac{\partial^2 u}{\partial r^2} + \frac{1}{r} \frac{\partial u}{\partial r} \right) = \frac{\partial u}{\partial t} - \frac{\partial q}{\partial t} \tag{3.20}$$

where c_h is the coefficient of consolidation in the radial direction, u is the excess pore-water pressure depending on both r and t, r is the radial co-ordinate measured from the centre of the drain, t is time and q is the external load that is a function of time. In equation 3.20 it is assumed that the water and soil particles are incompressible. The water flow in this equation is described by Darcy's law, soil is homogeneous and behaves as linear elastic material governed by the effective stresses and strain are small [9].

The boundary conditions to the solution of equation 3.20 are [4]:

$$\frac{\partial u}{\partial r} = 0 \qquad at \quad r = R \tag{3.21}$$

$$u = 0 \qquad at \quad r = r_d \tag{3.22}$$

The boundary conditions as presented in equation 3.21 and 3.22 are valid for the case of instantaneously applied load which is constant over time. Based on the constant load assumption applied to equation 3.20, the second term on the right side will disappear (*i.e.* $dq/dt = 0$). According to Barron [4], there are two types of vertical strain that may occur in the soil:

- Free vertical strain, resulting from a non-uniform distribution of the surface displacement
- Equal vertical strain, resulting from the imposing the same vertical deformation at the ground surface.

In the second strain condition, the first term on the right side of equation 3.20 is replaced by du_{avr}/dt, where u_{avr} is a function of time that represents the average excess pore water pressure over the radial direction between r_d and R. In his research Barron showed that the results obtained using the two formulations are very nearly the same, especially for large values of the ratio R/r_d. As a consequence, it was recommended to use the simpler equal-strain solution that is based on the following analytical relationship [9]:

$$u(r,t) = q\frac{F_1}{R^2F_0}exp\left(-\frac{2c_ht}{R^2F_0}\right) \tag{3.23}$$

with F_o in the form of:

$$F_o = \frac{N^2}{N^2-1}ln(N) - \frac{3N^2-1}{4N^2} \tag{3.24}$$

in which N is the ratio of R to the drain radius ($N = R/r_d$), and F_1 is a function of r given by:

$$F_1 = R^2 ln(\frac{r}{r_d}) - \frac{r^2-r_d^2}{2} \tag{3.25}$$

The excess pore-water pressure can be calculated analytically with the formulas as presented in equation 3.23, 3.24 and 3.25. Note that this approach is using many assumptions, and is only applicable for drains without stiffness. In the next section to contribution of drain stiffness to the consolidation process is taken into consideration.

3.3.3. Granular inclusions

Granular intrusions are made of compacted aggregate and are installed in weak soil as reinforcement to reduce the settlement of foundations and increase the bearing capacity of the soil, by increasing the shear resistance of the soil mass. The use of granular inclusions for improving the strength and consolidation characteristics of soft clays is one of the most common improvement techniques for foundation of embankments or structures on soft soils. Using granular inclusions is also cost-effective and environmentally ground-improvement technique [12]. The main effects usually considered with respect to the untreated ground conditions are: improvement of bearing capacity, reduction of total and differential settlements, acceleration of consolidation, improvement of the stability of embankments and natural slopes and reduction or liquefaction potential [3] [7].

The inclusions consist of granular material compacted in long cylindrical holes. The granular material can be like stone columns/granular piles, sand compaction piles and lime or cement columns, all with a higher stiffness and strength compared with the ambient soil. This research is primarily focused on the behaviour of sand piles; however, since the material properties and behaviour among granular materials are relative similar, research regarding the behaviour of stone columns is used as well [3] [18].

Drain stiffness and consolidation

In case the drains used to have a stiffness, which is the case with stone/sand columns, a different approach is needed in order to take the differences in stiffness into account. The approach of Han [16] suggest that the consolidation characteristics of a stone column reinforced foundation are different from those of fine-grained soils with drain wells. For the simplified and closed-form solutions of Han the following assumptions are made:

1. Stone columns are free-draining at any time, each column has a circular influence zone.
2. The surrounding soil is fully saturated, and water is incompressible.
3. Stone columns and the surrounding soil only deform vertically and have the equal strain at any depth.
4. The load is applied instantaneously through a rigid foundation and maintained constant during the consolidation period. At the moment the load is applied, uniform excess pore-water pressures within the surrounding soil carry all the loads.
5. Total vertical stresses with stone columns and the surrounding soil, respectively, are averaged and uniform.

The governing equation for the analytical approach of Han is also from the research of Barron. Considering that the reduction of soil volume is equal to the discharge of water from the soil, a partial differential equation for axisymmetric flow is presented in equation 3.26. Note that this formula is equal to the one presented by Barron (equation 3.8).

$$c_r\left(\frac{\partial^2 u}{\partial r^2}+\frac{1}{r}\frac{\partial u}{\partial r}\right)+c_v\frac{\partial^2 u}{\partial z^2}=\frac{\partial \overline{u}}{\partial t} \tag{3.26}$$

As can be noticed the horizontal coefficient of consolidation (c_v) is changed into a radial- and vertical coefficient of consolidation, c_r and c_v respectively. The average excess pore-water pressure is noted with $\overline{u}$, r and z are radial coordinates as defined in figure 3.2.

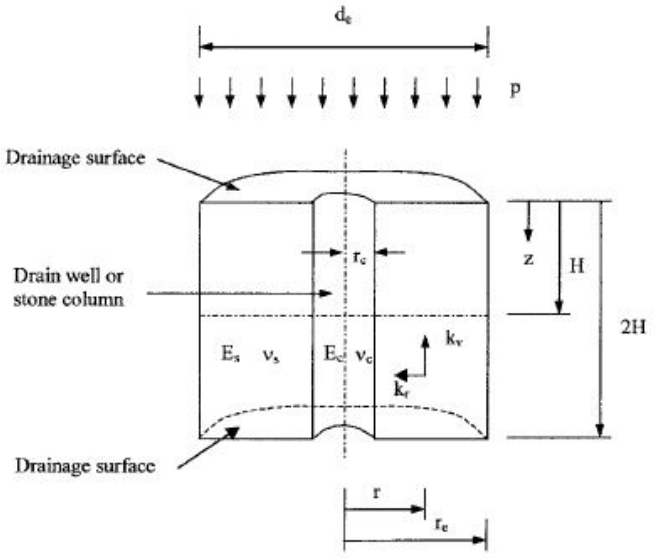

Figure 3.2: Schematised area of influence of vertical drain [16].

By composing the total flow of water into the radial and vertical flows, equation 3.26 can be expressed in two equations as:

$$\frac{\partial u_z}{\partial t}=c_v\frac{\partial^2 u_z}{\partial z^2} \tag{3.27}$$

$$\frac{\partial \overline{u}}{\partial t}=c_v\left(\frac{\partial^2 u_r}{\partial r^2}+\frac{1}{r}\frac{\partial u_r}{\partial r}\right) \tag{3.28}$$

where u_z is the excess pore-water pressure due to vertical flow only; u_r is the excess pore-water pressure due to radial flow only. Utilising the initial and boundary conditions, equation 3.28 can also be obtained as:

$$u_r=\frac{4\overline{u}}{d_e^2 F(M)}\left[r_e^2 ln\left(\frac{r}{r_d}\right)-\frac{r^2-r_d^2}{2}\right] \tag{3.29}$$

where $\overline{u}=u_0 e^{\lambda}$; $\lambda=-8T_r/F(N)$; u_0 = initial excess pore-water pressure; $F(M)=[M^2/(M^2-1)]ln(M)-(3M^2-1)/(4M^2)$; $M=d_e/d_d$ the diameter ratio; $T_r=c_r t/d_e^2$ time factor in a radial flow; r_c and r_e are radii of a drain well and its influence zone, respectively, as defined in figure 3.2; and d_d and d_c are the diameters of a drain well and its influence zone, respectively. The formula presented in equation 3.29 is equal to the formula presented in equation 3.23, only the notation is different. The average rate (or degree) of consolidation in the radial direction is:

$$U_r=1-e^{[-8/F(N)]T_r} \tag{3.30}$$

The boundary conditions in the simplified approach of Han [16] for modelling the consolidation around a column instead of a drain without strength, are similar to the boundary conditions as described by Barron [4]. Hence, the initial- and boundary conditions for the simplified approach are:

1. At t = 0, $u_0 = u_{t=0} = (A/A_s)p$ within the surrounding soil,
2. For t > 0, $u_{r=r_c} = 0 (t > 0)$,
3. $(\partial u/\partial r)_{r=r_e}$,
4. $u_{z=0} = 0 (t > 0)$,
5. $(\partial u/\partial z)_{z=H} = 0$

The initial and boundary conditions are used for the derivation of the governing equation for drainage around a stiff column. The formula used for analysing the consolidation around a stiff drain is presented in equation 3.31:

$$c_r' \left(\frac{1}{r} \frac{\partial u}{\partial r} + \frac{\partial^2 u}{\partial r^2} \right) + c_v' \frac{\partial^2 u}{\partial z^2} = \frac{\partial \overline{u}}{\partial t} \tag{3.31}$$

where c_r' is a modified coefficient of consolidation in the radial direction and c_v' a modified coefficient of consolidation in the vertical direction. As can be noticed equation 3.31 and 3.26 are identical in formats, only the coefficient of consolidation in radial- and vertical directions have been replaced by a modified coefficients of consolidation. Considering a combination effect of radial and vertical flows, the overall rate of consolidation can be expressed as[6]:

$$U_{rv} = 1 - (1 - U_r)(1 - U_v) \tag{3.32}$$

An approximate solution can be obtained as follows if U_{rv} is greater than 30% by:

$$U_{rv} = 1 - \frac{8}{\pi^2} e^{[-8/F(N)]\, T_r' - [\pi^2/4]\, T_v'} \tag{3.33}$$

where $T_r' = c_r' t / d_e^2$, a modified time factor in the radial flow; $T_v' = c_v' t / H^2$, a modified time factor in the vertical flow; and H is thickness of soil from a free draining horizontal surface to an impervious one. The earlier mentioned modified coefficients of consolidation (equation 3.31) are related to the original consolidation coefficients by the steady-stress concentration ratio (n_s) as the consolidation is complete and the diameter ratio (N). The modified coefficients of consolidation can be obtained by using the formulas in equation 3.34:

$$c_r' = c_r \left(1 + n_s \frac{1}{N^2 - 1} \right); \quad c_v' = c_v \left(1 + n_s \frac{1}{N^2 - 1} \right) \tag{3.34}$$

where (N) is the diameter ratio, previously defined in equation 3.29, and the stress concentration ratio can be found by equation 3.35. Note that the stress concentration ratio can also be defined as the ratio of the total vertical stress on the column to that on the soil at a certain time t:

$$n_s = \frac{\sigma_{cs}}{\sigma_{ss}} = \frac{m_{v,s}}{m_{v,c}} = \xi \frac{E_c}{E_s} \tag{3.35}$$

where the coefficient of compressibility of an elastic body (m_v) can be expressed as:

$$m_v = \frac{(1 + \nu)(1 - 2\nu)}{E(1 - \nu)} \tag{3.36}$$

where E is the elastic modulus; and ν is the Poisson ratio. With the simplified approach as described by Han [16], the excess pore water pressures can be calculated over time, while the soil is being loaded and drained by a stiff column. The effect of drain stiffness if captured in the coefficient of consolidation which is depending on the stiffness of both soil and column.

3.4. Sandpiles

In this section sandpiles as ground improvement technique is discussed. Sandpiles as granular inclusions are often used as soil improvement technique. Similar to PVDs, sandpiles have a high permeability and therefore contribute to an acceleration of the consolidation process. The main difference between soil improvement with PVDs and soil improvement with sandpiles is the drain stiffness. The stiffness of the sandpile influences the consolidation rate, as discussed in the previous section. In literature discussed in this section the terms sand/stone columns or granular inclusions are used, which indicate that the behaviour of these techniques is similar.

3.4.1. Bearing capacity

In this section the bearing capacity of sandpiles is analysed. First the bearing capacity of a single pile is reviewed, after which the bearing capacity and failure modes of pile groups are discussed.

Single piles

The bearing capacity of a single sandpile can be calculated by the formula of Hughes and Withers (1974) [18], based on performed laboratory studies. During these studies sand columns were placed within a cylindrical chamber filled with clay, and radiography was used to track the deformations inside and outside the column. After validation of the measurements it was proposed that the ultimate vertical stress (q) in a granular column could be predicted by:

$$q = \frac{1+sin\phi'}{1-sin\phi'}(\sigma'_r + 4c) \tag{3.37}$$

where ϕ' is the friction angle of the stone infill, σ'_r is the free-field lateral effective stress and c is the undrained strength [18]. This equation is still commonly used in daily practice [24]. In figure 3.3 the stresses in a stone column are visualised for both friction piles and stone columns.

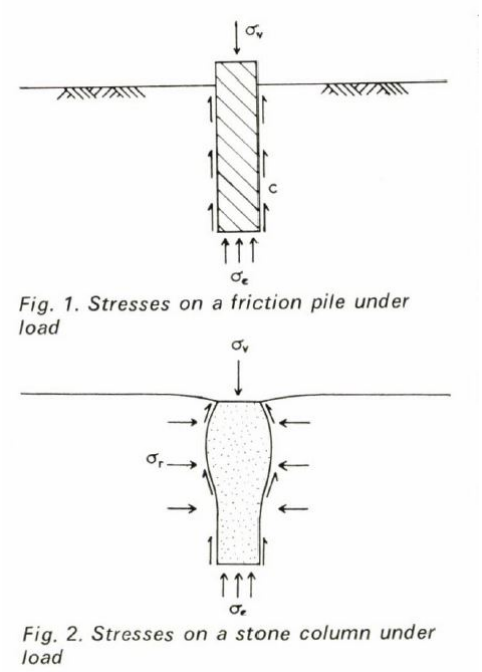

Figure 3.3: Stresses on friction pile (top) and stone column (bottom) under load [18].

As can be observed in the figure above the stone column is radially deforming at the top of the column. This radial deformation is referred to as bulging, and can cause failure of the column. Watts et al. [35] rewrote the equation as presented by Hughes and Withers assuming the column to be in a state of yielding shear (bulging failure mode) at a depth h as:

$$q_{ult} = K_{pc}(K_0[\gamma_s h - u_{so}] + u_{so} - u_s + 4c_u) \tag{3.38}$$

where K_{pc} is the coefficient of passive earth pressure for the column and is equal to $(1+sin\phi')/(1-sin\phi')$; K_0 is the coefficient of earth pressure at rest for unimproved soil and is equal to $(1-sin\phi_s)$; u_{so} is the initial pore water pressure at depth h; and u_s is the pore pressure at yield at depth h [27]. For single columns bulging behaviour is often causing failure of the pile. It is therefore an important requirement for granular columns, including sandpiles, to drive sufficient load-carrying capacity in the lateral confinement provided by the surrounding soft soil. A single granular column installed in very soft clay with an undrained strength of less then 15 kPa, might fail through excessive bulging that occurs near the top. For shorter granular columns, general shear failure is a more probable failure mechanism [17].

Pile groups

The analytical approach suggested by Etezad et al. [12] is dividing the soil underneath the embankment in three zones, which are used to determine the resistance of the improved soil against general, local or punching shear failure. The different failure modes are visualised in figure 3.4. Based upon the input parameters and the behaviour of sandpiles and stone columns it is assumed that the approach suggested by Etezad [12] is applicable for analysing the bearing capacity of sandpiles.

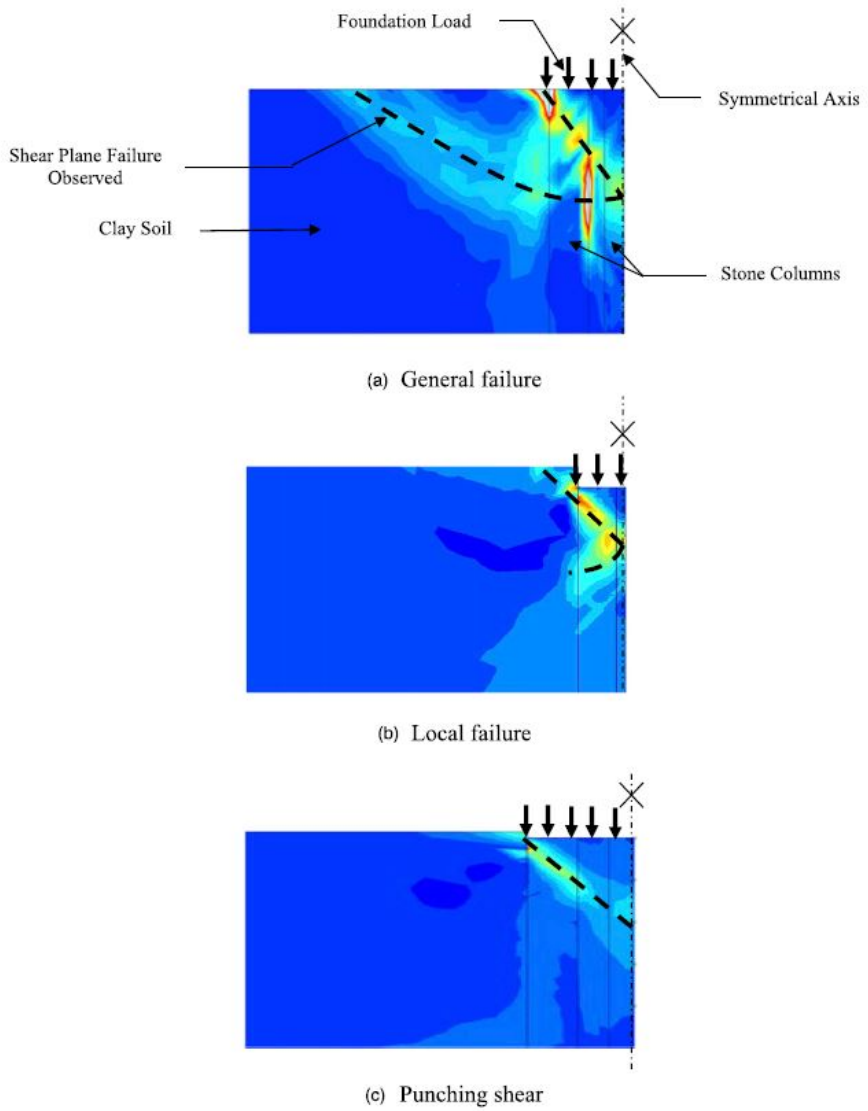

Figure 3.4: Different failure mechanisms of a group of stone columns [12].

In the case of general shear failure, the surrounding soil moves horizontally and vertically beyond the reinforced area, making the columns bulge (in the centre columns) and buckle (at the exterior columns). The analytical model developed by Etezad et al. [12] separates the reinforced soil into three zones:

1. Zone 1 is made out of a wedge shape (block ABC), located immediately under the foundation and making an angle ψ with the horizontal axis (i.e. with the soil surface). Following the classic theories for bearing capacity of shallow foundations, it is assumed that the wedge ABC moves together with the footing during loading.

2. Zone 2 consists of two log-spiral sections (curves CD and CF), which originate at the lower point of the wedge (point C). Owing the discontinuity of the materials at the boundaries between the composite

system and the soft soil, divergence of the log-spiral curves was noted. Consequently, each log-spiral section is made of two parts:"one part is within the composite soil and the other part is in the surrounding soft soil.

3. Zone 3 is known as the passive Rankine section, where the failure surfaces are made of planes (DE and FG). This zone connects the log-spiral part to the ground surface.

The zones listed above are visualised in figure 3.5:

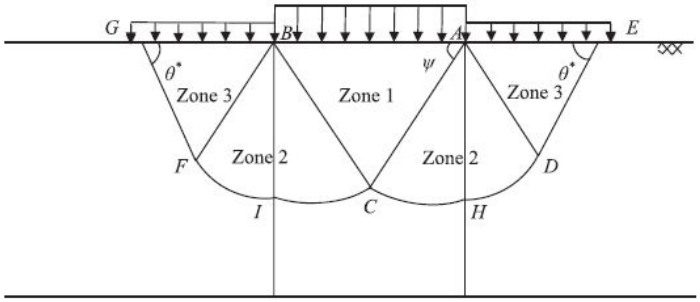

Figure 3.5: Idealised failure mechanisms [12].

As the analysis is not considering the failure of the reinforced soil, the analytical models for estimating the bearing capacity of the soil reinforced with sandpiles are not presented in this report. The analysis as performed in this research consider an uniform unit cell with constant loads acting on the cell. Over the depth of the unit cell the stresses on both sides are homogeneous, while the failure mechanisms as described by Etezad are caused by differences in horizontal stresses underneath and next to the structures.

3.4.2. Stiffness of soil/pile composite

Granular columns, including sandpiles, make very efficient use of the soil near the surface, unlike pile foundations. They are ideal for light loads but are less effective to support heavy loads because they cannot transfer the applied stresses to the deeper layers of soil [18]. Loading of the columns results not only in load transfer by shear stresses along the shaft, it also causes horizontal stresses in the soil by the bulging of the column (section 3.4.1).

Installing sandpiles in soft soil will improve the stiffness of the soil/pile composite, because the stiffness of the sand material inside the sandpile is higher than the stiffness of the surrounding soft soil. The load applied on the surface will be taken by the soil/pile composite. As the stiffness of the sandpile is high, more load transfer will occur through the pile, compared to the load transferred by the soft soil [18]. The stiffer elements carry more stress compared to the softer elements.

Deformation of reinforced soft soil

The deformation behaviour of soft ground reinforced by granular piles can be predicted by using the analytical approach of Alamgir [3]. The situation analysed by this approach is schematised in figure 3.6. As can be observed in this figure is the analytical approach considering the loading of a single granular column and the surrounded by (soft) soil. When performing the analysis a mesh is made to divide the sandpile and surrounding soils in multiple elements, after which for each elements the stresses and strains are calculated. The discretisation of the column and the stresses acting on the jth element are visualised in figure 3.7.

The assumptions made in the analytical approach of Alamgir are listed below:

1. The effect of drainage on the deformation is neglected.

2. The mesh only deforms in vertical direction.

3. The deformation behaviour is not time dependent, only the total displacements can be simulated with this approach.

4. Only shear stresses along the shaft of the piles are taken into consideration.

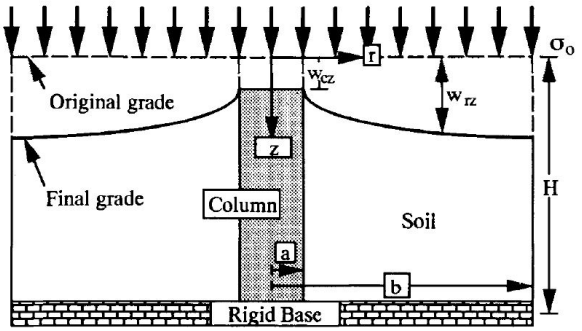

Figure 3.6: Assumed mode of deformation according to Alamgir [3].

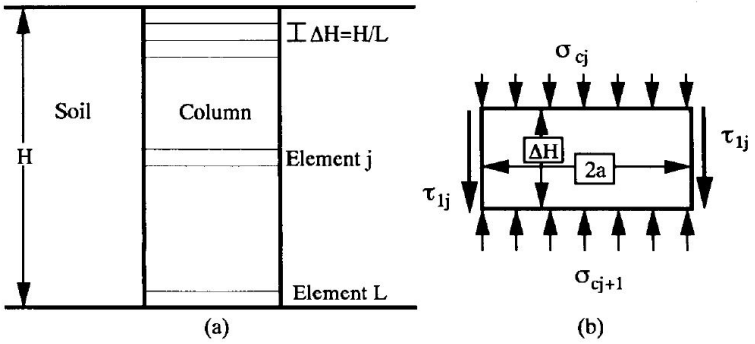

Figure 3.7: (a) Discretisation of column, (b) stresses on the jth element of column [3].

5. The tip of the pile is fixed; the pile is end-bearing.

The mode of deformation of the column-reinforced ground (visualised in figure 3.6) considered is expressed by the following equation:

$$w_{rz} = w_{cz} + \alpha_{cz}[r/a - e^{\beta_c(r/a-1)}] \quad for \quad a \leqslant r \leqslant b \tag{3.39}$$

where a and b are the radii of column and unit cell, respectively; r is the radial distance of the soil element at a depth z and at a radial distance r; w_{cz} is the displacement of the column element at a depth z; α_{cz} and β_c are the displacement parameters. The vertical displacement of the column-soil system varies both with depth and radial distance, the mobilised shear strain and shear stresses also vary in both directions. Differentiating equation (3.39) with respect to r and by substituting the value of shear modulus $G_s = E_s/2(1+\nu_s)$, the following expressions for the normal stress on the jth element of the column is obtained as:

$$\sigma_{c,j+1} = \sigma_{c,j} + \frac{(\Delta H/a)(1-\beta_c)E_s\alpha_{c,j}}{a^2(1+\nu_s)} \tag{3.40}$$

in which:

$$\beta_c e^{\beta_c(n-1)} - 1 = 0 \tag{3.41}$$

As can be seen in equation 3.41, β_c is only dependent on the spacing ratio ($n = b/a$) of the columns. The stresses $\sigma_{c,j}$ and $\sigma_{c,j+1}$ are the normal stresses acting on the top and bottom of the jth element of the column, respectively; j varies from 1 to L and α_{cj} is the displacement parameter. In the calculation of the deformations of the column only the axial deformation is considered. The vertical deformation of each element of the column is related to the stress acting at the mid section of that element and deformation modulus of the column material. Deformation of the jth element of the column, $w_{c,j}$ is derived from equation 3.40 as:

$$w_{c,j} = \frac{\Delta H}{E_c}\sigma_{c,j} + \frac{(\Delta H/a)^2(1-\beta_c)E_s\alpha_{cj}}{2E_c(1+\nu_s)} \tag{3.42}$$

The stresses in the column are transferred to the soil starting from the top op the pile. Over the length of the column these stresses decrease as more stress is transferred to the soil. The shear stress is maximum at the column-soil interface and decreases with an increase in radial distance and becomes zero at the outside boundary of the unit cell. Therefore, the normal stress acting on the surrounding soil varies with vertical and radial distances. To obtain the stresses in the soil and the column, the cell is divided into L number of vertical elements (the same amount as the column), and subdivided in N number of radial elements. These radial elements have a width of $\Delta r (= (b-a)/N$. The shear stress at the outside boundary of the unit cell is zero, i.e. at $r = b$, $\tau_{bz} = 0$. From the equilibrium of forces on the Nth element of the soil, the following formula is obtained:

$$(\sigma_{sNz} + \Delta\sigma_{sNz})[\pi b^2 - \pi(b-\Delta r)^2] - \sigma_{sNz}[\pi b^2 - \pi(b-\Delta r)^2] + \tau_{Nz} 2\pi(b-\Delta r)\Delta z = 0 \tag{3.43}$$

simplified as

$$\frac{d\sigma_{sNz}}{dz} = -\frac{(n-\Delta R)\tau_{Nz}}{a\Delta R(n-\Delta R/2)} \tag{3.44}$$

where τ_{Nz} is the shear stress acting at a radial distance $r/a = n - \Delta R$ and at a depth z, $\Delta R = r/a$. Integration of equation 3.44 numerically, the normal acting stress at the (N, j)th element is obtained as:

$$\sigma_{sNj+1} = \sigma_{sNj} - \frac{(\Delta H/a)(n-\Delta R)[1-\beta_c e^{\beta_c(n-\Delta R-1)}]E_s\alpha_{cj}}{2a\Delta R(n-\Delta R/2)(1+\nu_s)} \tag{3.45}$$

where σ_{sNj} and σ_{sNj+1} are the normal stresses acting at the top and bottom of the (N, j)th element, respectively. The vertical deformation of each supporting soil element surrounding the column is obtained from the uniform vertical stress acting at the mid section of the soil element and the deformation modulus of the soil. Compression of the (N,j)th element of soil (soil element adjacent to the boundary of unit cell), w_{sNj} is derived from equation 3.45 and expressed as:

$$w_{sNj} = \frac{\Delta H}{E_s}\sigma_{sNj} - \frac{(\Delta H/a)^2(n-\Delta R)[1-\beta_c e^{\beta_c(n-\Delta R-1)}]\alpha_{cj}}{4\Delta R(n-\Delta R/2)(1+\nu_s)} \tag{3.46}$$

From the equilibrium of vertical forces acting on a soil element(r, z) the following differential equation is obtained where the stress system is symmetric about the z-axis:

$$\sigma_{si+i,j+1} = \sigma_{si,j} - G_s[(\frac{\gamma_{i,j} - \gamma_{i+1,j}}{\Delta r}) + (\frac{\gamma_{i,j} + \gamma_{i+1,j}}{2r})]\partial z \tag{3.47}$$

where $\sigma_{si,j}$ and $\sigma_{si+1,j+1}$ are uniform stresses acting at the top and bottom of the (i, j)th element of soil, respectively; $\gamma_{i,j}$ and $\gamma_{i+1,j}$ are the shear strains for the (i, j)th and $(i+1, j)$th elements of soil, respectively. The shear strains are obtained by the following equations, in which the displacements, w_{rz} i.e. $w_{i,j}$ are predicted from equation 3.39 by substituting the values of unknown parameters as:

$$\gamma_{i,j} = \left(\frac{w_{i+1,j+1} + w_{i+1,j}}{2} - \frac{w_{i,j} + w_{i,j+1}}{2}\right)/\Delta r \tag{3.48}$$

$$\gamma_{i+1,j} = \left(\frac{w_{i+2,j+1} + w_{i+2,j}}{2} - \frac{w_{i+1,j} + w_{i+1,j+1}}{2}\right)/\Delta r \tag{3.49}$$

The displacement compatibility between the column and the soil element is considered here as an important criterion for the development of the proposed approach. For no slip conditions, the compatibility of column and soils along the full depth are considered. The displacements of the (j)th element of column, W_{cj} and (N, j)th element of soil, w_{sNj} is related as the following, obtained from equation 3.39 and by substituting for $r/a = n - \Delta R/2$:

$$w_{sNj} = w_{cj} + \alpha_{cj}[n - \Delta R/2 - e^{\beta_c(n-\Delta R/2-1)}] \tag{3.50}$$

Hence, evaluating w_{cj} from equation 3.42 and W_{sNj} from equation 3.46 and substituting in equation 3.50, α_{cj} is obtained as:

$$\alpha_{cj} = \frac{\left[\frac{\sigma_{sNj}}{E_s} - \frac{\sigma_{cj}}{E_c}\right]\Delta H}{(A_1 + A_2 + A_3)} \tag{3.51}$$

in which

$$A_1 = \frac{(\Delta H/a)^2(1-\beta_c)E_s}{2E_c(1+\nu_s)} \tag{3.52}$$

$$A_2 = \frac{(\Delta H/a)^2(n-\Delta R)[1-\beta_c e^{\beta_c(n-\Delta R-1)}]}{4\Delta R(n-\Delta R/2)(1+\nu_s)} \tag{3.53}$$

$$A_3 = n-\Delta R/2-e^{\beta_c(n-\Delta R/s-1)} \tag{3.54}$$

Due to the free strain consideration, at the surface the stresses on the column and soil are the same as the applied stresses, i.e. $\sigma_{c1} = \sigma_{s1} = \sigma_0$. Applying this condition, equation 3.51 can be solved for all the elements, i.e. $j = 1$ to L. Once the values of $\alpha_{c,j}$ and β_c are known, the displacements, the shear stresses, the stresses on the column and soil for all elements are calculated with equation 3.39, 3.41, 3.40 and 3.47, respectively. Since the stresses on the soil surrounding the column vary with depth and radial distance, the stress concentration ratio n_c (ratio of stress on column to stress on soil), varies with depth and radial distance as:

$$n_{cij} = \frac{\sigma_{cj}}{\sigma_{sij}} \tag{3.55}$$

The overall settlement at the surface of the column reinforced ground is evaluated by adding the displacements of all shear elements ($j = 1$ to L). Thus the general equation for the settlement (S_{ti}) of the column-treated ground is obtained as:

$$S_{ti} = \sum_{j=1}^{j=L} w_{ij} \tag{3.56}$$

The settlement of the untreated ground (S_0) is estimated as:

$$S_0 = \frac{\sigma_0}{E_s} H \tag{3.57}$$

and a settlement ratio, β_{si} is defined as:

$$\beta_{si} = \frac{S_{ti}}{S_0} \tag{3.58}$$

The method as proposed by Alamgir [3] can be used for the determination of the settlement ratio between the untreated ground and the reinforced ground. The method is based upon the principle that shear stresses between the column and the soil are causing a transfer of loads in the radial direction, resulting in a stress reduction and therefore a settlement reduction for the column surrounding soil. However, this method does not include the horizontal (elastic-plastic) deformation of the column or the influence of drainage on the consolidation rate. Therefore this approach is only suitable for a first approach estimation of the settlements of a reinforced ground regime.

3.4.3. Influence sandpile deformation on consolidation

The rate of consolidations in soft soils can be improved by the installation of granular inclusions, as described in section 3.3.3. The column/soil stiffness ratio varies over time due to the decrease in soil volume during consolidation. Therefore, the fraction of vertical load carried by the columns also varies. The columns deform and bulge under this vertical load, exerting horizontal pressure against the surrounding soil. This horizontal pressure, also variable with time, has an influence on the consolidation process of the surrounding soil [7].

In order to determine the influence of the installation of a sandpile in soft ground on the consolidation behaviour, Castro et al. [7] presented a method for calculating the consolidation of a pile/soil composite. In this method both the elastic- and the elastic-plastic response of the pile are taken into consideration.

Final and undrained state

The analysis of the stress distribution between columns and soil is based on imposing the conditions of vertical equilibrium and compatibility of vertical deformations. Under embankments on large uniform loaded areas, it is convenient to consider a representative cylindrical unit cell formed by a column and it surrounding soil. The boundary conditions at the outer wall are: zero shear stress, zero radial displacements and no discharge of water. The top (surface) and bottom (stiff layer) boundaries are considered as smooth (zero shear stress). When a vertical uniform unit load p_a is applied at the surface, the equilibrium condition in vertical direction is as follows:

$$p_a = \overline{\sigma}_{zc} a_r + \overline{\sigma}_{zs}(1 - a_r) \tag{3.59}$$

where σ_{zc} and σ_{zs} are the total vertical stress increments for the column and for the soil, respectively. The upper bar indicates the average value of the variable along the radius. a_r is the area replacement ratio (area of column A_s divided by the area of the cell, A_c), sometimes denoted in terms of radii; $N = r_1/r_2 = (1/a_r)^{1/2}$. In the first approach only the elastic behaviour of the columns is taken into account. The following elastic parameters are used; Young's (E), shear (G), bulk (K) and oedometric (E_m) moduli, Lamé constant (λ), Poisson's ratio (ν), of which only the Young's modulus and Poisson's ratio are independent.

The proposed analytical solution considers both the horizontal and vertical component of deformation simultaneously. The vertical soil stress can be calculated by the following formula:

$$\sigma_{zs,f} = \frac{p_a}{1 + a_r\left(\frac{E_{mc} - 2\lambda_c F}{E_{ms} + 2\lambda_s F a_r/(1-a_r)} - 1\right)} \tag{3.60}$$

where

$$F = \frac{(1 - a_r)(\lambda_c - \lambda_s)}{2[a_r(\lambda_s + G_s - \lambda_c - G_c) + \lambda_c + G_c + G_s]} \tag{3.61}$$

The improvement factor (n) becomes

$$n = 1 + a_r\left(\frac{E_{ms} - 2(\lambda_c - \lambda_s)F}{E_{ms}} - 1\right) \tag{3.62}$$

The lateral deformations always reduce the stress concentration ratio by subtracting a term to the oedometric modulus of the column and adding another term to that of the soil. The stress concentration factor (SCF) is higher than observed in reality. This is caused by the assumption of pure elastic behaviour of the column.

Elastic solution

In figure 3.8 a horizontal slice of the elementary cell is shown. The column is a vertical solid cylinder subjected to an uniform pressure (σ_{zc}) and radial pressure (σ_{rc}) at its lateral wall. The soil is modelled as a cylinder with a central cylindrical cavity, subjected to a vertical uniform effective pressure (σ'_{zs}), a radial pressure ($\sigma_{rs}(=\sigma_{rc})$) and an internal excess pore pressure ($\overline{u}$). These five pressures determine the stresses and strains at any point of the soil and the column.

The conditions of vertical and radial equilibrium and vertical and radial compatibility of deformation at the soil-column interface must be imposed. These four equations allow to express the above four vertical or radial pressures in terms of the pore pressure ($\overline{u}$) and the applied vertical pressure (p_a) only. The consolidation equation for pure radial equation is [4]:

$$c_{vr} = \left[\frac{\partial^2 u}{\partial u^2} + \frac{1}{r}\frac{\partial u}{\partial r}\right] = \frac{\partial \overline{u}}{\partial t} \tag{3.63}$$

updated with a new modified coefficient of consolidation:

$$c_{vr}^{zre} = c_{vr}\frac{[a_r(\lambda_c + 2G_s) + (1 - a_r)(\lambda_s + 2G_s)][H - (\lambda_c - \lambda_s)] - (1 - a_r)(\lambda_c - \lambda_s)^2}{(\lambda_s + 2G_s)[H - (1 - 3a_r)(G_c - G_s)]} \tag{3.64}$$

with $H = (1/a_r)(\lambda_c + G_c + G_s) - (G_c - G_s)$. The ratio of (c_{vr}^{zre}/c_{vr}) depends on the Poisson's ratio of both soil and column, the modular ratio (E_c/E_s) and the area replacement ratio (a_r).The superscript zre refers to the influence of vertical and radial elastic deformation of the column. The value of c_{vr}^{zre} can be calculated once the stresses are known in the final and undrained stages.

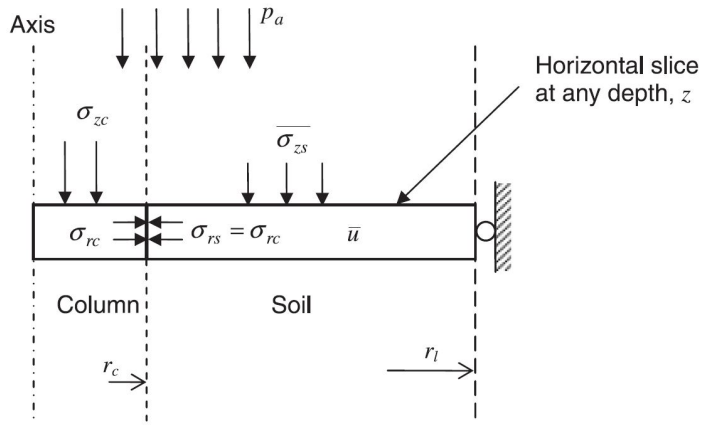

Figure 3.8: Equilibrium and compatibility conditions between soil and column in the elastic case [3].

With use of the modified coefficient of consolidation (c_{vr}^{zre}) the variation of the average degree of consolidation with time can be obtained, after which the degree of consolidation can be determined.

Plastic deformations

In case the deformation of the column is assumed to be plastic, the plastic strains of the column can be determined by using the Mohr-Coulomb yielding criterion and a non-associated flow rule for the plastic strains. This flow rule assumes a constant dilatancy angle ($\psi_c \neq \phi_c$). Based upon the before mentioned criteria, the following formulas can be derived:

$$\frac{\sigma_{rc}}{\sigma zc} = \frac{1 - sin\phi_c}{1 + sin\phi_c} = k_{ac} \tag{3.65}$$

$$-\frac{\epsilon_{zc}^p}{2\epsilon_{rc}^p} = \frac{1 - sin\psi_c}{1 + sin\psi_c} = k_{\psi c} \tag{3.66}$$

The increments of elastic strains in the column during plastic deformation are neglected. The plastic components, when they exist, are equal to the total strains, therefore superscript p can be suppressed. In the elastic-plastic analysis, the effective stresses in the yield condition (3.65) must also include the previous stresses existing before the load application. As these stresses in general vary over depth, the analysis must be carried out in terms of z. Being an elastic-plastic analysis, the final state is highly dependent on the loading path followed. Therefore, the analysis must be performed in the time, keeping track of the development of stresses and strains at each depth during the process.

In figure 3.9 the stress paths in the (σ_{rc},σ_{zc}) are plotted. When the effects of column installation are neglected, the initial stresses (point I) are:

$$\sigma_{zc,i} = \gamma_s' z, \quad \sigma zc, i = \gamma_c' z, \quad \sigma_{rs,i}' = \sigma_{rc,i} = k_{0s}\sigma_{zs,i}' \quad and \quad u_i = 0 \tag{3.67}$$

The column starts in an elastic state, because $k_{0s} > k_{as}$ in every case. Immediately after the load is applied, the soil undrained stiffness is higher than the drained stiffness of the column. At this time the soil takes more vertical load than the column does. Therefore, at this point the column is well confined by the surrounding soil, with a vertical stress increment even lower than the radial one (point U).

Direct after loading the soil starts to consolidate, part of the vertical stress is progressively transferred from the soil to the column, and at the same time the lateral stress in the column-soil interface decreases. The column remains elastic until the end of the consolidation (case a), point (F), or reach the plastic state at a given time (case b), point (Y).

Since the initial stresses increase with z and their increments are independent of depth, the worst conditions occur at the surface. Once yielding is reached, the vertical stiffness of the column decreases, and also its radial deformability increases due to dilatancy. This affects the transfer of vertical load from the soil. The vertical load on the column varies with depth, which means that for vertical equilibrium some shear stresses

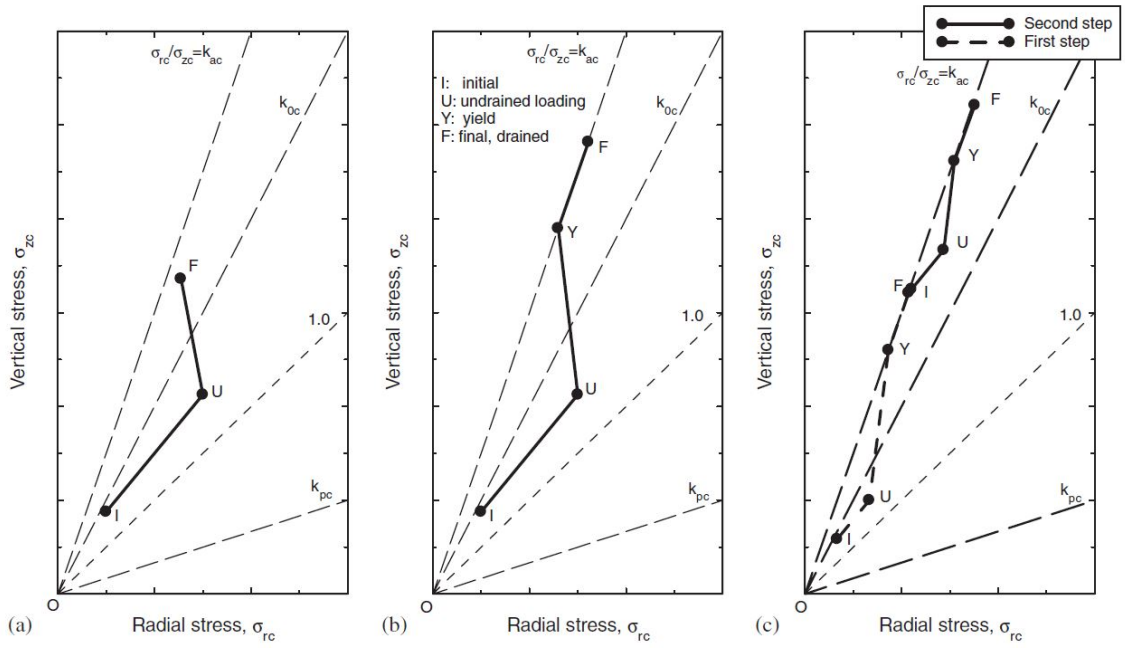

Figure 3.9: Stress path in the column in typical conditions; (a) elastic case; (b) elastic-plastic case; and (c) two-step load[7].

must appear at the column-soil interface. However, this second order effect is not included in the presented approach. Below the limit of the plastic zone stresses are constant over depth, and the preceding elastic solution is valid.

At any depth z the time of yielding can be obtained from the yield condition (equation 3.65) applied to the elastic solution at the elastic-plastic interface:

$$\frac{\sigma_{rc,y}}{\sigma_{zc,y}} = \frac{k_0\gamma'_s z + \partial\sigma_{rc,y}}{\gamma'_c + \partial\sigma_{zc,y}} = \frac{1-sin\phi_c}{1+sin\phi_c} = k_{ac} \tag{3.68}$$

where the stress increments (denoted as $\Delta\sigma$) are due to the load application and the suffix 'y' refers to the moment of yielding. Each increment can now be expressed as;

$$\Delta\sigma_y = \Delta\sigma_u + U_y^e(\Delta\sigma_f^e - \Delta\sigma_u) \tag{3.69}$$

where U_y^e is the elastic degree of consolidation at the moment of column yielding at the depth considered, defined as the interpolation factor between the undrained stress increments and the final ones if the column would behave elastically until the end of consolidation, $\Delta\sigma_f^e$.

For the pore pressure the final value is unchanged with respect to the elastic case ($u_f = 0$), so;

$$\overline{u}_y = (1-U_y^e)u_u \tag{3.70}$$

Hence, U_y^e is the true degree of consolidation in terms of average excess pore pressures at the time of yielding:

$$U_y^e = \frac{(k_0\gamma'_s - k_{ac}\gamma'_c)z + \Delta\sigma_{rc,u} - k_{ac}\Delta\sigma_{zc,u}}{k_{ac}\Delta\sigma^e_{zc,f} - \Delta\sigma_{rc,f} + \Delta\sigma_{rc,u} - k_{ac}\Delta\sigma_{zc,u}} \tag{3.71}$$

In the equation above only the first term in the numerator is dependent on z. The rest are undrained or final elastic stress increments, all of them proportional to the applied load p_a. Hence, U_y^e depends on the depth z and the load p_a only through the factor $(k_0\gamma'_s - k_a c\gamma'_c)z/p_a$.

Once the undrained and final situations are defined for the plastic phase, the consolidation process for the plastic increment can be studied using any of the available solutions of the radial consolidation equation, in the same way as it was done for the elastic column. The modified coefficient of consolidation considering plastic behaviour becomes:

$$c_{vr}^{zrp} = c_{vr} \frac{(1-a_r) + \frac{a_r}{(\lambda_s+2G_s)}\left(\frac{\lambda_s}{k_{\psi c}} + \frac{J}{k_{ac}}\right)}{\left[1+\frac{a_r}{(1-a_r)k_{\psi c}}\right]\left((1-a_r+\frac{a_r}{k_{ac}}\right)} \tag{3.72}$$

with $J = \lambda_s + G_s + a_r(\lambda_c + G_s)/(1-a_r)k_{\psi c}$. The ratio (c_{vr}^{zrp}/c_{vr}) depends only on the Poisson's ratio of the soil (ν_s), the plastic parameters of the column (ϕ_c, ψ_c), and the area replacement ratio (a_r). With the resulting value of c_{vr}^{zrp}, the solution follows the same procedure as for the elastic phase.

Integration for the whole column

As the moment for yielding U_y^e is different for each depth, the surface settlement at any time can be obtained by integration of the vertical strain along the column length L. Options are: analytical integration, numerical integration or use of the situation at a representative point for the whole column (mean depth $z = L/2$).

The settlement-time law is by far the most important result of the analysis, because surface settlement is the variable most often monitored in actual cases. For this reason, the result of the analytical integration is given, using the Barron-Hansbo closed form solution for the consolidation at any depth z. By integration of the consolidation rate for the whole column, the following expressions are obtained for the settlement of column head, s, in three different phases:

1. Phase A; $(z_c \leq 0)$, the whole column is elastic:

$$s_z = L[\epsilon_{z,u} + (\epsilon_{z,f} - \epsilon_{z,u})(1 - e^{-8(T_r/f(a_r))c_{vr}^{zre}/c_{vr}})] \tag{3.73}$$

2. Phase B; $(0 < z_c < L)$, the upper part of the column $(z \leq z_c)$ is plastic and the rest $(z \geqslant z_c)$ is elastic:

$$s_z = (L-z_c)[\epsilon_{z,u} + (\epsilon_{z,f}^e - \epsilon_{z,u})(1 - e^{-8(T_r/f(a_r))c_{vr}^{zre}/c_{vr}})] + z_c[\epsilon_{z,u} + (\epsilon_{z,f}^e - \epsilon_{z,u})P(z_c)] + \frac{\Delta\epsilon_z^p}{\overline{u}^y} u_u \left[z_c[1-P(z_c)] + Q(z_c)e^{-8(T_r/f(a_r))c_{vr}^{zre}/c_{vr}}\right] \tag{3.74}$$

3. Phase C; $(L \leq z_c)$, the whole column is plastic:

$$s_z = L[\epsilon_{z,u} + (\epsilon z, f^e - \epsilon_{z,u})P(L)] + \frac{\Delta\epsilon_z^p}{\overline{u}^y} u_u [L[1-P(L)] + Q(L)e^{-8(T_r/f(a_r))c_{vr}^{zre}/c_{vr}} \tag{3.75}$$

where

$$P(z) = \frac{\eta\frac{z}{2} - \kappa_u}{\kappa_f^e - \kappa_u}, \qquad Q(z) = \frac{\kappa_f^e - \kappa_u}{(2-\lambda_{ep})\eta}\left[\left(\frac{\kappa_f^e - \eta z}{\kappa_f^e - \kappa_u}\right)^{2-\lambda_{ep}} - \left(\frac{\kappa_f^e}{k_f^{e-\kappa_u}}\right)^{2-\lambda_{ep}}\right]$$
$$\kappa = \frac{k_{ac}\Delta\sigma_{zc} - \Delta\sigma_{rc}}{k_{ac}}, \qquad \eta = \frac{k_0\gamma_s' - k_{ac}\gamma_c'}{k_{ac}}, \qquad \lambda_{ep} = \frac{c_{vr}^{zrp}}{c_{vr}^{zre}} \tag{3.76}$$

and where $(\kappa_u, \epsilon_{z,u})$ and $(\kappa_f^e, \epsilon_{z,f}^e)$ refer, respectively, to the undrained state and to the final one in the assumption of elastic behaviour, as defined in equation (3.69).

The analytical approach as proposed by Castro et al. [7] can be used for analysing the behaviour of the sandpiles. One of the main findings of the research of Castro et al. was the effect of the radial deformation on the modified coefficient of consolidation $(c_{vr}^{zre}/c_{vr},\ c_{vr}^{ze}/c_{vr})$ and the area displacement ratio (a_r) for modular ratio (E_c/E_s) (figure 3.10).

As can be seen in figure 3.10 the introduction of radial deformations of the column reduce the extreme high stress ratio between the soil and column. The reduction of the stress ratio in the analytical model by enabling lateral deformations results in more realistic values of the stresses calculated.

3.5. Installation of sandpiles

In this section the installation procedure of the sandpiles is discussed. First, the installation method is described, after which the different installation effects are analysed.

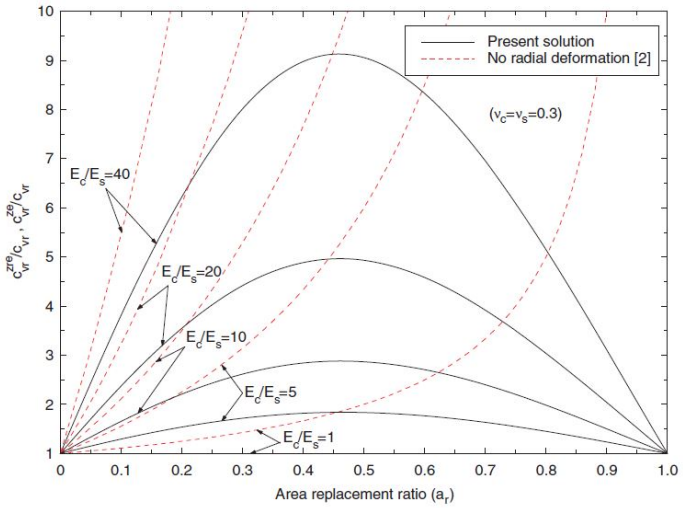

Figure 3.10: Equivalent coefficient of consolidation. Elastic column. Influence of modular ratio [7].

3.5.1. Installation procedure

There are installation methods for granular inclusions, which include installation by vibro- compaction, vibro-replacement, cased bore hole (rammed stone columns/granular piles), or by simple auger boring methods [22]. This research is focused on the behaviour of sand piles, therefore the installation technique used for installing sand piles will be discussed. The sandpile installation method used at the NAICM site is static placement in combination with vibrations and air pressure. The installation method involves a hollow casing which is pushed by a rig into the soft soil layers until it reaches the designed depth. The soft soil in the casing is then being removed by an auger. After removal of the soil, sand is inserted under pressure at the end of the tube, while the tube itself is pulled upwards. The casing is being vibrated while pulling out in order to prevent soil-arching of the sand in the tube, which could block the stream of sand. In applications where sand compaction is desired, the sand inside the casing can be compacted by vibrations, dynamic impacting or static excitation. The sandpiles at the test embankment at the NAICM site are installed without additional compaction [2].

3.5.2. Installation effects

The installation of sandpiles with the methods as described in section 3.5.1 will affect the material properties of the surrounding soft soils. The effects which can be observed during and after the installation of piles are the occurrence of smear- and transition zones around the piles. The strengthening effect of the installation method on the surrounding soil is depending on the chosen installation technique.

Smear zone

During the installation of the piles the soil adjacent to the casing is displaced and dragged down in order to produce space for the casing. These displacements create a zone of disturbed soil around the tube in which the strength and hydraulic conductivity in the horizontal direction decrease, and the compressibility increases. This reduction in hydraulic conductivity delays the consolidation process. The soil in this smear zone is completely remoulded, resulting in a spatially uniform hydraulic conductivity (k_s) which is smaller than the in-situ hydraulic conductivity (k_c). The degree of disturbance qualified with the ratio k_s/k_c and the extent of smear zone have been researched thoroughly. Based upon back analysis of case histories, laboratory tests and samples collected from field, model experiments, studies of pile driving, practical considerations and experience, the degree of disturbance varies between 0.1 and 0.33. However, some studies proposed a value as low as 0.001, while others suggest that the ratio ranges from 0.5 to 0.66 [5]. The large range of the degree of disturbances proposed indicate that this disturbance is not captured accurately. The position of the smear zone with respect to the vertical drain is visualised in figure 3.11.

The extent of the smear zone around prefabricated vertical drains installed by a mandrel is analysed by Sathananthan et al. [31], based on the cavity expansion theory for soft clay. In the analysis the modified Cam-clay model is used. It was proposed that the extent of the smear zone is considered as the region in which

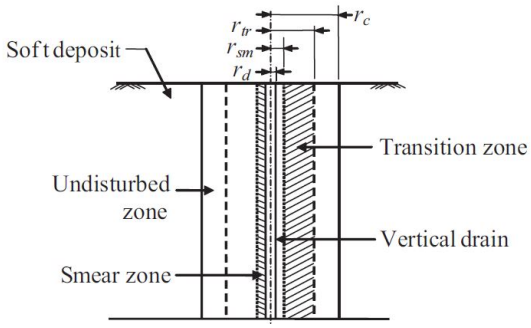

Figure 3.11: Position of smear zone and disturbance zone [5].

the pore water pressure is greater than the initial overburden stress (total). This is based on the assumption that the soil is severely disturbed, although the plastic zone might extend beyond this point. The anisotropy with respect to its permeability coefficient is almost entirely destroyed when $u = \sigma_{v0}$ [31]. According to the findings of Sathananthan et al. the radius of the plastic (smear) zone depends on the Poisson's ratio (v), the slope of the swelling- and compression lines in $v - lnp'$ space, κ and λ, respectively. Furthermore the slope of the critical state line (M) and the isotropic overconsolidation ratio (R) influence the radius of the smear zone. Although the properties and development of the smear zone along the prefabricated vertical drains is thoroughly researched, the research conducted on the smear zone development around sandpiles is very limited. As the installation procedure of sandpiles indicated that there is a smear zone development, the properties and geometry of this zone cannot be estimated.

Transition zone

Next to the smear zone in which the soil is completely remoulded, a transition zone is located in which the soil changes from being completely remoulded until being completely unaffected by the installation of the pile (figure 3.11). The dimensions and shape of this disturbance zone depends on many factors, such as the shape and size of the tube, the compaction method and the soil properties. In case of circular sand piles, the smear- and transition zone is assumed to be circular.

The distribution of the ratio of hydraulic conductivity's over the width of the smear- and the transition zone is not linear, according to experimental investigations. Multiple different distributions of hydraulic conductivity over the width of the zones are proposed, named Case A t/m Case E [5]:

1. Case A: the hydraulic conductivity (HC) over the width of the smear zone is constant; the HC in the transition zone is equal to the HC of the natural soil;

2. Case B: the HC over the width of the smear zone is constant; the HC in the transition zone is linear, starting from the HC of the smear zone to the HC of the natural soil;

3. Case C: the HC over both zones is bi-linear, starting from the HC of the smear zone towards the HC of the natural soil. Between the two zones the HC gets a lower gradient when entering the transition zone;

4. Case D: the HC is linear over both layers, starting from HC of the smear zone until HC of the natural soil;

5. Case E: the HC over the smear zone is constant, the HC over the transition zone is bi-linear. At a certain distance in the transition zone the HC gets a lower gradient towards the natural soil.

Based on the research of Basu [5], in which the various cases are compared, it is not possible to state which case is the most accurate for modelling the hydraulic conductivity in the affected zone. The five different cases with the different hydraulic conductivity's are visualised in figure 3.12.

Concluding on the theorem available on the development of smear- and transition zones around sandpiles is that it is know that these zones develop upon pile installation. However, the properties and range of these zones is rather unknown and hard to predict, as these are dependent on several parameters.

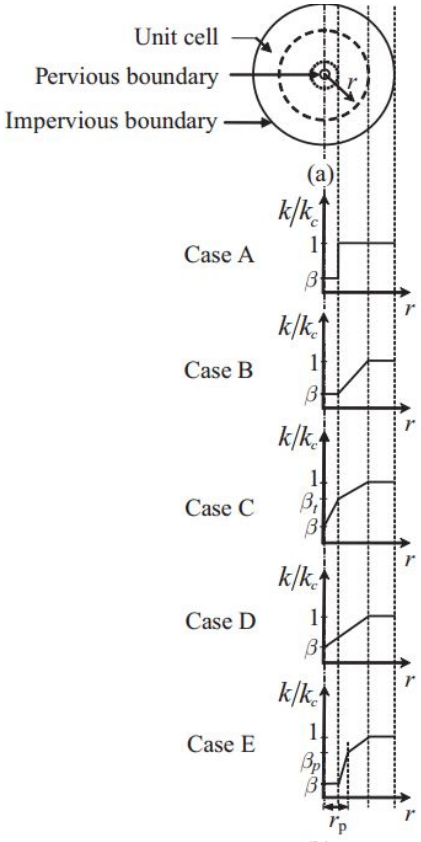

Figure 3.12: Variation of the hydraulic conductivity with distance from the centre of the drain for different cases [5].

3.6. Material models

The numerical analyses are performed in the finite element (FE) software Plaxis 2D. The material models used for analysing the behaviour of the sandpiles and the surrounding soil, namely the Mohr-Coulomb model, the Hardening Soil model and the Soft Soil model, are briefly described in this section.

The numerical analysis of the sandpile behaviour is performed in the FE software Plaxis 2D. With use of a FE program the development of stresses and strains in the sandpiles and soil upon loading can be estimated. The material models applied for simulating the behaviour of the analysed soils is important, as the selected models may or may not include the right material behaviour for a given problem. In this research, the first FE models are using a simple material model, the Mohr-Coulomb model. This model is based on linear elastic perfectly plastic material behaviour. This model is suitable for a first estimate, for accurate modelling more advanced models are needed, i.e. the Hardening Soil and the Soft Soil Creep model.

Note that using FEM software for analysing the behaviour of soils requires special attention to the model input. Using input data which is not correct or a soil model which not captures the right material behaviour may results in output data which does not represent the actual situation. Therefore all the input data, including the default settings, need to be checked before running the simulations.

3.6.1. The Mohr-Coulomb model

The Mohr-Coulomb (MC) model is a linear elastic perfectly plastic model, often used as a first approximation of soil behaviour. The linear elastic part is based on Hooke's law of isotropic elasticity, the perfectly plastic part is based on the MC failure criteria, formulated in a non-associated plasticity framework [1].

The MC model is using a yield function (f_s) in order to evaluate whether or not plasticity occurs during a simulation. When the effective stresses in the soil are reaching this yield function ($f_s = 0$), plastic straining will occur. In the MC model the yield function is fixed and is not affected by (plastic) straining. For stress states represented inside the yield contour, the behaviour is purely elastic and all strains are reversible. A stress state outside the yield contour is physically not possible. In figure 3.13 the principle of an elastic perfectly plastic model is visualised.

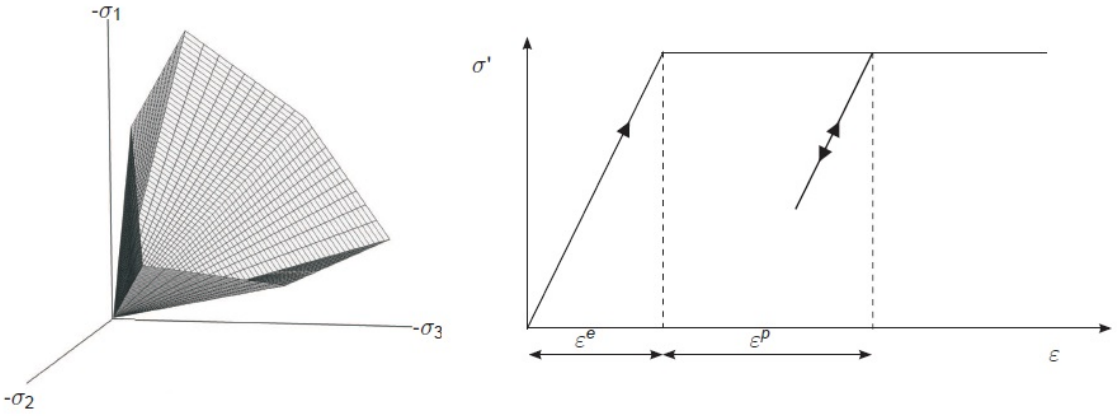

Figure 3.13: The Mohr-Coulomb yield surface in principle stress state (left); The basic idea of an elastic perfectly plastic model (right) [1].

The characteristics of the Mohr-Coulomb model are:

1. Constant material stiffness over depth.
2. Fixed yield surface.
3. Elastic unloading / reloading.
4. Failure of material according to the Mohr-Coulomb failure criteria.

The MC model requires the input of six parameters, which can be obtained from basic tests on soil samples. The input parameters of the MC model are listed in table 3.2.

Table 3.2: Input parameters of the Mohr Coulomb material model [1]

Input	**Parameter**	**Unit**
Young's modulus	E	$[kN/m^2]$
Friction angle	ϕ'	[°]
Cohesion	c'	$[kN/m^2]$
Dilatancy angle	ψ'	[°]
Poisson's ratio	ν_{ur}	[−]
Tension cut-off and tensile strength	σ_t	$[kN/m^2]$

3.6.2. The Hardening Soil model

The hardening soil (HS) model is an advanced soil model used for modelling the behaviour of stiffer- and soft soils. The main characteristic of this model is the presence of a cap in the principle stress space, which enables modelling of plastic straining of the soil. In contrast with the Mohr-Coulomb model the yield surface can develop as result of plastic straining, changing the stiffness of the soil upon loading and reloading. The yield surface in the principle stress space and cap- and friction hardening are visualised in figure 3.14.
The characteristics of the hardening soil model are:

1. Stress dependent stiffness (power law).
2. Plastic straining due to primary deviatoric loading (shear hardening).
3. Plastic straining due to primary compression (compression hardening).
4. Elastic unloading / reloading.
5. Failure according to the Mohr-Coulomb failure criteria.

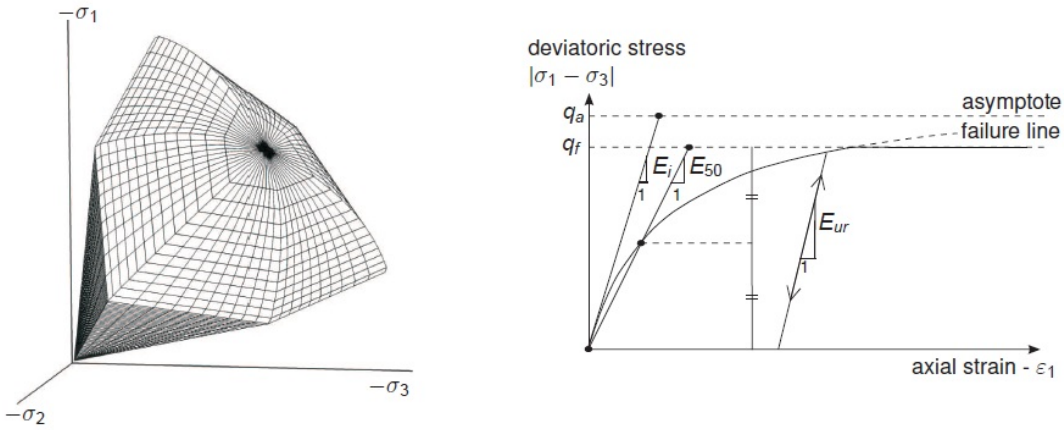

Figure 3.14: The Hardening Soil yield surface in principle stress space (c=0) (left); The principles of a strain hardening model (right) [1].

The yield surface as presented in figure 3.14 is able to expand as a result of plastic straining, which enables the model to incorporate the hardening behaviour of the soil. In the HS model two types of hardening are distinguished, namely shear hardening and compression hardening. Both hardening types enlarge the yield contour upon straining, increasing the region inside the contour governing the elastic behaviour of the material. The input parameters used in the HS model are presented in the table 3.3.

Table 3.3: Input parameters of the hardening soil material model [1]

Input	**Parameter**	**Unit**
Effective friction angle	ϕ'	[°]
Effective cohesion	c'	$[kN/m^2]$
Dilatancy angle	ψ'	[°]
Secant stiffness modulus	$E_{50;ref}$	$[kN/m^2]$
Unloading/reloading stiffness	$E_{ur;ref}$	$[kN/m^2]$
Tangent stiffness modulus	$E_{oed;ref}$	$[kN/m^2]$
Poisson's ratio unloading/reloading	ν_{ur}	[−]
Power law for stress-level dependency of stiffness	m	[−]
Ratio of failure	R_f	[−]
Reference stress for stiffness	P^{ref}	$[kN/m^2]$
Neutral lateral stress coefficient (NC)	$K_{0;nc}$	[−]

The HS model is an advanced material model including stress dependent stiffness of soft and stiffer soils. However, this model does not include some of the features of real soil material. In the model softening behaviour due to soil dilatancy and de-bonding effects are not incorporated. Other material aspects which are not captured in the material model include cyclic and dynamic loading, small strain stiffness and secondary consolidation.

3.6.3. The Soft Soil Creep model

The Soft Soil Creep model (SSC) model is an advanced soil model used for modelling the behaviour of soft soils, including near-normally consolidated clays, clayey silts and peat. These materials are characterised by their high degree of compressibility. The HS model is capable of modelling the behaviour of compressive soils as well, but for very soft soils with a high compressibility ($E_{oed}^{ref}/E_{50}^{ref} < 0.5$) this model is not suitable, for these soils the SSC model may be used. The characteristics of the soft soil creep model are [1]:

1. Stress dependent stiffness (logarithmic compression behaviour).
2. Distinction between primary loading and unloading-reloading.

3. Ageing of pre-consolidation stress.
4. Secondary (time dependent) compression.
5. Failure according to the Mohr-Coulomb failure criterion.

The parameters required when using the SSC model are listed in table 3.4.

Table 3.4: Input parameters of the soft soil creep material model [1]

Input	**Parameter**	**Unit**
Modified compression index	λ^*	$[-]$
Modified swelling index	κ^*	$[-]$
Modified creep index	μ^*	$[-]$
Effective cohesion	c'	$[kN/m^2]$
Friction angle	ϕ	$[°]$
Dilatancy angle	ψ	$[°]$
Tensile strength	σ_t	$[kN/m^2]$
Poisson's ratio unloading/reloading	ν_{ur}	$[-]$
Neutral lateral stress coefficient (NC)	$K_{0;nc}$	$[-]$
$K_{0;nc}$-parameter	M	$[-]$

The SSC model is neither using the elastic bulk modulus (K_{ur}) nor the elastic Young's modulus (E_{ur}) but is using the modified swelling index, (κ^*) instead. This index is used as input constant for computing the elastic strains. In the loading situating in which yield occurs, the plastic strains are governed by the modified compression index λ^*, which determines the compressibilty of the material in primary loading. The secondary time dependent compression is captured by the modified creep index μ^*. This parameter can be obtained by measuring long term volumetric strain development and plotting it over time. In figure 3.15 the relation between volumetric strain and mean stress is visualised.

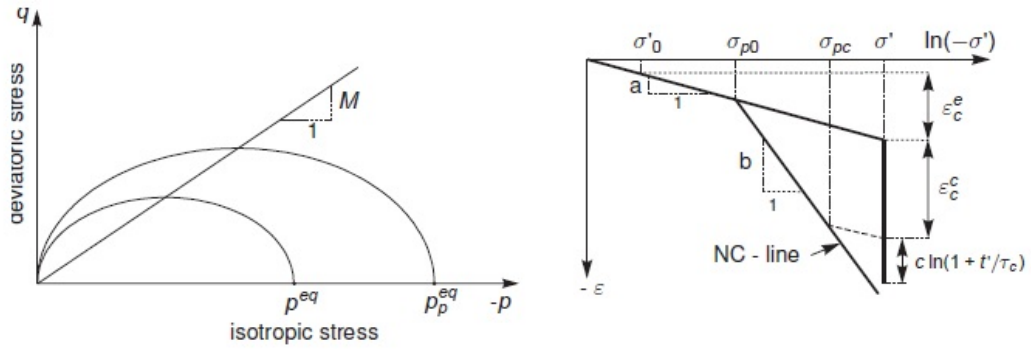

Figure 3.15: The Soft Soil Creep yield surface in principle stress space (c=0) (left); The logarithmic relation between volumetric strain and mean stress (right). In the right figure the strain development until the NC line is reached is governed by (*a*), which is κ^* parameter in the SSC model. The strain development at the moment the NC is reached is governed by (*b*), which is a combination of λ^* and μ^* in the SSC model. [1].

The soft soil creep model is applicable for modelling the behaviour of compressible soils. In contrast to the soft soil model, the soft soil creep model is capable of modelling secondary compression. The SSC model is sensitive to the OCR value, when a normally consolidated soil is analysed, an OCR value of 1.0 would lead to unrealistic large creep strain rates. Recommended is to use a value of OCR value in the order to 1.2-1.4 or even higher [1].

4

Analytical Modelling

The analytical models used to estimate the behaviour of the sandpiles is discussed in this chapter. The findings of the analytical approach are used for qualitative understanding of the behaviour of the sandpiles upon loading, used as verification of the finite element (FE) modelling results, as researched in chapter 5.

4.1. Introduction

The behaviour of sandpiles in soft soils is time dependent and non-linear. Therefore it is hard to capture the fully coupled behaviour with a single analytical model. In order to take all the different behavioural aspects into account, finite element (FE) software is needed. However, the results of the FE modelling can be inaccurate, even when the software is generating results. It is therefore important to understand the behaviour of the sandpile qualitatively, and knowing what magnitude to expect before using FE software. The use of analytical models is therefore necessary to obtain a first estimate of the results. In the following sections multiple analytical models are discussed for simulating the behaviour of sandpiles. Note that it is important to know the assumptions and limitations made in each model, therefore these have been listed in each section.

4.2. Unit cell definition

Most of the analytical models are considering an axisymmetrical problem in which both the sandpiles and the surrounding soil are modelled. The 2D representation is only taking half of the sandpile- and surrounding soil diameter into account, assuming that the problem is axisymmetrical around the y-axis. This representation in 2D is referred to as the unit cell, which will be used as geometry input for the analytical models. The horizontal displacements at the vertical boundaries of this unit cell are assumed to be zero, as the unit cell is mirrored over these boundaries. The forces acting at each side of the boundary are equal due to this mirroring, resulting in zero horizontal displacements. In figure 4.1 the unit cell as 3D representation of the sandpile reinforced soil is visualised. In figure 4.2 the axisymmetrical model is presented.

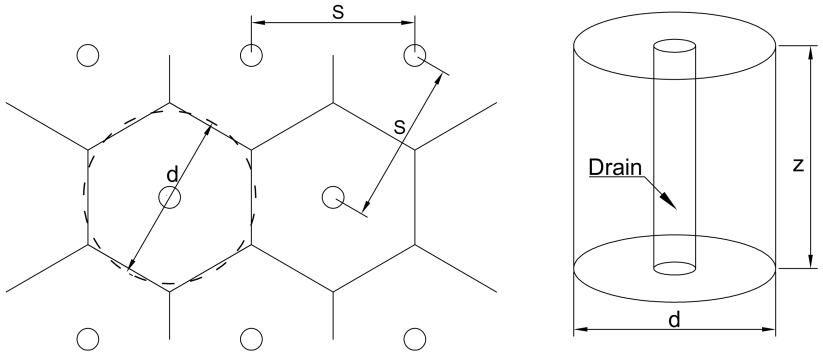

Figure 4.1: Transition from reinforced soil area (left) towards unit cell (right).

As can be observed in figure 4.1 the 3D unit cell has a depth (z) and a diameter (d). This depth is de-

pendent on the problem analysed, in this research the depth of the unit cell is 30.0m. The centre to centre distance between two piles (S) differs from the diameter of the unit cell (d), which is indicated by the dotted line in figure 4.1. The equivalent area of soil surrounding the sandpile is hexagonal shaped, but its closely approximated as an equivalent circle having the same total area. The equivalent circle for a triangular grid has a diameter of $d = 1.05 \cdot S$. For a square grid this diameter is $d = 1.13 \cdot S$ [10].

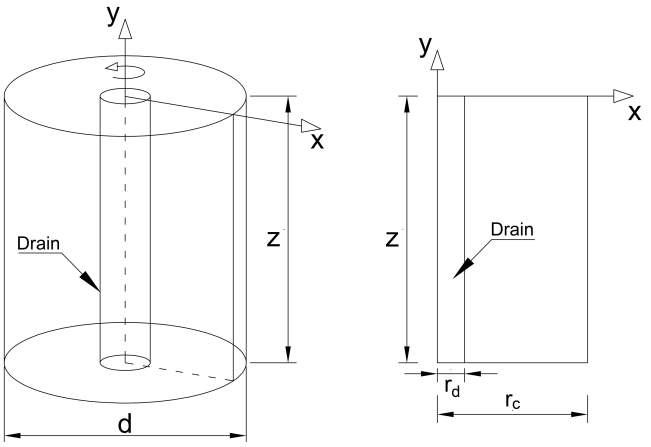

Figure 4.2: Representation of the unit cell in 3D (left) and axisymmetrical (right)

The groundwater table in the analytical models is positioned at the ground level, therefore all of the soil volume is fully saturated. The surcharge load applied on top is set to 60 kPa, a value based on the weight of 2 meters of light weight embankment material ($2 \cdot 12.5$ kPa) and 2 meters of surcharge load ($2 \cdot 18$ kPa). This loads are based on the unit weights of both the embankment and surcharge load above groundwater level.

The properties of the unit cell used in the analytical models are summarised in table 4.1. Furthermore it is assumed that the y_{min} boundary is fixed in horizontal and radial direction, the x_{min} and x_{max} boundaries are fixed in radial direction but can move upward or downwards. The x boundaries are impermeable, the water can only dissipate from the unit cell through the y_{min}- and y_{max} axis.

Table 4.1: Material properties of clay and sand used in the analytical approach

Description	**Parameter**	**Value**	**Unit**
Radius unit cell	r_c	1.58	[m]
Radius sandpile	r_d	0.20	[m]
Depth unit cell	z	30.0	[m]
Surcharge load	p_a	60.0	[kPa]

The material properties of the clay inside the unit cell have been selected from a representative clay layer at the NAICM site. The chosen layer is the FAS A layer, which has a thickness of 10.60 meter and is characterised by its high initial void ratio and large friction angle [2]. The material properties of the sand used for constructing the sandpiles in the trial are not researched in the TASANA reports, therefore the soil properties are chosen corresponding to a medium dense sand. The dilatancy angle (ψ') is set to 10 degrees, which is a high value. The latter is chosen in order to make the differences between the elastic- and elastic-plastic behaviour of the piles clearer (see section 4.5). The material properties of both clay and sand as used in the analytical approach are listed in table 4.2.

In table 4.2 the parameter γ is the wet unit weight, E' is the Young's modulus, $\nu'$the Poisson's ratio, e_0 the initial void ratio, ϕ' and ψ' the internal friction angle and the dilatancy angle, respectively, c is the cohesion, and k_r and k_v are the radial- and vertical hydraulic conductivity respectively.

The values of the clay properties in table 4.2 have been rounded off slightly. It is assumed that this will not affect the accuracy of the results of the analytical methods. The stiffness of the clay layer was not listed in the TASANA report, the Young's modulus (E) used is chosen based on the modulus of normal consolidated weak clay. Note that the horizontal hydraulic conductivity (k_h) is equal to the radial hydraulic conductivity (k_r) of the soil material when applying the axisymmetrical unit cell concept.

Table 4.2: Material properties of clay and sand used in the analytical approach

Material	γ [kN/m3]	**E'** [kPa]	ν' [-]	**e0** [-]	ϕ' [°]	ψ' [°]	**c** [kPa]	k_r [m/day]	k_v [m/day]
FAS A	12,10	3,000	0,30	7,9	37,00	0,00	0,00	2,23E-05	3,03E-04
Sand	18,00	30,000	0,33	0,5	30,00	10,0	0,00	10,00	10,00

4.3. Consolidation

The consolidation of the soft soil surrounding the pile is estimated with the help of the analytical model as presented by Barron, which takes the radial consolidation of the soil into account. In his derivation, Barron assumed that [4];

1. Water in saturated soil is incompressible and at the moment of loading, excess pore water pressure carries all the vertical loads;
2. Soil mass only deforms vertically;
3. Each drain well has a circular influence zone;
4. Loads distribute uniformly over the compressible soil zone.
5. The influence of vertical consolidation on the total consolidation process is neglected.

The analytical approach as presented by Barron can be found in chapter (3.2.3). In this chapter only the results of the analytical model are discussed. The properties of the unit cell and the soil parameters used in the model can be found in section 4.2. In figure 4.3 the average degree of consolidation is plotted over time. In the figure the vertical average degree of consolidation based on Terzaghi's 1D consolidation theorem and the average radial degree of consolidation based the Kjellman-Barron solution are plotted. Secondly, the combined average degree of consolidation of both the radial- (Kjellman-Barron) and vertical consolidation (Terzaghi), based on Carrilo's theorem [6][4].

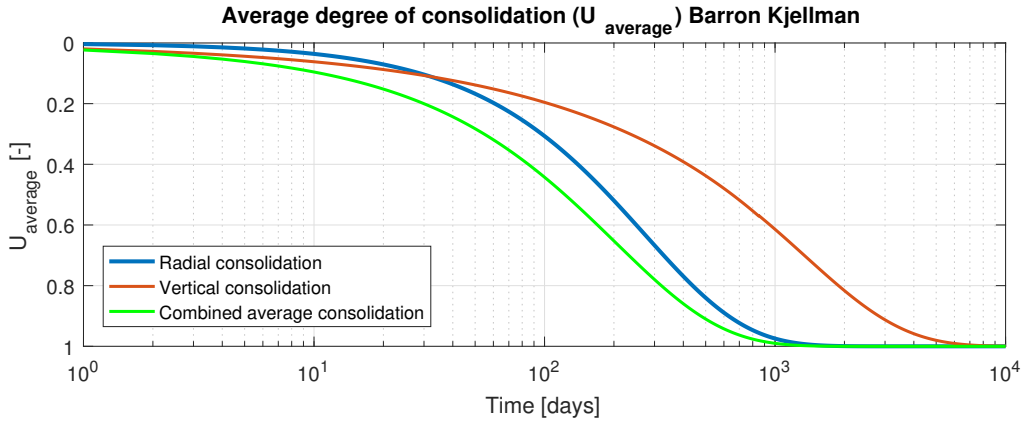

Figure 4.3: Plot of average degree of consolidation over depth in radial and vertical direction and combined, based on the theorem of Barron [4].

As can be observed in figure 4.3, the rate of consolidation in radial direction is relatively high compared with the vertical consolidation rate. This is according to the expectations as the flow path in which the pore water can dissipate is much smaller in radial direction than in vertical direction. For further analysis the vertical rate of consolidation, contributing to the total consolidation, is neglected.

4.4. Effects column stiffness on deformations

The effects of differences in stiffness between the sand column and the surrounding soft soils is researched by Alamgir et al. [3]. The analytical model proposed is using the deformation properties of both the column

and the soil for analysing the vertical (settlement) behaviour of the unit cell. The interaction between the shear stresses at the interface between the column and surrounding soil are accounting for the stress transfer between the column and soil. The model of Alamgir is described in more detail in section 3.4.2. The analytical model is based upon the following assumptions:

1. The vertical deformations of the column and soil are only depending on the stiffness parameters, effects of consolidation is not taken into account.
2. Vertical deformations of the column tip are zero; the columns are end-bearing.
3. The deformation behaviour is not time dependent, only the total displacements can be simulated with this approach.
4. Only shear stresses along the shaft of the piles are taken into consideration.
5. The column and soil are both behaving elastic.
6. There are no horizontal deformations.
7. The stresses acting on the column and soil are constant.

The analytical model only uses the Young's modulus (E) and the Poisson's ratio (ν) of both the column and soil into account. Since the behaviour is elastic and assuming that no slip occurs at the column/soil interface, the settlements of the column and soil at the interface are equal.

4.4.1. Effects stiffness difference on settlements

The effects of installing the stiffer sand columns in the soft soil is analysed by modelling the unit cell, with the geometry and parameters as described in section 4.2. The result of the analytical model is visualised in figure 4.4, in which the settlement at different depths z are plotted against the ratio of radii of the sandpile (r_d) and unit cell (r_c).

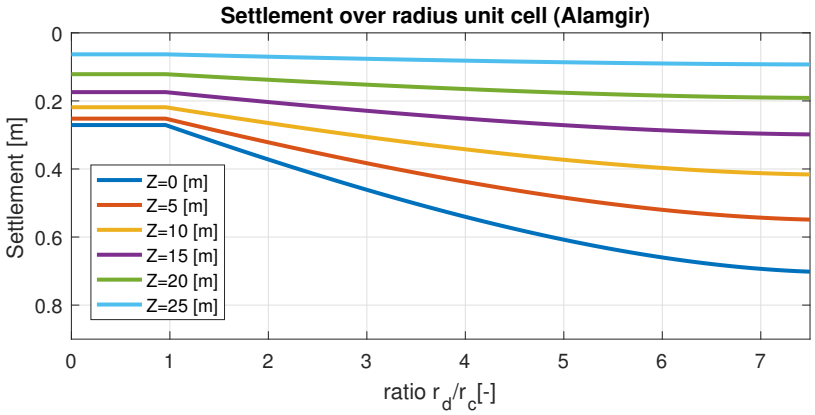

Figure 4.4: Plot of settlement versus radius unit cell, based on the simplified approach of Alamgir [3].

The plot in figure 4.4 shows that the settlement in the first 0.20 meter of the unit cell radius is constant. This makes sense as this is equal to the column radius in which the stiffness is constant and the material is assumed to deform only vertically. Starting from 0.20 meter the unit cell radius the settlement increases until the unit cell boundary, which represents the settlement of the clay material. The stiffness of the column is influences the settlement behaviour of the surrounding soil, near the column the settlements of the clay are reduced via transfer of shear stresses towards the stiffer column. The transfer of stresses reduces as the radius from the clay towards the column increases. From the simplified settlement analysis as formulated by Alamgir [3] it can be concluded that the expected effect of the installation of sandpiles is the stiffening of the sandpile and soft soil composite in the direct surrounding of the pile. This effect will reduce as the radius towards the pile increases. Note that this model is based on a list of assumptions and the magnitude of the results are not likely to be accurate. This analysis is therefore used for qualifying the phenomenon rather than quantifying it.

4.5. Effects of column deformations on soil behaviour

In this section the influence of column deformation on the consolidation behaviour is researched. The analytical approach used is presented by Castro and Segaseta [7], and is primarily used for analysing the behaviour of stone columns. Considering the used parameters in the model and the similarities in material behaviour, it is assumed that the model is applicable for sandpiles as well. In this chapter only the results of the model are discussed, the model itself is explained in more detail in section 3.4.3.

Before presenting the results of the analytical model, the assumptions made are listed. Note that the assumptions made enable the model to simulate the behaviour, but the simulated behaviour is only an approximation of the actual behaviour [7].

1. The soil is fully saturated.
2. Vertical deformations of the column tip are zero; the columns are end-bearing.
3. The load applied on top of the unit cell is constant over time.
4. The water and soil particles are incompressible; i.e. the change in volume is only due to the leak of water.
5. Darcy's law is obeyed.
6. The soil vertical strain, (ϵ_{zs}), and stress (σ'_{zs}) are uniform in any horizontal plane.
7. The average total vertical stress in the soil is constant with time, but different from the applied load.
8. Shear stresses at the column/soil interface are ignored.

The model is primarily used to calculate the stress increments over time in the column and the surrounding soil. These increments are fully elastic- or elastic-plastic depending on the ratio between the natural effective stress at a given depth and the effective stress increment due to the surcharge load and consolidation over time. With the calculated stress increments over time the expected settlement of the column and soil can be determined.

4.5.1. Effect of yielding on consolidation

The coefficient of consolidation in radial direction (c_{vr}) is updated according to either the elastic (c_{vr}^{zre}) or elastic-plastic (c_{vr}^{zrp}) behaviour of the column [7]. As explained in section 3.4.3, it is expected that the coefficient of consolidation lowers after the moment of yield and therefore the consolidation rate decreases. The average degree of consolidation (U) is plotted over the time for both elastic and elastic-plastic material behaviour in figure 4.5.

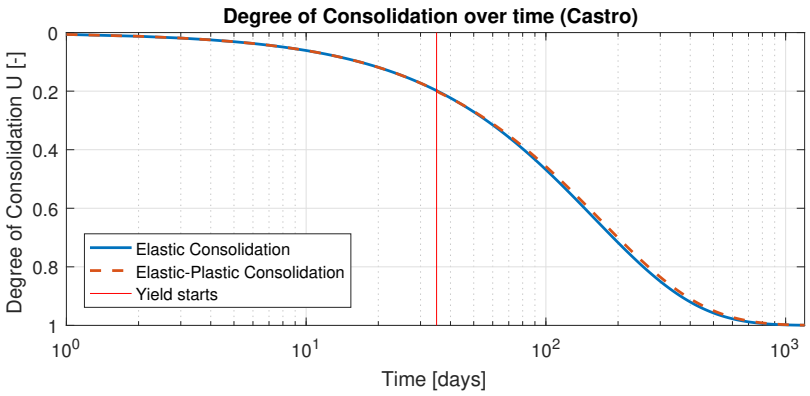

Figure 4.5: Plot of average degree of consolidation (U) versus time, based on the analytical approach of Castro et al. [7].

In figure 4.5 it can be observed that after the moment of yielding, the consolidation rate is indeed lowered and the curve reduces in steepness. However, the magnitude of this effect is negligible for the situation presented in this graph.

4.5.2. Effect of yielding on radial deformations

The deformations of both sandpile and surrounding clay in radial direction have been analysed for both the elastic phase and the elastic-plastic phase. Since the sandpile is subjected to higher vertical stresses compared with the surrounding soft soil, the radial stresses in the column are also higher. This difference in stresses will force the interface between the sandpile and soil to deform in radial direction. The biggest deformation is expected to occur at this interface, as the axisymmetrical model is not allowing radial deformations at the boundaries. The radial deformations for different radii, modelled based on the approach of Castro et al., are plotted in figure 4.6.

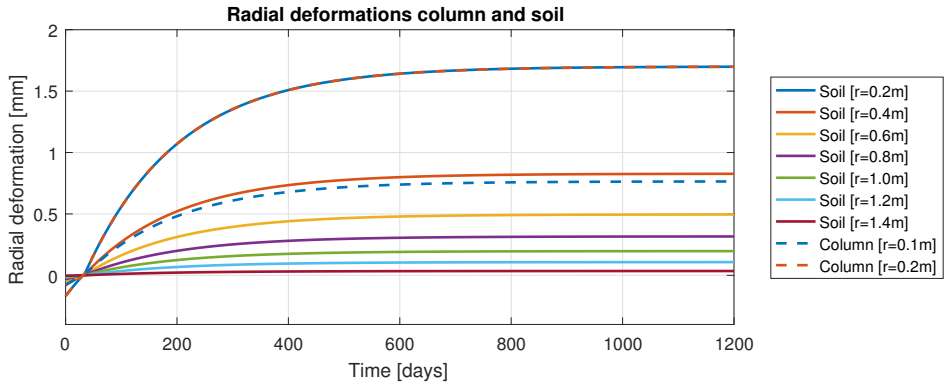

Figure 4.6: Plot of the radial deformations at different radii over time, based on the analytical approach of Castro et al. [7].

The deformations are as expected increasing when the interface between the sandpile and soft soil is approached, and reaches a maximum at the interface ($r = 0.2m$). The plot also indicates the increase in radial deformation after yielding. This increase makes sense, as the material in an elastic-plastic phase tends to deform more compared to pure elastic deformations.

4.5.3. Effect of yielding on effective stresses

Next to the deformations and consolidation rate, the vertical and horizontal deformations of the column and soil are researched. In figure 4.7 the vertical and radial effective stresses in the column and soil are plotted over the time. The moment of yielding, in which the behaviour transits from elastic to elastic-plastic, is indicated with the red line (t=36 days).

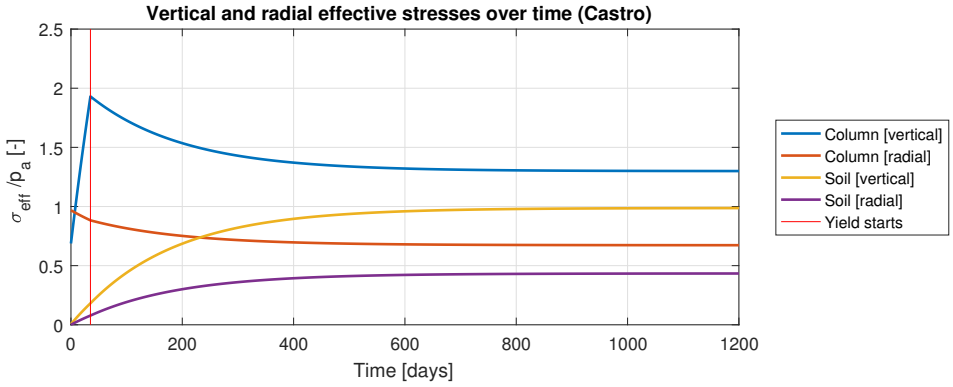

Figure 4.7: Plot of effective stresses in column and soil before and after yielding over time, based on the analytical approach of Castro et al. [7].

As can be observed from the figure above is the effective stress in the column decreasing after the transition between elastic and elastic-plastic behaviour, which is according to the expectation. The influence of the plastic deformation makes the column softer, thus reducing its capacity to carry loads.

4.6. Floating piles versus end bearing piles

The sandpiles as constructed at the NAICM trial embankment are not connected to the silty sand layer underlaying the top soft clay layers. The end of the sandpiles are positioned 3 meter above the sandy silt layer, as explained in section 2.4.4. The piles are therefore 'floating' in the clay layer. In order to estimate the effect of this floating of the sandpiles on the consolidation of the whole unit cell, two alternatives have been researched. The first alternative considers the floating piles, in which the unit cell has been divided into two blocks. Block 1 has a height of 27 meters and is representing the soft soil reinforced with sandpiles, block 2 has a height of 3 meters and is located below block1, representing the natural soft soil. The analysis performed in this section is used for estimating the change in settlements rate by the change in loading scenarios, in which the amount of stress transferred directly from block 1 towards block 2 is varied. The configuration of the blocks is visualised in figure 4.8.

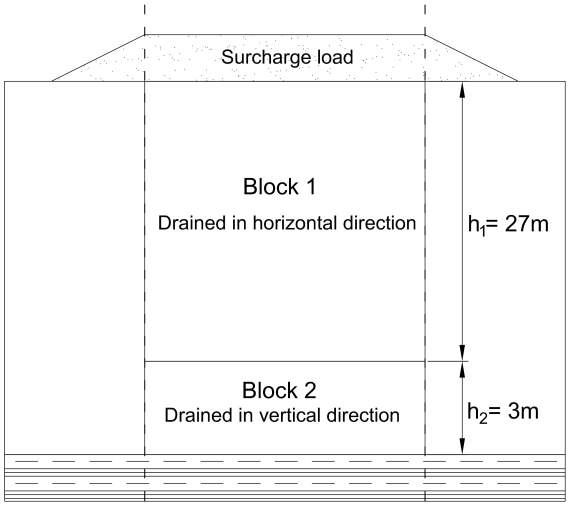

Figure 4.8: Visualisation of alternative 1, with block 1 representing the soil layer improved with sandpiles and block 2 the natural soil layer. Alternative 2 only considers block 1 over the depth of the unit cell.

The second scenario is when the piles are attached to the silty sand layer positioned underneath the clay layers. Hence, the total depth of the unit cell consists of Block 1.

In order to simulate the consolidation of the soft soil reinforced with floating piles, the following assumptions have been made;

1. Block 1 only considers consolidation in radial direction.
2. Block 2 only considers two sided consolidation in vertical direction.
3. The load active on block 2 is equal to the surcharge load on top of the unit cell.
4. The influence of the sandpile stiffness on the settlements is not taken into account.

The rate of consolidation of both blocks is equal to the rates of consolidation visualised in figure 4.3, in which the vertical- and radial (Barron) consolidation curves correspond with Block 2 and Block 1, respectively.

4.6.1. Change in settlement

The settlements over time have been plotted for both alternatives and for multiple loading scenarios. The B1 in the plot represents the percentage of surcharge load carried by block 1, i.e. the percentage of load not directly transferred to block 2 by the sandpiles.

As can be observed in figure 4.9 the amount of settlement for the end-bearing piles is less than the alternative of the floating piles. This reduction in settlement is explained by the load transfer of the sandpiles towards the stiffer soil layers. In case of end-bearing piles the load is (partly) transferred towards the stiff layer, hence reducing the load carried by the soft clay layers. In case of a floating pile, the soft clay layer positioned underneath the pile will always be subjected to a load equal to the applied load on top of the soil.

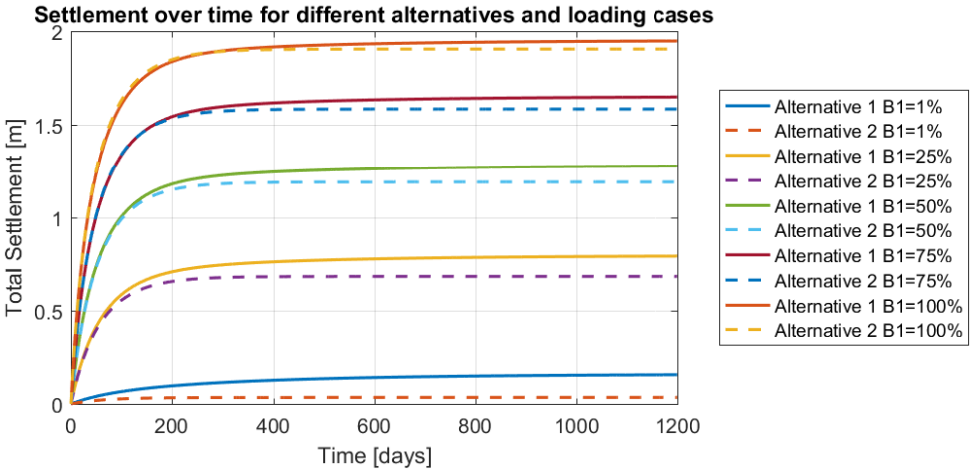

Figure 4.9: Plot of settlements versus time, plotted for floating piles (alternative 1) and end-bearing piles (alternative 2). The different loading scenarios are plotted for each alternative, B1 is the percentage of load carried by block 1.

Because of this, the settlements in case of a floating pile are assumed to be larger than the alternative with the end-bearing piles.

Secondly, when looking at the different loading scenarios it can be observed that the differences between both alternatives are becoming less significant when the load carried by the clay layers increases. When almost all the load is carried by the top block the calculated settlements are almost equal. Therefore it can be concluded that when the sandpile becomes stiffer and transfers more load from the top soil towards the deeper stiff layers, the end-bearing piles result is significantly less settlement compared to the floating piles.

5

Numerical Modelling

In this chapter the development of the numerical model is presented. The software used for creating the numerical model is the Finite Element (FE) software Plaxis 2D. The model type used for this analysis is the axisymmetric model, which can be compared with the unit cell approach used in the analytical models in chapter 4. At the end of this chapter a numerical model is presented capable of simulating the behaviour of the sandpile. This model will be verified in chapter 6.

5.1. Introduction

In the previous chapter the behaviour of sandpiles in soft soils has been investigated by using analytical formulas. These formulas provide a first estimate of the expected behaviour of the piles, but each of the analytical solutions is based on a list of assumptions. Hence, the obtained results are based on simplifications and are not accurate enough as a starting point for an actual design.

In this chapter the sandpiles will be modelled in the FE software Plaxis 2D, in an axisymmetric model set-up. The same model dimensions as the unit cell described in section 4.2 are used. The first FE model is based upon the soil layer and material properties as used in the unit cell in chapter 4. The material model used for the soil and sandpile in the first model is the Mohr-Coulomb model, described in section 3.6.1. The results of this first model are validated with the results of the analytical models.

The second model (Model 2) uses advanced material models for simulating the sandpile- and soil behaviour. The material model used for simulating the sandpile- and soil behaviour are the hardening soil model and the soft soil creep model, respectively. Secondly, the sandpile is shortened from being end-bearing towards an configuration in which the sandpile 'floats' 3 meter above the bottom of the unit cell.

The third and final model incorporates the soil layers and material properties conform the design report of TASANA [34]. The geometry and material properties of the soil layers are obtained from the trial embankment at the NAICM site, as described in section 2.3.2. The performance of the sandpile is then being analysed, with respect to the improved consolidation rate and increase in soil stiffness. In chapter 6 the final numerical model is adjusted to fit the monitored behaviour of the trial embankments at the NAICM site.

5.2. Model set-up

The selected model type used in Plaxis 2D for simulating the behaviour of the sandpile is the axisymmetrical model, which is introduced in section 5.2.1. In section 5.2.2 the mesh size used in the analysis is presented. The different stages in developing the axisymmetric model are discussed in section 5.2.3.

5.2.1. Axisymmetric modelling

The type of model used in the numerical analysis is the axisymmetric model type of Plaxis 2D. This model resembles the principle of the unit cell, a radial cross section of the cell is modelled as a 2D model. In the simulations of Plaxis 2D this cross section is being rotated along the y-axis to represent the (uniform) soil around the y-axis. The deformations and stress states are assumed to be identical in any radial direction [1]. In figure 5.1 the concept of the axisymmetrical model is visualised.

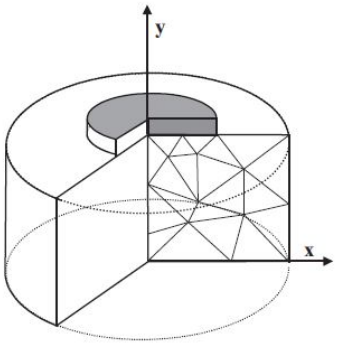

Figure 5.1: Visualisation of the concept of axisymmetry [1].

5.2.2. Mesh sizes

The soil and sandpile in the Plaxis model are discretized by a mesh, which divides the materials into multiple triangular elements. These elements contain several nodes (6 or 15) in which the deformations and stress states are updated. A mesh with more elements will result in more nodes and therefore more calculations. Therefore, a finer mesh with smaller elements can be used to get more accurate results of the simulation. The downside of generating more elements is the increase in calculation time. In the numerical simulations of the sandpile and surrounding soil the mesh size selected is very fine. The mesh obtained by selecting this mesh size is visualised in figure 5.2.

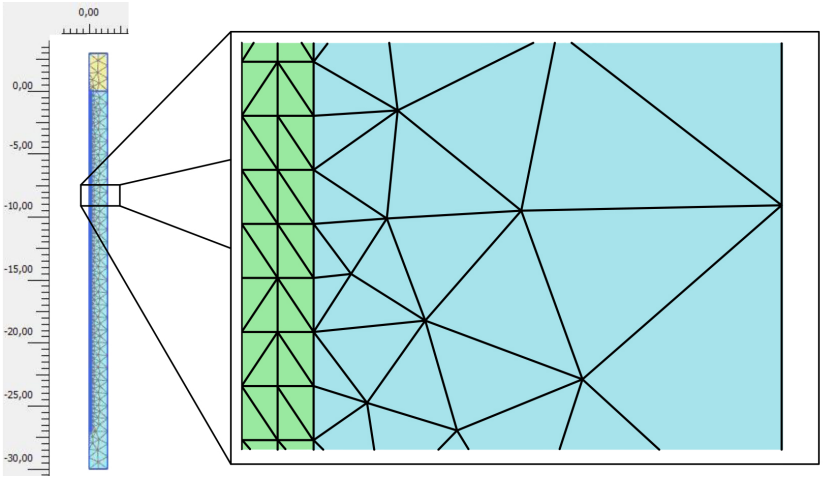

Figure 5.2: Mesh generated by Plaxis 2D in the axisymmetric model, mesh size setting very fine. In green the material inside the sandpile is presented, in blue the material of the surrounding soft soil.

The mesh of the unit cell is only partially presented in figure 5.2 because of the large dimensions of the cross section. Note that the mesh sizes are smaller inside the sandpile and the direct adjacent soil, and increase in size when the distance to the sandpile increases. The mesh in the model is rotated along the y-axis, which is located at the left boundary of the sandpile.

5.2.3. Model stages

The build up of the numerical model is performed in stages. The reasoning for this is that the output of the numerical model is first compared with the results of the analytical models. By comparing these results the simulated behaviour can be verified. The model is then adjusted step-wise, verifying the changes in the results for each adjustment. The different model staged used in this research are listed in table 5.1.

Table 5.1 shows that there are three main model phases distinguished, each phase increasing the accuracy in which the model approaches the real behaviour. The last model is a geometry similar to the subsoil at the NAICM site, based on the report of TASANA [34]. The geometry and material properties of the soil presented in this report are based on field- and laboratory tests.

Table 5.1: Description of the model stages distinguished during the numerical model analysis.

Model name	Material model	Geometry unit cell
Model 1	Mohr-Coulomb	Analytical model
Model 2	Hardening Soil & Soft Soil Creep	Analytical & floating pile
Model 3	Hardening Soil & Soft Soil Creep	TASANA design report*

**Geometry is based on the design report of TASANA [34].*

5.3. Model 1: Basic material model

The first FE model in the numerical analysis uses the Mohr-Coulomb (MC) material model, which is described in more detail in section 3.6.1. In this section the properties of the model are presented and the results of the model are discussed.

5.3.1. Model properties

The geometry of the first Plaxis 2D model is conform the unit cell used in the analytical approach (section 4.2). The soft soils surrounding the sandpile are simplified as an uniform clay layer with material properties equal to those used in the analytical models. The embankment on top of the unit cell is modelled as a line load and the groundwater table is located at the top of the unit cell. The properties of the unit cell are listed in table 5.2.

Table 5.2: Dimensions of unit cell and applied load on top of the cell.

Description	Parameter	Value	Unit
Radius unit cell	r_c	1.58	[m]
Radius sandpile	r_d	0.20	[m]
Depth unit cell	z	30.0	[m]
Surcharge load	p_a	60.0	[kPa]

The dimensions of the unit cell as listed in table 5.2 remain constant for the first numerical models. In the models multiple calculation phases have been implemented in order to accurately simulate the sandpile behaviour. The phases are required for calculating the right in-situ stresses, installing the sandpile, applying the right loads and simulating the consolidation behaviour. The different loading phases implemented in the numerical models are listed in table 5.3.

Table 5.3: Material properties of clay and sand used in Plaxis 2D model 1

Phase	Calculation type	Loading type	Description
Initial phase	K_0 procedure	Staged construction	Initial stage
Phase 1	Plastic	Staged construction	Installation of sandpile
Phase 2	Plastic	Staged construction	Apply line loads on top of unit cell
Phase 3	Consolidation	Degree of consolidation	Consolidation analysis

As presented in table 5.3, phase 1 and phase 2 are both plastic calculation types with a staged construction as loading type. During the initial phase the stresses in the natural soil are calculated. The sandpiles installed during phase 1 are then modelled. Note that the pile is 'wished in place', the installation effects including the disturbance of the soil caused by the installation are not simulated. When the sandpile is installed the load of 60 kPa is applied on top of the cell. In the consolidation phase the loaded cell is consolidated until the degree of consolidation reaches 99%.

The Mohr-Coulomb material properties of the different soils in the first model are listed in table 5.4. Note that the value of each material property is equal to that used in the analytical approach (section 4.2).

In table 5.4 the volumetric weight is denoted by γ_{sat}; E' is the Young's modulus, ν' the Poisson's ratio; e_0

Table 5.4: Material properties of clay and sand used in Plaxis 2D model 1.

Material	**Model**	γ_{sat} [kN/m3]	**E'** [kPa]	ν' [-]	e_0 [-]	ϕ' [°]	ψ' [°]	**c** [kPa]	k_r [m/day]	k_v [m/day]
FAS A	MC	14.00	3.000	0.30	7.9	37.00	0.00	0.00	2.23E-05	3.03E-06
Sand	MC	18.00	30.000	0.33	0.5	30.00	10.0	0.00	10.00	10.00

the initial void ratio; ϕ' and ψ' the friction angle and the dilatancy angle, respectively; c is the cohesion and k_r and k_v the radial and vertical hydraulic conductivity of the soil, respectively.

5.3.2. Comparison analytical and numerical calculations

The first numerical model is verified by comparing the results with the results of the analytical models. The simplifications and assumptions made in the analytical models are expected to result in some deviations from the results of the numerical model. However, the results of the analytical models present a first indication in expected behaviour of the sandpile, and will therefore be used to verify the numerical model.

Consolidation (Kjellman-Barron)

The consolidation as calculated with the analytical approach of Kjellman-Barron (section 4.3) is plotted together with the consolidation as simulated by Plaxis 2D over time, as visualised in figure 5.3.

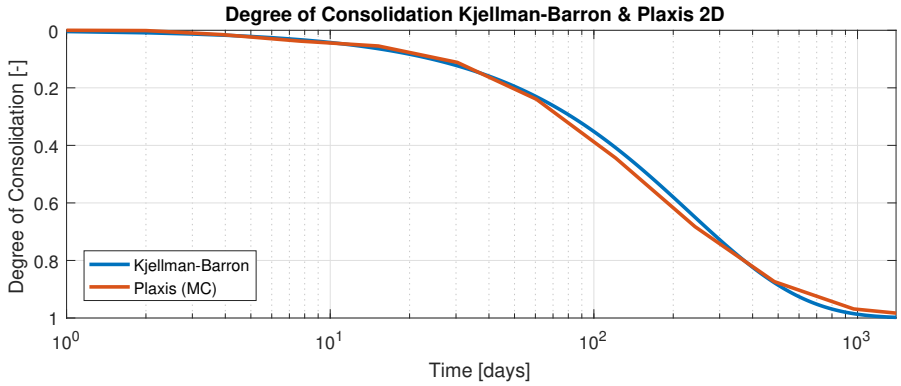

Figure 5.3: Consolidation over time of analytical (Kjellman-Barron) and numerical (Plaxis 2D) models.

As can be observed in the figure above, there are small deviations of the Plaxis MC model compared with the Kjellman-Barron solution. The differences are relative small and are caused by the limited time steps taken in the Plaxis 2D simulation. The curves however show that the numerical model is providing a close fit to the analytical solution, therefore it is assumed that the numerical model is presenting accurate results regarding the consolidation rate.

Settlements over radius (Alamgir)

The settlements over the radius are estimated by using the analytical approach as presented by Alamgir et al. [3] and by a simulation using the Plaxis 2D software. The results of both models are plotted in figure 5.4.

As can be observed in figure 5.4 there is a difference in the settlement behaviour between the analytical and numerical model. The analytical approach is showing an increase in settlements starting from the radius of the sandpile towards the boundary of the unit cell. In the numerical simulation, this behaviour is not observed. This difference in behaviour may be caused by two assumptions made in the analytical model.

The first assumption is that the settlement at the boundary of the unit cell obtained with the Alamgir model is based on the maximum elastic deformation of the unimproved clay upon loading. This implies that the settlement at the border of the unit cell only depends on the stiffness of the clay, not on the distance to the sandpile. In the Plaxis 2D model the settlement at the boundary is dependent on the distance from the stiffer pile. Hence the soil at the border of the unit cell might be stiffer due to the presence of the sandpile, compared to the stiffness estimated with the Alamgir model.

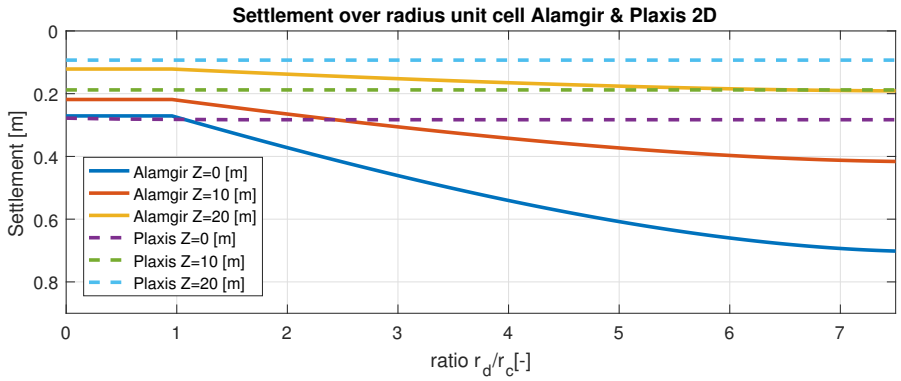

Figure 5.4: Consolidation over time of analytical (Alamgir) and numerical (Plaxis 2D) models.

Besides the fixed deformation at the boundary of the unit cell, the model of Alamgir is only considering vertical deformations. As was described in section 4.5, the horizontal deformation of the pile generates a lower stiffness ratio between the sandpile and the surrounding soft soil. By assuming that the sandpile is fixed in horizontal direction the stiffness ratio between the sandpile and soil remains very high. This results in a larger difference in settlement between the two material bodies.

Consolidation (Castro)

In the consolidation analysis described in the analytical approach of Castro et al. [7], the stiffness of both the sandpile and the surrounding soft soil are influencing the consolidation rate. In figure 5.5 the consolidation over time of both the method by Castro and the simulation by Plaxis 2D are presented.

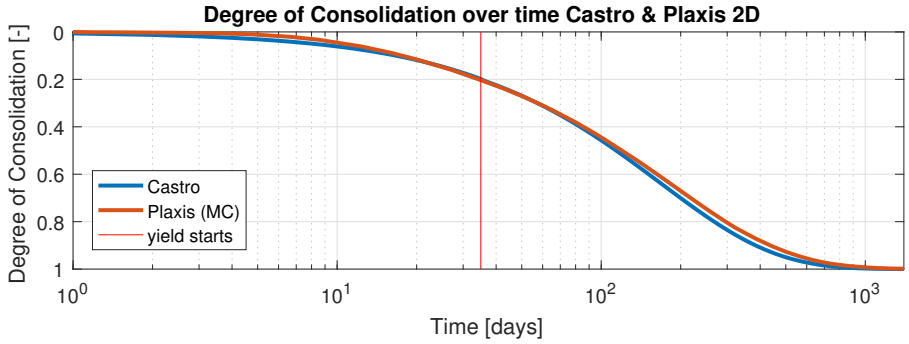

Figure 5.5: Consolidation over time of analytical (Castro) and numerical (Plaxis 2D) models.

As can be observed in figure 5.5, there is a slight difference in consolidation rate between the two models. The model based on Castro is slightly under-estimating the rate of consolidation, compared to the consolidation rate simulated with the Plaxis 2D model. Since the models show a close fit it is assumed that the numerical model is simulating the correct behaviour of the unit cell.

Effective stresses over time (Castro)

The effective stresses on both the sandpile and surrounding soil are obtained by the Plaxis 2D simulation, plotted against those obtained by the analytical solution by Castro et al. [7]. The results are presented in figure 5.6.

As can be observed in figure 5.6, the development of the effective stresses over time as modelled with the Plaxis 2D software are similar to those obtained by the analytical solution. The vertical effective stresses in the column are increasing rapidly until yield occurs, after which the effective stress decreases. The shape of these curves, of both analytical and numerical solution, shows a sharp turn at the time of yielding. This yield is obtained roughly at the same time in both models. However, the magnitude of the final vertical effective stress are different. The numerical model shows less deterioration of effective vertical stress after yielding, compared with the analytical model. The other stress curves of both methods are not far apart and are there-

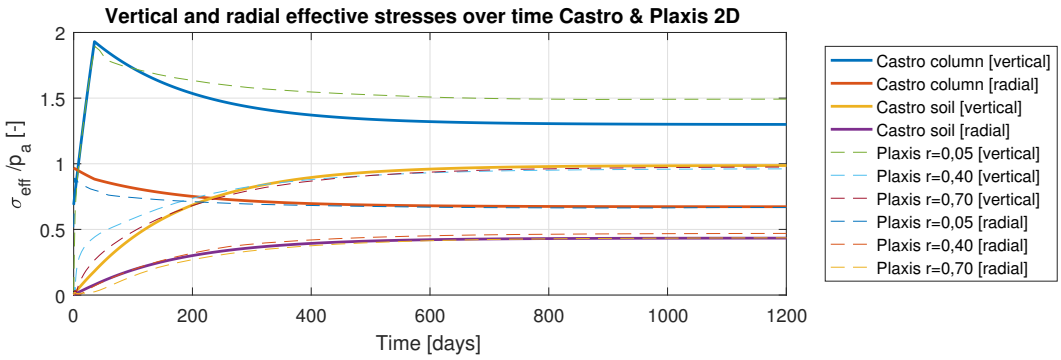

Figure 5.6: Effective stresses over time of analytical (Castro) and numerical (Plaxis 2D) models.

fore assumed to be modelled correctly. The obtained results of the effective stresses over time indicated the importance of yield in the behaviour of the sandpile.

Radial deformations (Castro)

The radial deformations in both the sandpile and the surrounding soft soil are calculated with the analytical approach by Castro et al. [7] and simulated with a numerical model in Plaxis 2D. The results of both models are presented in figure 5.7.

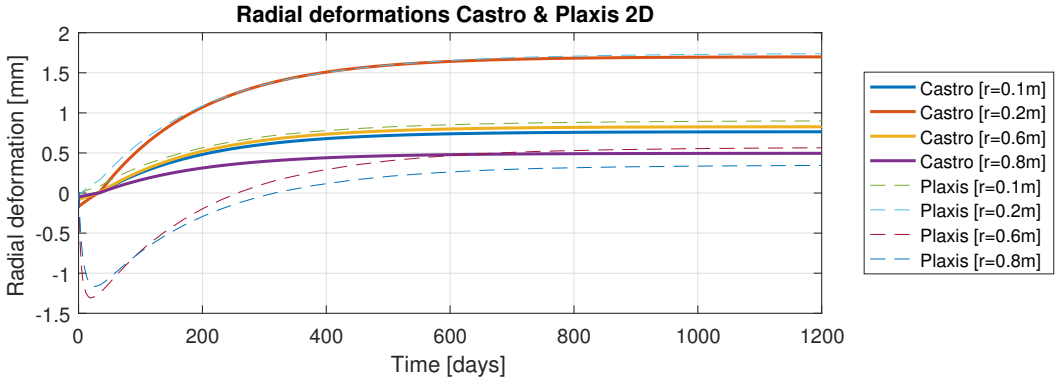

Figure 5.7: Radial deformations over time of analytical (Castro) and numerical (Plaxis 2D) models.

As can be observed in the figure above is the progress of radial deformation within the sandpile ($r = 0.1m$ and $r = 0.2m$) for both models similar. However, the radial deformations in the clay simulated with Plaxis 2D show a different trend. In the first days the clay is rapidly moving towards the sandpile, after which the clay is moving in the opposite direction for the remaining time. This effect is explained by the difference in material response of the sand and the clay. At the early time steps the sandpile is drained while the clay has an undrained response. Upon loading the response of the clay is undrained and deformation is only possible in the direction of the sandpile, as the other boundaries (x_{max} and y_{min}) are fixed. At the first time steps the clay therefore compresses the sandpile and during consolidation the sandpile is pushing the clay in the positive radial direction. The inward movement is therefore a numerical error in the Plaxis 2D model. In reality this behaviour will not occur.

5.4. Model 2: Advanced material models

The second stage in the numerical modelling is the implementation of advanced material models. The advanced material models used for simulating the behaviour of the sandpile and surrounding soft clay are the hardening soil (HS) model and the soft soil creep (SSC) model, respectively. The updated material properties of both the sandpile and the clay are listed in table 5.5. The values in this table are based upon the values as presented in the TASANA report [34]. The characteristic of the advanced material models are explained in section 3.6.2 and 3.6.3.

Table 5.5: General material properties of clay and sand used in Plaxis 2D model 3.

Material	**Model**	$\gamma_{unsat}/\gamma_{sat}$ [kN/m3]	ν' [-]	**e0** [-]	ϕ' [°]	ψ' [°]	**c** kPa	k_r [m/day]	k_v [m/day]	c_k [-]
FAS A	SSC	12.1/12.1	0.30	7.6	34.00	0.00	0.10	2.27E-04	2.27E-04	2.270
Sandpile	HS	17.0/19.0	0.33	0.5	33.00	3.00	0.10	7.69	7.69	1E15

What can be observed in table 5.6 is a value for POP (pre-overburden pressure) assigned to the sandpile, which takes account for the history of previous loading [25]. This prevents all points in the material to start on the yield surface, causing direct yielding upon loading. Furthermore the cohesion is increased from 0.00 to 0.10, which is a minimum required for modelling with the SS and HS models. The c_k parameter governs the change of permeability of the soil during consolidation, as explained in section 3.2.4. In table 5.6 the values of the material model specific properties are listed, for both the HS model and the SSC model,

Table 5.6: Material model specific properties of clay and sand used in Plaxis 2D model 3.

Material	**Model**	**OCR** [-]	**POP** [kPa]	E_{50}^{ref} [kPa]	E_{50}^{oed} [kPa]	E_{ur}^{ref} [kPa]	m [-]	λ^* [-]	κ^* [-]	μ^* [-]
FAS A	SSC	1.767	-	-	-	-	-	0.2963	0.03155	0.01264
Sand	HS	-	10	30.0E3	30.0E3	90.0E3	0.5	-	-	-

in which the OCR and the POP are the over-consolidation ratio and the pre-overburden pressure, respectively; the E_{50}^{ref}, E_{50}^{oed} and the E_{ur}^{ref} are the secant stiffness, unloading/reloading stiffness and the tangent stiffness modulus, respectively; m is the power law governing the stress dependency of the stiffness; and λ^*, κ^* and μ^* are the modified indices of compression, swelling and creep, respectively. The parameters listed in the table above for both the FAS A layer and the sandpile are elaborated in section 3.6.3 and section 3.6.2, respectively.

5.4.1. Change in sandpile behaviour

In this section the simulations of the model using the advanced material models (Model 2) are compared with the obtained results simulated with the model using the Mohr-Coulomb (MC) model (Model 1). The changes in consolidation rate, deformations and stresses are discussed.

Consolidation rate

The rate of consolidation in the soft soil simulated with Model 1 (Mohr-Coulomb) and Model 2 (HS & SSC) are plotted in figure 5.8.

When comparing the consolidation rates of both Model 1 and Model 2, some deviations can be observed. First, the increase in consolidation rate when using the advanced soil models. This is caused by the use of the over-consolidation ratio (OCR). The Mohr-Coulomb model is assuming a single stiffness of the soil material, captured in the Young's modulus (E'). In the Soft Soil Creep model the stiffness is dependent on the effective stress and strain rate. When the stress in the soil is lower than the NC pressure, the soil material has a relative high stiffness, governed by the modified swelling index (κ^*). After the NC yield stress has been reached, the stiffness is governed by the modified compression index (λ^*). The stiffness of the material is relative low during this virgin compression of the soil.

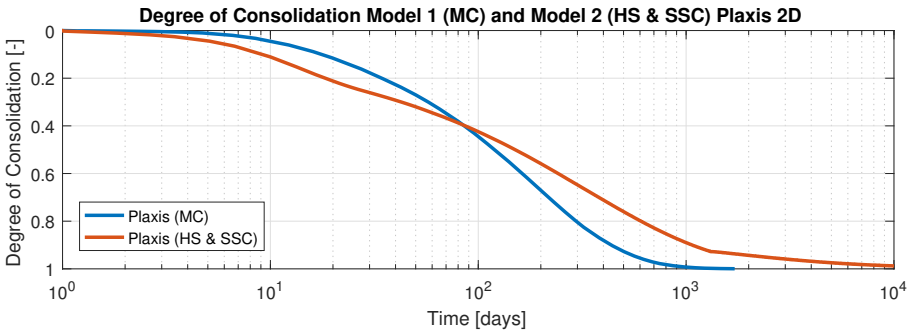

Figure 5.8: Consolidation rates Model 1 (MC) and Model 2 (HS & SSC).

Secondly, Model 2 shows a bend in the consolidation graph when the degree of consolidation is around 0.90. When this degree of consolidation is reached, the rate in which the soil consolidates is reduced. This reduced rate is caused by the generation of excess pore water pressure by the creep of the soft soil material. When the modified creep index is lowered, the excess pore water pressures generated by creep are reduced and this bend in the graph shifts over time. When creep is not considered, this bend in the graph is not observed.

The advanced material models incorporate the change of permeability during consolidation. During consolidation the voids between the solids in the soil material reduces, lowering the permeability of the material. The change in permeability during consolidation is captured in the c_k parameter (table 5.5). The MC model uses a constant permeability in the different soil materials, hence the consolidation rate in soft soil layers is higher in Model 1 than in Model 2.

Radial deformations

The radial deformations simulated with both Model 1 (MC) and Model 2 (HS & SSC) are compared with another in figure 5.9.

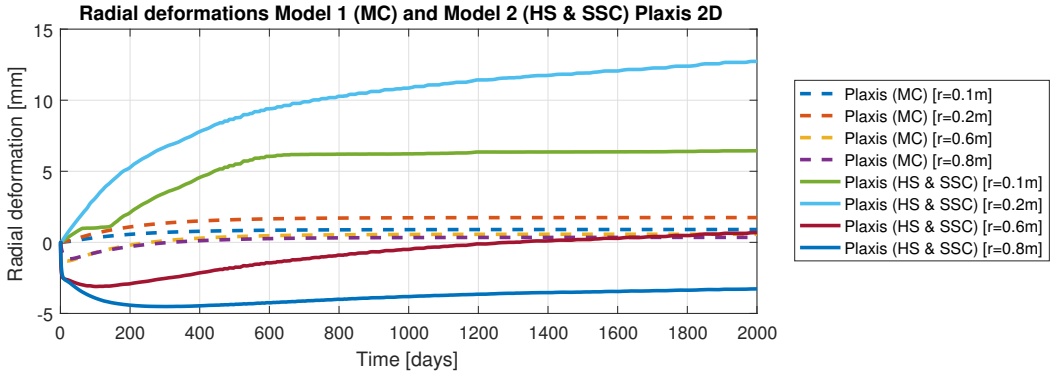

Figure 5.9: Radial deformations Model 1 (MC) and Model 2 (HS & SSC).

As can be observed in figure 5.9, there is a large difference in the magnitude of radial deformations between Model 1 (MC) and Model 2 (HS & SSC). This difference in magnitude is caused by differences in stiffness between the soft soil layers in both models. The MC model uses a constant stiffness governed by the Young's modulus (E'), while the advanced model use a stress dependent stiffness. The relation between the stress and stiffness is logarithmic in the advanced models and therefore hard to compare with the constant stiffness used in the MC model.

However, the trend observed in both simulations are similar. The sandpile starts to deform in radial direction upon loading, at the border of the pile roughly twice as much as at half of the pile radius. The clay soil moves towards the sandpile at the beginning of the loading. This is similar to the behaviour observed for clayey soil in Model 1. Over time the soil moves back in the positive direction of the pile. In section 5.3.2 this behaviour is explained in more detail. The radial deformation of both the sandpile and the surrounding soil is still ongoing after t=1200 days in Model 2, unlike the plots obtained with Model 1. The long term

deformations of the pile are governed by the modified creep index. When creep is not considered, the radial deformations reach an equilibrium after consolidation.

Effective stress development

The changes in effective stress development in both the sandpile and the surrounding soil are analysed. In figure 5.10 the effective vertical and effective radial stresses are plotted for the clay layer in both Model 1 and Model 2.

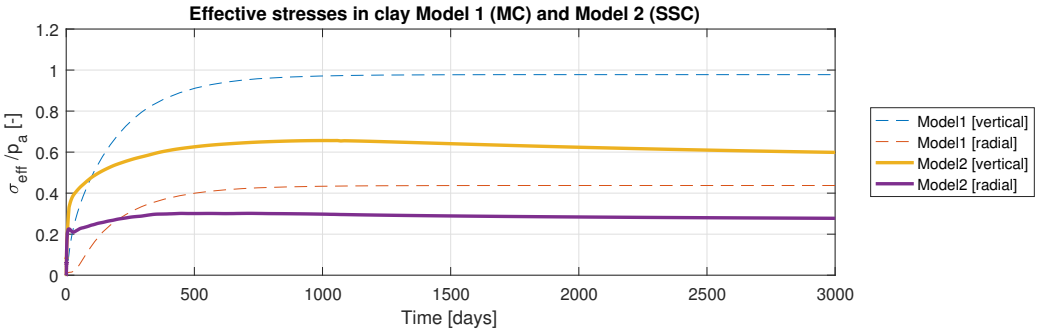

Figure 5.10: Stresses in clay layer surrounding the sandpile (r=0.40m) for both Model 1 (MC) and Model 2 (SSC).

The plot in figure 5.10 shows that the effective stress increase in the clay layers in Model 2 is lower than simulated in Model 1. As the stiffness of the clay is lower in the advanced models, the soft soil carries less stress compared to the sandpile. A second trend which can be observed is the deterioration of effective vertical and radial stress over time in Model 2. The ongoing settlement of the soil and therefore the submerging of the embankment applied on top of the unit cell results in a decrease in stresses in the underlaying soil, hence the developed effective stresses are decreasing over time.

In figure 5.11 the effective vertical and effective radial stresses are plotted for the sandpile, simulated with model 1 as well as Model 2.

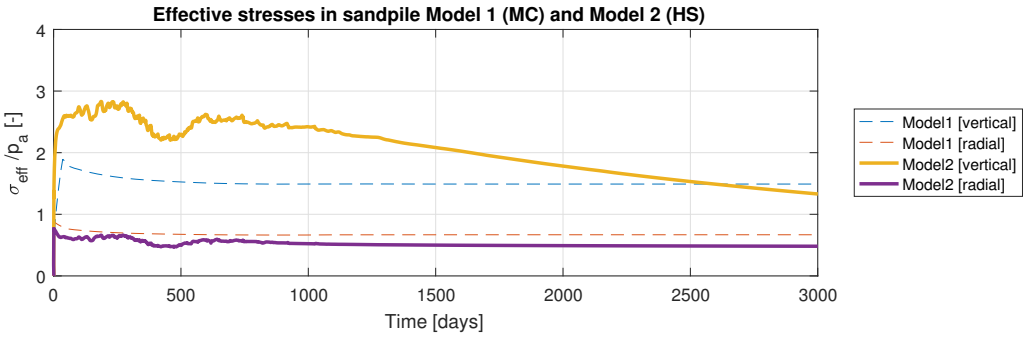

Figure 5.11: Stresses in sandpile (r=0.18m) for both Model 1 (MC) and Model 2 (SSC).

The plots in figure 5.11 show a higher vertical effective stress in Model 2 compared to Model 1. This deviation is explained by the difference in sandpile stiffness defined in each model. In Model 1 the stiffness of the sandpile is constant and described by the Young's modulus (E'). In model 2 this stiffness is stress dependent and governed by either the unloading/reloading stiffness (E_{ur}^{ref}) and the oedometer- and reference stiffness for primary loading, (E_{50}^{oed} and E_{50}^{ref}). A higher stress level in the sandpile results in a higher stiffness, thus the sandpile attracts more of the applied load (p_a). At the same time, the soft soil around the pile is compressed by both the horizontal and vertical forces acting on the soil and the secondary settlement of the soil itself. The horizontal compression of the soft soil causes radial deformation of the pile, which results in a reduction in pile stiffness. The oscillations in stresses observed in figure 5.11 are caused an error in the numerical model, elaborated in section 5.7.

5.4.2. Floating piles

After the alteration of the material models, the sandpile has been shortened in Model 2. Instead of positioning the pile tip at the bottom of the unit cell (z=30.0m), the pile tip is now modelled at z=27.0m. This new geometry of the pile is conform the design of the sandpile at the trial embankment. A required minimal distance of 3.0m between the tip of the sandpile and the drained layer underneath is a result of the difference in hydraulic head between the upper soil layers and the drained layer positioned underneath, see section 2.4.4. The influence of shortening of the pile is measured by the surface settlement of the unit cell and the settlement at z=27.0m, the new position of the pile tip. In figure 5.12 the settlement simulated with Model 2 for both end-bearing piles and floating piles is presented.

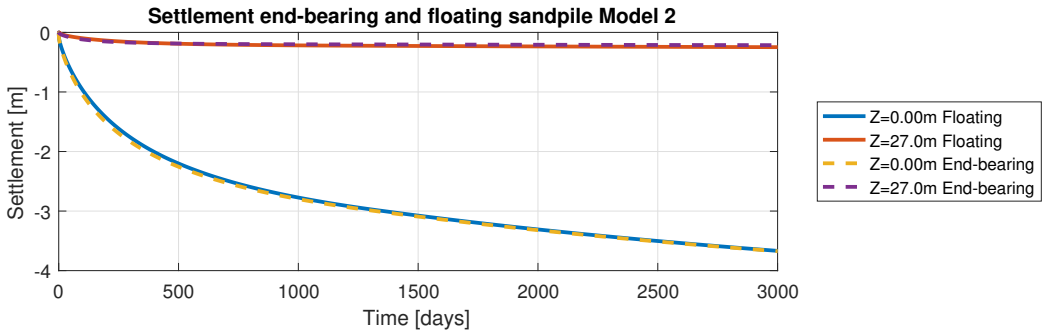

Figure 5.12: Settlement over time for end-bearing and floating piles. Both simulations are performed with Model 2.

The settlement graphs of the end-bearing pile model and the simulation with the floating piles are almost identical, as can be observed in figure 5.12. The surface of the floating pile deviates slightly during the the first 600 days, but afterwards this difference becomes negligible. This difference can be explained by the presence of a soft soil layer underneath the sandpile in the floating pile simulation. This results in an increased drainage path for the soil underneath the sandpile and therefore a lower consolidation rate at this specific location.

5.4.3. Advanced model features

The change from a basic material model (MC) towards advanced models (HS & SSC) is affecting the behaviour of the sandpile. Two of the main changes observed in the models is the bulging behaviour of the pile at a shallow depth and the changing rate of consolidation over the depth of the soil.

Bulging behaviour

The soft soil creep (SSC) material model used for simulating the behaviour of the clay layer has a stress dependent stiffness. The stiffness of the clay is therefore increasing in depth, in contrast with the Mohr-Coulomb (MC) model which assumes a constant stiffness over depth. This difference results in a constant radial displacement of the sandpile over depth in the MC simulation, while using the advanced SSC material model results in larger radial deformations closer to the ground surface. These deformations are decreasing over the depth of the pile. In figure 5.13 the radial deformations of the top 5 meter of the sandpile are plotted for model 1 (MC) and model 2 (advanced material models).

What can be observed in the figure 5.13 is the radial deformation at the MC model more or less continuous over the length of the pile during the first 5 meter. The radial deformation of the advanced model is resulting in large radial deformations at the top of the sandpile, which reduces with depth. The stress dependent stiffness of the advanced models are causing this decrease in radial deformations over the depth.

Stress dependent excess pore water pressure

The second phenomenon observed in the transition from basic MC material model towards the advanced SSC material model is the change in the distribution of excess pore water pressure during consolidation. In the previous section it is explained that the stiffness of the soft soil is constant in the MC model, but stress dependent in the SSC model. The coefficient of consolidation which governs the consolidation rate is dependent on the stiffness of the soil. The relation between the material stiffness and the coefficient of consolidation is explained in section 3.3.3. As the stiffness increases, the coefficient and the consolidation rate increase as

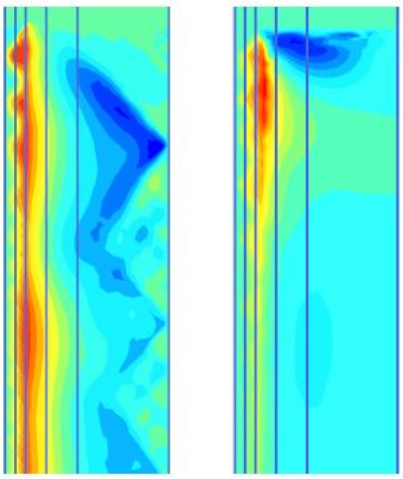

Figure 5.13: Radial displacement at top 5.0m of the unit cell for both the MC model (left) and the advanced soil model (right). Note that the scale of the legend is different for both models. Red are displacements in positive direction, blue in negative direction.

well. In figure 5.14 the excess pore water distribution is visualised for both the MC model (Model 1) and the SSC model (Model 2).

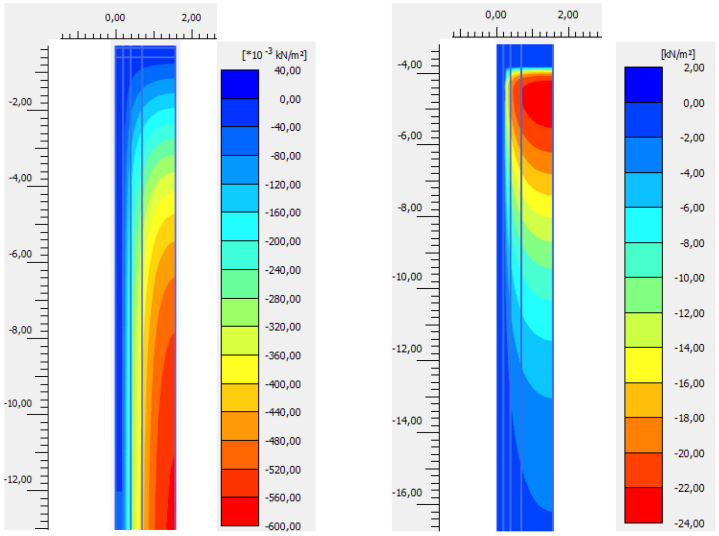

Figure 5.14: Excess pore water pressure distribution over the top half of the sandpile. The MC model (left) shows an increase in excess pore water pressure over the radius of the unit cell. The SSC model (right) shows in increase in pore water pressures with an increase in radius and decrease in depth.

When looking at the left visualisation in figure 5.14 it can be observed that the excess pore water pressure at the soft soil depends on the distance towards the drained boundary. In figure 5.14 these are the top horizontal boundary and the left vertical boundary. The right visualisation represents the distribution of excess pore water pressure in Model 2. What can be observed is the highest excess pore pressure found at the shallow surface, just below the ground surface. The stiffness of the soft soil is the lowest at that position. Hence, the transition towards the SSC model causes the consolidation rate to be stress dependent.

5.5. Model 3: Realistic model

In this section the numerical model described in the previous section is adjusted to match the realistic geometry and properties of the subsoil at the NAICM site. The input properties are based upon both the design report of TASANA [34] and UNAM [2]. The main difference between the realistic design and the model analysed in section 5.4.3 is the addition of the deeper soil layers and the adjustment of hydraulic heads. The differences between the previous model (Model 2) are only analysed in terms of settlement, as the material models do not change. The realistic model as presented in this section is verified in chapter 6.

5.5.1. Geometry of the soil

In order to match the subsoil conditions at the NAICM site, the deeper soil layers are added underneath the unit cell. The phreatic surface at the NAICM site is located at -1.0m below surface level. The new soil geometry is based on the design report of TASANA [34] and is listed in table 5.7.

Table 5.7: Geometry and head distribution of the soil layers as modelled in the realistic model (Model 3).

Subsoil NAICM site		**Geometry**		**Hydraulic head**	
Soil layer	**Description**	**Top [m]**	**Bottom [m]**	**Top**	**Bottom**
Desiccated crust	Remoulded soil	0.00	-0.70	Phreatic	Phreatic
FAS A	First top clay layer	-0.70	-9.60	Phreatic	Phreatic
FAS B	Second top clay layer	-9.60	-23.40	Phreatic	Phreatic
FAS C	Third top clay layer	-23.40	-30.20	Phreatic	-4m
CD	Silty sand layer	-30.20	-31.30	-4m	-4m
FAI	Top deep clay layer	-31.30	-44.10	-4m	-9m
SES	Silty sand layer	-44.10	-50.00	-9m	-9m
FAP	Bottom deep clay layer	-50.00	-60.00	-9m	Linear
FEP	Deep sand layer	-60.00	-62.00	-50m	-50m

The table above shows that at the NAICM site two clay layers are present underneath the CD layer. The addition of these clay layers will result in extra settlement, as the total thickness of compressible layers is increased. At a depth of -60.00m groundwater is being extracted from the deeper aquifer. The water extraction causes a jump in hydraulic head in the adjacent clay layer (FEP) from -9.0m to -50.0m with respect to the surface level. The complete list of soil properties can be found in appendix E. The sandpile is modelled conform the field embankment test at the NAICM site, as described in the UNAM [2] report. The geometry of the sandpile is listed in table 5.8.

Table 5.8: Dimensions of sandpile in the realistic model.

Description	**Parameter**	**Value**	**Unit**
Radius sandpile	r_d	0.20	[m]
Length sandpile	L	27.0	[m]

In order to model the behaviour of the two drained layers underneath the FAS layers (CD and SES), numerical drains have been added in the model. The x_{min} and x_{max} boundaries are impermeable, therefore the water inside the drained layers is trapped between the adjacent clay layers. In the numerical model this results in excess pore water pressures in the sand layers. In order to ensure the sand layers are drained, two drains have been added in the model. The location of these drains are listed in table 5.9.

As can be observed in the table above and table 5.7 are the drains positioned at the x_{max} boundary of both the CD and the SES soil layer.

5.5.2. Settlement of deeper clay layers

The addition of the deeper clay layers and the change of the single FAS A layer into three soft soil layers (FAS A, FAS B and FAS C) affects the rate of settlement. The plot of settlement over time for different locations in the unit cell are presented in figure 5.15.

Table 5.9: Position of numerical drains added to the Plaxis 2D model.

Position	Drain 1	Drain 2
Top	(1.58,-30.20)	(1.58,-44.10)
Bottom	(1.58,-31.30)	(1.58,-50.00)

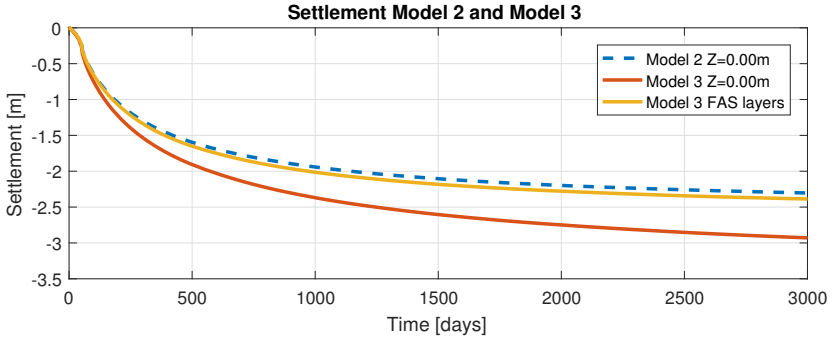

Figure 5.15: Settlement simulated in Model 2 and Model 3.

The plots in figure 5.15 show the total surface settlement (Z=0.00m) simulated with Model 2 and the realistic model, Model 3. The settlement of the FAS layers of Model 3 is slightly larger than the settlement of the FAS A layer in Model 2. The addition of the deeper soil layers to the unit cell is contributing to an increase in settlement. In figure 5.15 the surface settlement of the realistic model, including the deep soil layers, results in an increase of settlement of almost 0.50m over 3000 days. This 0.50m is the contribution of the deep soil layers to the surface settlement at the unit cell.

5.6. Sandpile performance

In chapter 2.4 it is explained that sandpiles as soil improvement method increase the stiffness of soft soils and accelerate the consolidation process. Those two aspects of the pile performance are investigated by using the realistic model (chapter 5.5). The performance of the sandpile is measured by the rate of settlement (consolidation) and the total settlements (stiffness).

5.6.1. Improving consolidation rate

Upon installation, sandpiles provide a reduction in drainage path to the surrounding soft soils. This allows the excess pore water pressure to dissipate faster from the soil, hence increasing the consolidation rate (chapter 2.4). The increase in consolidation rate can be visualised by plotting the rate of average degree of consolidation for both the improved and unimproved soil. In figure 5.16 the average consolidation is plotted for both cases.

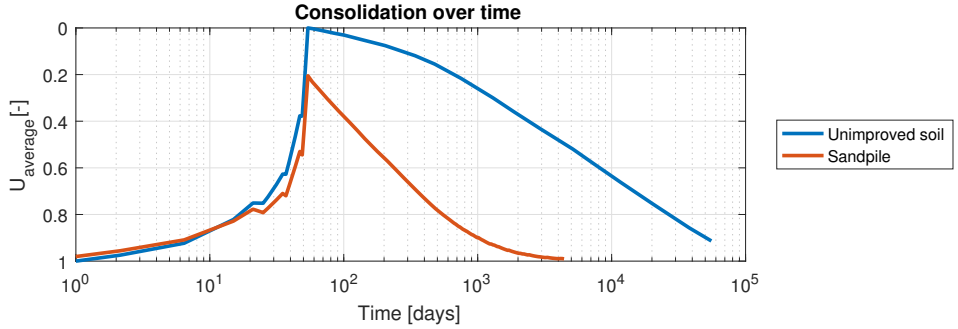

Figure 5.16: Settlement over time for both unimproved soft soils and soils improved with sandpiles.

As can be observed in figure 5.16, the consolidation rate is significantly increased by the sandpiles. The

observed increase in consolidation rate conforms the expectation regarding the drainage behaviour of the sandpile (chapter 3.3). Based upon the results of the simulation it is concluded that the sandpiles are effective in accelerating the consolidation process.

5.6.2. Increasing soil stiffness

The stiffness of sandpiles is high compared to the stiffness of the soft soils. Upon installation, sandpiles increase the total stiffness of the soil generally. The increased stiffness of the soil results in a reduction in total settlements (section 2.4). However, the numerical simulation show only minor changes in total settlement for soils improved with sandpiles compared to unimproved soils. In figure 5.17 the simulated settlement curves are presented.

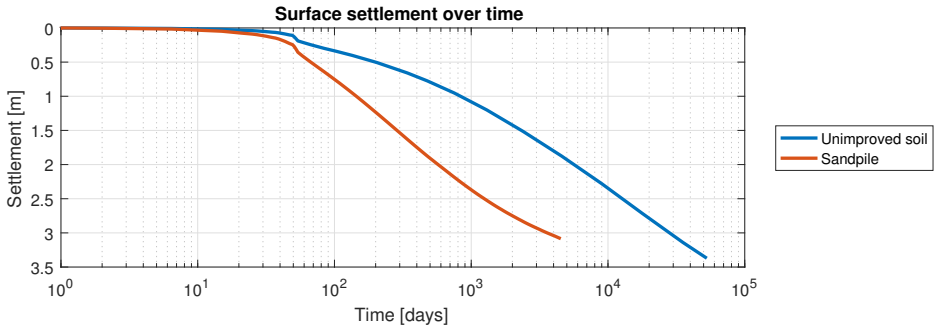

Figure 5.17: Settlement over time for both unimproved soft soils and soils improved with sandpiles.

The reason for this is the following: the radial- and vertical deformations of the sandpile during consolidation prevent stress transfer from the soft soils towards the sandpile. The shear stresses are not able to develop around the pile, as the pile deforms together with the soil. When the radial deformations of the sandpile are limited, shear stresses are able to transfer stresses towards the pile, hence reducing the total settlements. Note that this behaviour is observed at sandpiles installed in the specific soil conditions at the NAICM site. In figure 5.18 the settlements of soft soil improved with the a sandpile is visualised, together with the settlements of a sandpile with limited radial deformations (confined sandpile).

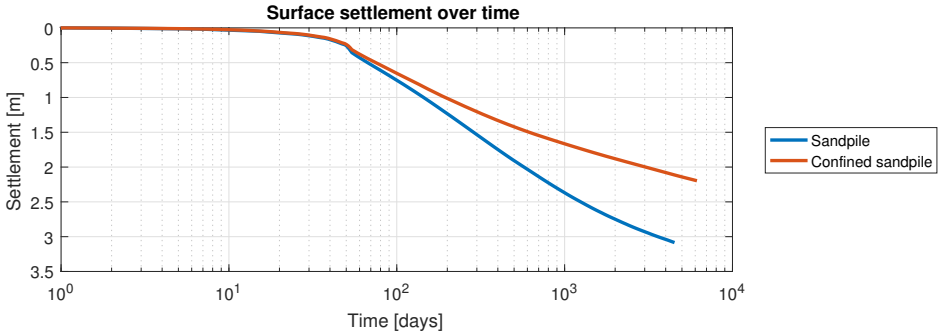

Figure 5.18: Settlement over time for sandpiles and sandpiles with limited radial deformations (confined sandpiles).

The plot in figure 5.18 indicated that when radial deformations are limited the stiffness of the soil is increased, a reduction in total settlements is observed. In figure 5.19 the shear stresses developed around both the sandpile and the confined sandpile are presented.

Figure 5.19 shows the difference in shear stress development around the sandpile and the confined sandpile. The sandpile with limited radial deformations develops maximum shear stresses are around the top two meters of the sandpile. Furthermore, a difference in settlement between the soil and sandpile is observed. The shear stress development at the top meters of the soil indicates that stresses are being transferred towards the confined sandpile, resulting in a settlement reduction of 0.70m (figure 5.18). The sandpile which is non-restricted, shows a different shear stress development. At the top of the sandpile the shear stress development is very limited, with an increase in depth the shear stress developed is also increasing. The settlement of the sandpile is equal to the settlement of the soft surrounding soil. Due to the radial deformations the sandpile

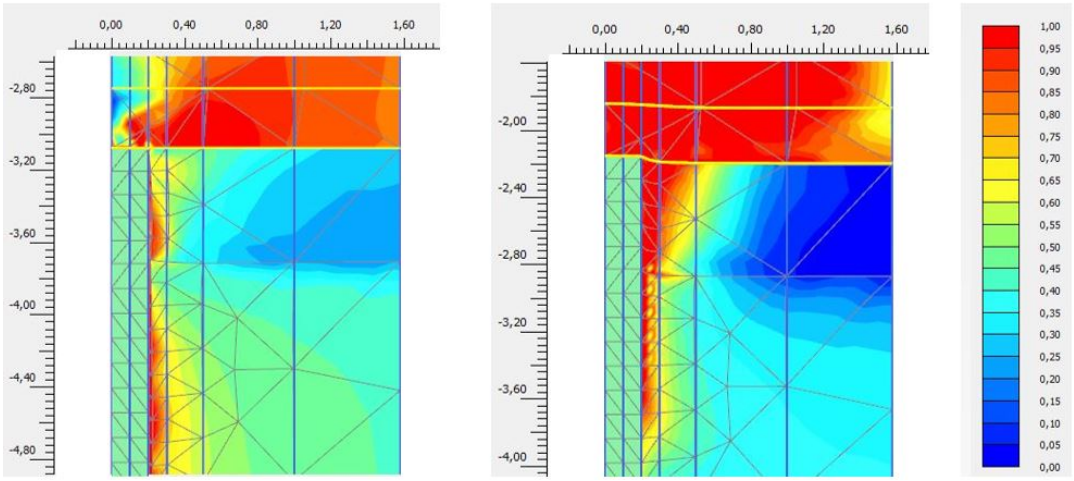

Figure 5.19: Relative shear stress development around the top of the sandpile (left) and the confined sandpile (right). The red colours indicate maximum shear stress development ($\tau_{rel} = 1$), in blue the minimum shear stresses are indicated ($\tau_{rel} = 0$).

itself is decreasing in length, allowing the pile to settle together with the soil. As a result the stresses in the soft soils cannot be transferred towards the sandpile by shear stresses. An increase in depth lowers the pile deformations, allowing more shear stresses to develop around the pile. In figure 5.20 the relative shear stresses around the bottom of the sandpiles are presented.

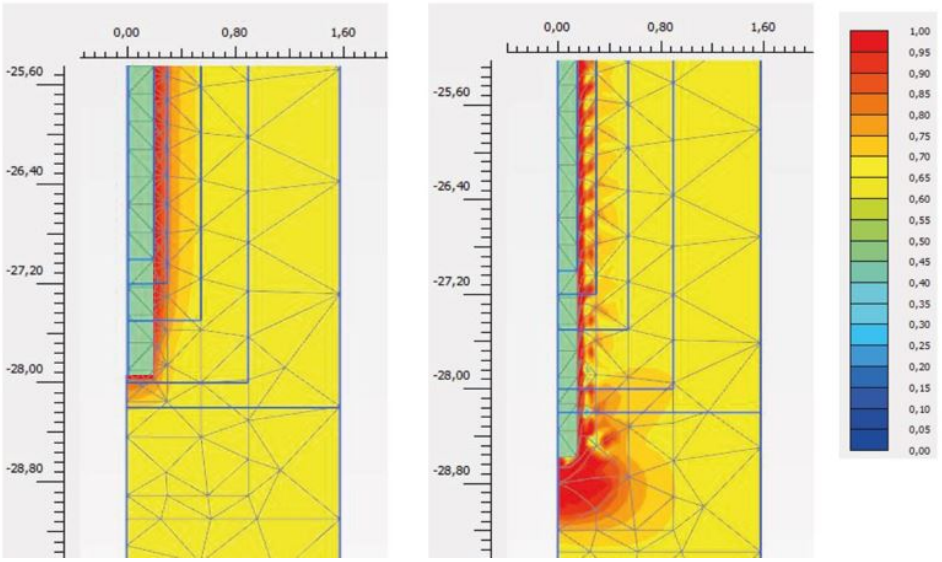

Figure 5.20: Relative shear stress development around the bottom of the sandpile (left) and the confined sandpile (right). The red colours indicate maximum shear stress development ($\tau_{rel} = 1$), in blue the minimum shear stresses are indicated ($\tau_{rel} = 0$).

The left picture in figure 5.20 shows the shear stress development around the bottom of the sandpiles, on the right the shear stress development around the confined sandpile is presented. As can be seen is the shear stress increase underneath the sandpile significant less compared to the shear stress development of the confined sandpile. The transfer of stresses by the sandpile are therefore less compared to the confined sandpile, indicating that the transfer of stresses from soft soil towards sandpile are less effective in sandpiles deforming in radial and vertical direction. In conclusion, the radial- and vertical deformations of the sandpile limit the stress transfer from soft soil towards sandpile. For this reason, the reduction in total settlements is minor. When limiting the radial deformations of the sandpile, the stress transfer increases and therefore a significant reduction of 0.7m in total settlements is achieved.

5.7. Model Errors

The stress oscillations observed in section 5.4.1 simulated in the sandpile are caused by an error in the numerical model. Plaxis 2D uses a critical time step in the consolidation analysis, which is the minimum value of the time increment used to prevent a reduction in accuracy in the simulation. The critical time step ($\Delta t_{critical}$) in the consolidation analysis of Plaxis 2D is governed by the following formula:

$$\Delta t_{critical} = \frac{H^2}{\eta \alpha c_v} \tag{5.1}$$

in which H is the height of the element used, η is a constant parameter which is determined for each types of element, α is the time integration coefficient which is equal to 1 for fully implicit integration scheme and c_v is the consolidation coefficient. The 2D elements used in Plaxis 2D are 15-node triangular elements, therefore formula 5.1 can be reformulated as [1]:

$$\Delta t_{critical} = \frac{H^2 \gamma_w}{80 k_y} \left(\frac{1}{E_{oed}} + \frac{n}{K_w} \right) \tag{5.2}$$

with γ_w is the unit weight of the pore fluid, k_y is the coefficient of permeability, E_{oed} is the oedometer modulus, n is the porosity and K_w is the elastic bulk modulus of water. As can be observed in formula 5.2 is the element size the only variable which can be adjusted without changing the properties of the soil. In order to reduce the stress oscillations simulated the elements are reduced in size. In figure 5.21 the total stresses in the sandpile for different mesh sizes are presented.

Figure 5.21 shows the stress oscillations in the total stresses for different mesh sizes. Note that the stresses are simulated in a reduced time span, as the increase in mesh size induces a smaller time step generated in the calculations. This results in a smaller total time span covered in the 10,000 steps of the simulation.

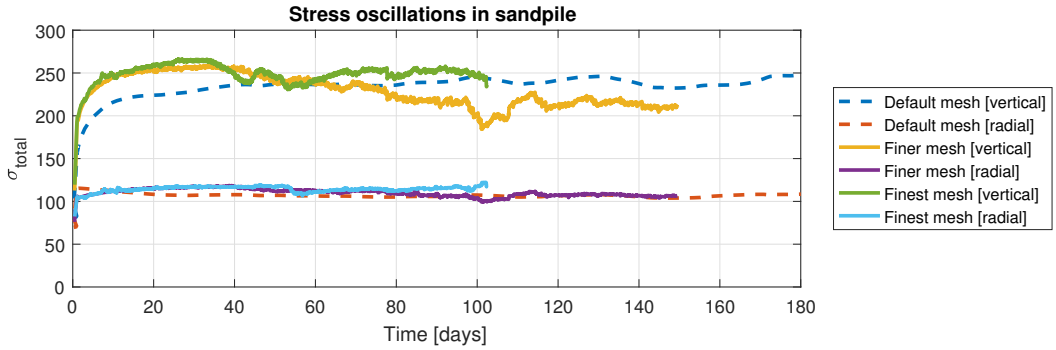

Figure 5.21: Stress oscillations for default and refined mesh sizes.

The maximum value of the critical time step is automatically adopted as the 'First step' in a consolidation analysis [1]. The mesh refinement in combination with a manually adjusted value of the first step did not result in an decrease in the stress oscillations. The stresses oscillations generated by Plaxis 2D are believed to a result of a numerical instability, caused by the large difference in hydraulic conductivity of the clay compared to the sandpile. In the numerical model the critical time step is generated for the whole model, one value of $t_{critical}$ is used in the simulation. This minimum time step could be generated based upon the properties of the mesh in the clay and the corresponding soil properties, while this critical time-step is to large for a stable simulation of stresses in the sandpile.

The tolerated error in the consolidation phase was adjusted to investigate the influence on the stress oscillations. In the numerical models the tolerated error used is 0.10. The model error is varied and the changes in stress development inside the sandpile (node K, positioned at a depth of 5.0m and a radius of 0.19m) and surface settlements are presented in figure 5.22.

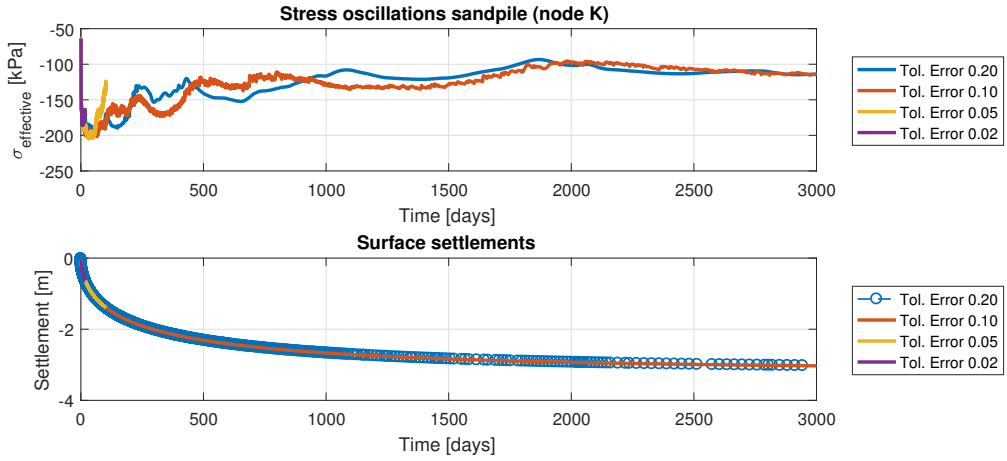

Figure 5.22: Stress oscillations and surface settlements for different values of tolerated error.

From figure 5.22 it can be observed that lowering the model error does not result in a reduction of stress oscillations inside the sandpile. The surface settlements simulated by the different models remain constant when lowering the tolerated error, therefore it is concluded that the consolidation and settlements simulated with the Plaxis 2D numerical model closely represents the real soil behaviour. The stress oscillations in the sandpile can be discarded in the consolidation and settlement analysis. In Appendix C the development of stresses and settlements are represented for a smaller time span.

6

Model Verification

In this chapter the verification of the numerical models is performed using the measured data obtained from the trial embankments. The verified model is used for the sandpile sensitivity analysis in chapter 7.

6.1. Introduction

The numerical Plaxis 2D model as described in chapter 5 is verified before using it in the sandpile sensitivity analysis. The verification is done by using the data obtained from trial embankments constructed at the NAICM site and comparing those to the data simulated with the numerical models. Prior to the design of the runways, trial embankments have been constructed for monitoring the behaviour of the subsoil upon loading. The soil underlaying the trial embankments is improved by different soil improvements methods, including prefabricated vertical drains (PVDs), sandpiles and rigid inclusions. The position of the different trial embankments at the NAICM site is visualised in figure 6.1.

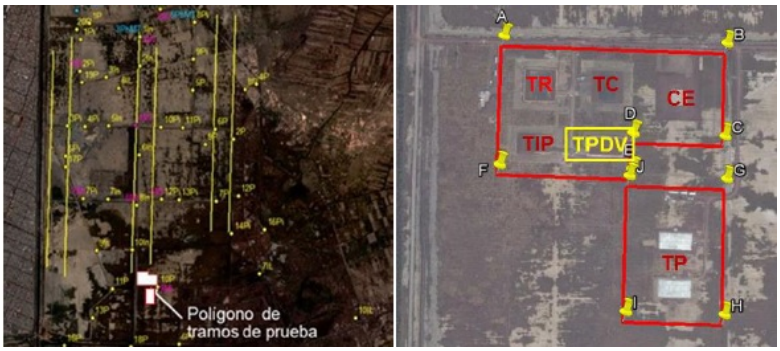

Figure 6.1: On the left side the location of the trial embankments at the NAICM site [2]. On the right side the positions of the trial embankments with respect to one another. In yellow the position of the TPDV embankment (Terraplén de prueba con Precarga y Drenes Verticales) is highlighted, this is the embankment with sandpiles and PVDs on each side.

The measured data of the trial embankment positioned on top of the sandpiles (Terraplen Drenes de Arena, TDA) is used in the verification of the numerical model. In figure 6.2 the geometry of this trial embankment is shown, positioned on soil improved both with sandpiles (left side) and PVDs (right side).

The measurement devices installed underneath the trial embankments include pressure cells and piezometers for measuring the pressure increase underneath the embankment and the increase in pore water pressure in the soil, respectively. In addition to the applied load and the increase in pore pressures, the settlement at different locations of the embankment has been monitored. In section 6.2 the procedure used in the fitting of the modelled and measured data is discussed. In section 6.3 the verification of the model based on the TDA trial data is performed.

After the numerical model is verified for the TDA trial, the verified model is applied on the PVD trial in section 6.4. Finally in section 6.5 the errors occurring during the model verification are discussed.

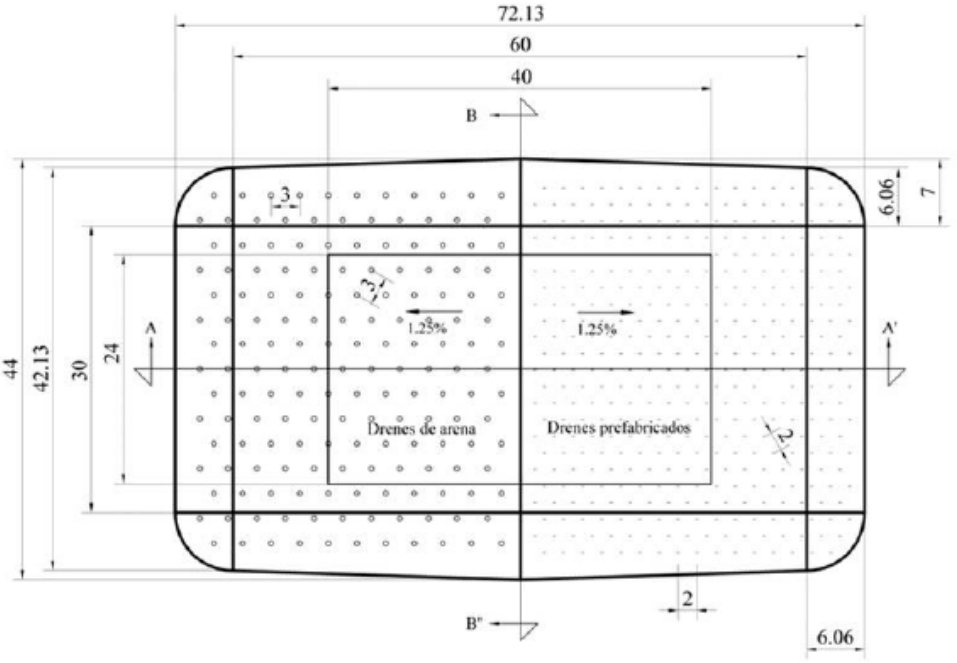

Figure 6.2: Geometry of trial embankment with sandpiles installed on the left side (drenes de arena) and PVDs installed on the right side (drenes de prefabricados) [2].

6.2. Fitting procedure

The verification of the numerical model in Plaxis 2D is performed by matching the simulated behaviour of the sandpile with the monitored data from the TDA trial. The process of adjusting the input parameters for obtaining a match in data is referred to as 'fitting' of the material properties. Prior to the verification of the input parameters, the sensitivity of those parameters is investigated. The effect of a change in material properties on the settlement rate is visualised in appendix D. The reference data in the figures presented in this appendix are based upon the values conform TASANA [34]. The high- and low parameter plots represent an increase and decrease of the original input parameters with a magnitude of +20% and -20%, respectively. The results of the analyses are presented in table 6.1. For each simulation the increase in settlement between t=600 days and t=2920 days is listed. The settlement occurring in this time period is referred to as the performance, explained in detail in section 7.1.

Table 6.1: Sensitivity of material model parameters of the soft soil layers. The input parameters have been adjusted by plus- and minus 20%. The results of the analysis are presented in terms of performance, which is the settlement between t=600 days and t=2920 days (8 years).

		Performance [m]			**Relative performance [%]**	
Parameter	**Symbol**	**-20%**	**0%**	**+20%**	**-20%**	**+20%**
Over consolidation ratio	OCR	1.08	0.88	0.72	122.7	81.8
Horizontal hydraulic conductivity	k_x	0.95	0.88	0.83	108.0	94.3
Vertical hydraulic conductivity	k_y	0.88	0.88	0.87	100.0	98.9
Modified swelling index	λ^*	0.91	0.88	0.87	103.4	98.9
Modified compression index	κ^*	0.89	0.88	0.88	101.1	100.0
Modified creep index	μ^*	0.80	0.88	0.97	90.9	110.2

The sensitivity analysis of the material model parameters indicates that the over- consolidation ratio (OCR), the horizontal permeability (k_x) and the modified creep index (μ^*) are the most influential. The selection of the parameter values providing the right fit is performed by manual adjustment of the different input parameters. In the verification analysis there exist no 'perfect' fit, as there are uncertainties in both the measured- and simulated data (section 6.5). There are multiple different sets of parameters providing a rea-

sonable fit, therefore the chosen set of parameters is arbitrary. The values of the input parameters conform the TASANA report [34] (default) together with the updated values providing the chosen 'best' fit are listed in table 6.2.

Table 6.2: Original and updated material properties of different soil layers.

	FAS A		FAS B		FAS C		
Parameter	Default	Updated	Default	Updated	Default	Updated	**Unit**
OCR	1.767	1.850	1.767	1.650	1.586	1.650	[-]
k_x	2.270E-4	2.400E-4	2.270E-4	1.700E-4	2.270E-4	1.700E-4	[m/day]
k_y	2.270E-4	2.400E-4	2.270E-4	1.700E-4	2.270E-4	1.700E-4	[m/day]
λ^*	0.315	0.315	0.340	0.380	0.387	0.380	[-]
κ^*	0.035	0.040	0.037	0.044	0.038	0.044	[-]
μ^*	0.013	0.013	0.014	0.014	0.015	0.015	[-]

As can be observed in table 6.2 the permeability is the parameter which is changed the most during the verification analysis. The difference in permeability of approximately -25% can be explained by the fact that the default input parameters conform the TASANA report [34] are used for simulating soil improved with PVDs, not with sandpiles. The differences in permeability can therefore be explained by the differences in permeability and installation effects between both techniques.

6.3. TDA verification

In this section the numerical model is verified by using the measured data obtained from the trial. By comparing the results of both the trial and the model, the input of the numerical model can be adjusted in order to match the measured data. The position of the measurement devices used in the TDA trial are presented in figure 6.3.

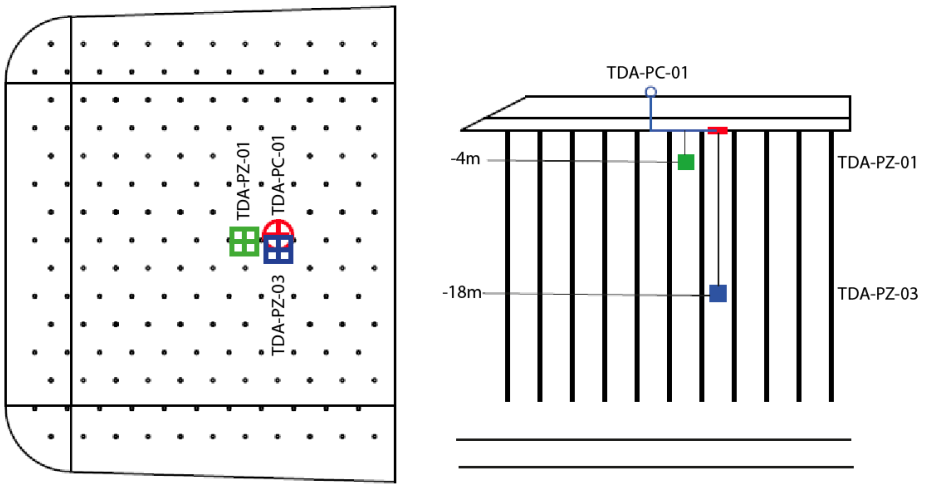

Figure 6.3: Position of the pressure cell (TDA-PC-01) and the piezometers (TDA-PZ-01 and TDA-PZ-02) at the TDA, used in the verification analysis [2]. The figure on the left shows the positions in top view, on the right the positions in cross section is presented.

In the following subsections the results of the trial embankment are plotted together with the data obtained from the fitted numerical model.

6.3.1. Applied load

The pressure cells underneath the embankment measure the increase in total stress during the construction of the embankment. This data is used to verify the magnitude of the load applied in the numerical model. In figure 6.4 the measured load and modelled load over time are visualised.

The measured stresses over time fluctuate during the construction phase, as heavy machinery is used to construct the embankment. The peaks in stresses are very short, it is assumed that these peak stresses will not

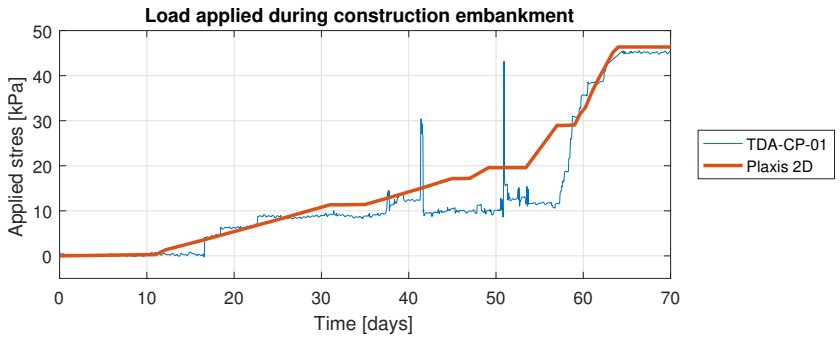

Figure 6.4: Measured and simulated (Plaxis 2D) load applied by embankment.

influence the consolidation process of the underlying soil layers and therefore are not taken into account in the numerical model. The modelled construction of the embankment overestimates the increase in applied load between 43 and 58 days. As the duration is short this overestimation is assumed not to influence the results of the analysis.

6.3.2. Excess pore water pressures

The simulated excess pore water pressure is adjusted in order to match the data measured by the piezometers. The piezometers installed at depths of 4.0m and 18.0m measure the excess pore water pressure at the corresponding depths. The piezometers itself will settle simultaneously with the soil. Therefore the measured excess pore water pressure includes the relative increase in head, resulting in an over-estimate of the excess pore water pressure over time. This effect is taken into account by adding the additional increase in water pressure due to settlement to the simulated excess pore water pressure.

Secondly, the simulated behaviour of the sandpiles does not include subsidence. Due to water extraction at the deep aquifer, the hydraulic head at the deeper clay layers (FAI and FAP) reduces over time. This reduction in hydraulic head is causing settlements at these layers, resulting in a relative constant extra settlement over the whole NAICM site.

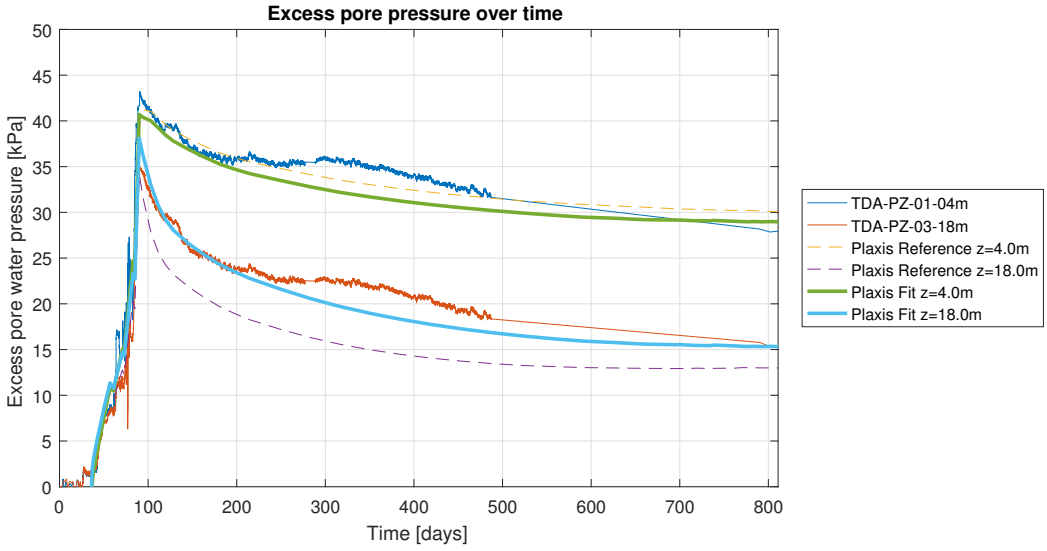

Figure 6.5: Measured settlement and simulated settlement (Plaxis 2D).

The resulting graphs are presented in figure 6.5. The excess pore water pressures measured in the period between 80 and 200 days and the pressures around 770 and 800 days are used for fitting the model.

The measured data shows an increase in excess pore water pressure in the time period starting from 200 until 300 days. This increase corresponds to the increase in water table during the rain season. The precipitation is not included in the numerical model, therefore deviations from the measured results are obtained.

Furthermore the subsidence is not modelled in the numerical model, hence an subsidence of 100mm a year is added to the calculated settlements to take this effect into account [20].

The results of the fitted Plaxis 2D model shows a close fit to the measured data, therefore this model is assumed to simulate the behaviour of the clay layers more accurate than the default model. Note that there is no 'perfect fit' as more possible configurations of properties providing a close fit can be found. Secondly, the errors in both the measurements and the modelled data are causing a bandwidth of reasonable fits. In section 6.5 the errors affecting the accuracy of the fit are described.

6.3.3. Settlement

The settlement of different positions at the embankment were monitored starting from the installation of the embankment in July 2014 until April 2017. However, after August 2016 an unknown external event influenced the measurements [20]. Therefore, the measured data until August 2016 was used for fitting the settlement curves.

As stated before, the numerical model does not include the subsidence of the whole site due to groundwater extraction at the deep aquifers. Therefore, an additional settlement of 100mm per year is added to the calculated settlement to account for this effect (section 2.2.2). In figure 6.6, the measured data of the trial embankment positioned on top of the sandpiles (TDA side) is plotted together with the results of the default and fitted Plaxis 2D models.

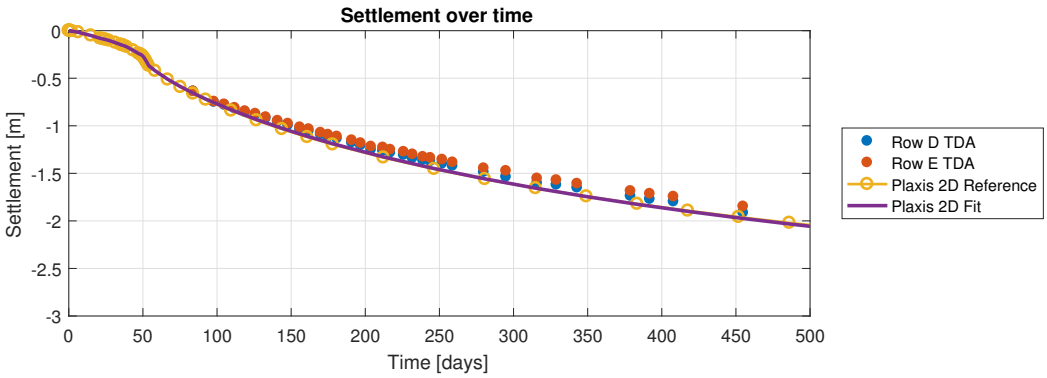

Figure 6.6: Excess pore water pressures, both measured and simulated (Plaxis 2D).

The simulated settlements of both the default and fitted model are almost similar and fit very closely with the measured settlements of the TDA embankment. A slight overestimate of settlements is expected when using the unit cell approach, as the load applied on top of the cell is assumed to be infinite in width and length. This causes a relative higher stress increase in the deeper soil layers compared to the real situation (load limited in dimensions), resulting in increased settlements.

6.4. TDP verification

The model verification concludes with the comparison of the new model parameters with the data from the TDP (embankment with PVDs) trial. The stiffness and radius of the sandpile are reduced to match the properties of the PVDs by assigning the stiffness of the surrounding clay to the sandpile material. The TDP verification only includes the measured excess pore water pressures and the settlement of the embankment. The location of the measurement devices at the TDP embankment is visualised in figure 6.7. In table 6.3 the updated properties of the sandpile are listed.

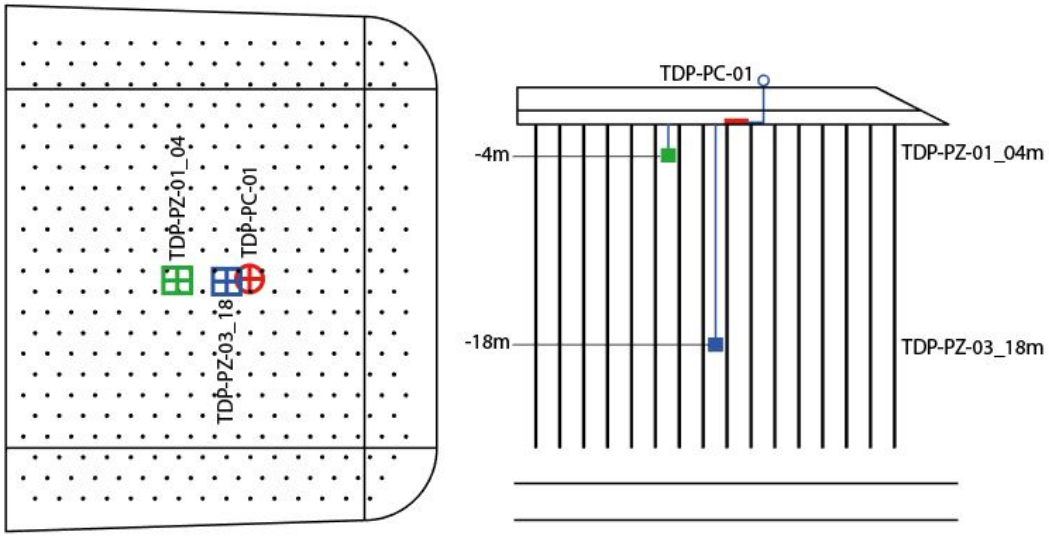

Figure 6.7: Position of the measurement devices at the TDP trial [2], in top view (left) and cross section (right).

Table 6.3: Updated properties of the sandpile in order to simulate the PVD behaviour.

Input parameter	Name	Sandpile	PVD	Unit
General				
Unit weight (wet)	γ_{unsat}	16.00	12.10	$[kN/m^3]$
Unit weight (wet)	γ_{sat}	18.00	13.00	$[kN/m^3]$
Radius drain	r	0.20	0.05	$[m]$
Parameters				
Secant stiffness*	E_{50}^{ref}	30.0E3	3.0E3	$[kN/m^2]$
Tangent stiffness**	E_{oed}^{ref}	30.0E3	3.0E3	$[kN/m^2]$
Unloading/reloading stiffness	E_{ur}^{ref}	90.0E3	9.0E3	$[kN/m^2]$

Note that the geometry of the PVDs is not exactly correct; the PVDs as used in the TDP trial have a rectangular shape of 100mm by 3mm. In a axisymetric model only circular shapes can be modelled, hence the geometry listed in table 6.3.

6.4.1. Excess pore water pressures

The excess pore water pressure as measured at the TDP embankment is compared with the data simulated with Plaxis 2D. In figure 6.8 both data is plotted.

As can be observed in figure 6.8 matches the simulated data with the measured data at a depth (z) of 4.0m. At a depth of 18.0m the simulation gives a reasonable fit at the first 250 days, but with when time progresses the simulation underestimates the increase in excess pore water pressure. The measured data at the depth of 18.0m shows a different trend compared to the data measured at the TDA trial, the excess pore pressure barely decreases between t=500 days and t=811 days. Based on this unexpected trend in the dissipation of

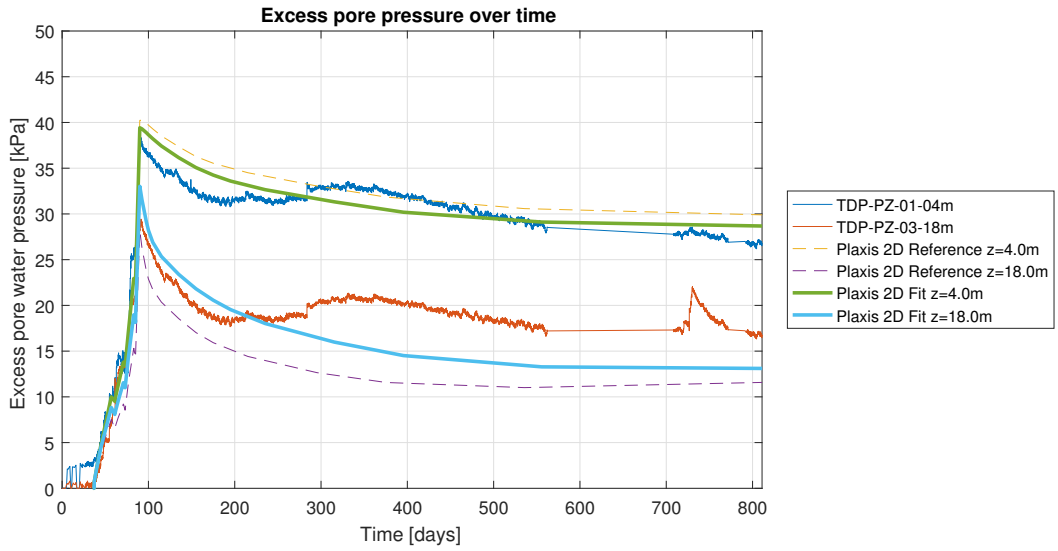

Figure 6.8: Excess pore water pressure measured at the TDP side of the embankment and the excess pore water pressure simulated with Plaxis 2D.

pore water pressure it is assumed that there might have been an event around t=720 days which disturbed the measured data.

6.4.2. Settlement

The settlement as measured at the TDP embankment is compared with the data simulated with Plaxis 2D. The results are visualised by the plots in figure 6.9.

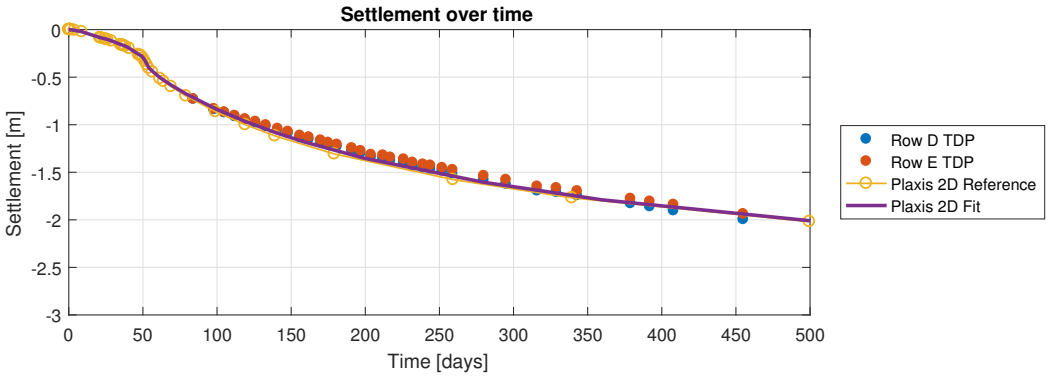

Figure 6.9: Settlement measured at the TDP side of the embankment and settlement simulated with Plaxis 2D.

Figure 6.9 shows that the Plaxis 2D model is slightly underestimating the settlements underneath the embankment. However, the trend in both the measured data and modelled results are relative similar. The Plaxis 2D model is therefore considered to be applicable for simulating of the behaviour of the TDP embankment, as the underestimation of settlement is almost negligible.

6.5. Verification limitations

The verification analysis performed in the previous sections is subjected to several limitations and uncertainties, found at the measured data and the numerical model. Therefore, it is not possible to conclude the fitting analysis with 'the best fit', as there is no single best solution. This results in a bandwidth of valid solutions to this problem. In this section the limitations and uncertainties encountered during the model verification are described qualitatively.

6.5.1. Measurement uncertainties

In this subsection the different measurement uncertainties are described.

Limited data available

The data obtained from the trial embankments is very limited, the model is verified based on only four measurements. The piezometers are installed at a depth of 4.0m and 18.0m; these two points are used for fitting the soil material properties. The progression of pore water pressures at every other point remains unknown.

Subsidence of the NAICM site

The subsidence of the total area is assumed to be 100mm each year. It is assumed that during the whole year the subsidence rate is constant and also the magnitude is constant over the whole area. Possibly the actual subsidence deviates slightly from this assumed value, therefore introducing a small uncertainty in the interpretation of the measured results.

6.5.2. Model limitations

The errors encountered when using a numerical model to simulate the soil behaviour are listed in this subsection.

Unit cell method

The unit cell used for simulating the sandpile behaviour overestimates the increase of stresses at the deeper soil layers. The x-dimension of the embankment on top of the unit cell is infinite in length, meaning that an embankment with an infinite footprint is positioned on top of the unit cell. In reality the dimensions of the embankment are limited and the applied stress decreasing over depth as stresses are transferred to the soil next to the embankment. The limitation in the models results in an increase in settlement in the deep soft soil layers.

Subsoil simplification

The model itself is a simulation of the real behaviour of the different soil layers. The subsoil present in the unit cell is a simplification of the soil layers present at the site. The geometry of these layers is based upon limited data, the subsoil modelled is therefore an estimate of the real situation.

Material models

The modelling of the behaviour of soils is done with constitutive models. The models used, even the advanced models, are still not capable of perfectly modelling the behaviour of soils. In the analysis the model that captures the behaviour the best is chosen, but it remains a simulation of the real behaviour. It is not possible to capture all the different aspects of the behaviour of a material in a single soil model.

Change in groundwater table

The model does not include changes in hydraulic head during the rain season. The excess pore water pressures as simulated do not fit the measured excess pore water pressures. It is assumed that the trend in the measured data between t=81 and t=200 days represents the 'real' development of these pore pressures. Between t=480 days and t=795 days there is no data reported, after t=795 days some measurements have been obtained. The model is also fitted by these few measurements. However, it is not certain if the measured pore water pressure is affected by a large recharge of water during the rain season or not.

Installation effects

The numerical model is not capable of simulating installation effects. The sandpiles are 'wished in place', effects of pile installation of the stiffness of the surrounding soil are not included. As the data measured at the test embankment includes these effects, the influence of these effects is taken into account in the model properties. For example, the effect of smear due to pile installation is taken into account in the horizontal permeability of the surrounding clayey soils.

7

Sandpile Sensitivity Analysis

In this chapter the sandpile sensitivity analysis is performed. The aim of this analysis is to gain knowledge about the sandpile properties and configurations influencing the performance of this improvement method. In this chapter both single and multi-variable analyses are performed for assessing the optimal sandpile performance. The optimal sandpile performance is compared with the performance of PVDs and rigid inclusions at the end of this chapter.

7.1. Introduction

In this chapter the model validated in chapter 6 is used for performing the sandpile sensitivity analysis. The properties of the sandpile used in this analysis are the stiffness, length, radius, centre to centre distance and the permeability of the pile. In section 7.2 the parameters are changed one at a time to research the influence of changing each property on the total performance of the pile. In section 7.3 multiple-variable analyses are conducted in order to search for the best performing pile configuration. The input parameters and their reference values used in the sensitivity analysis are listed in table 7.1.

Table 7.1: Reference input parameters of the sandpile, conform report TASANA [34].

Sandpile parameter	**Name**	**Value**	**Unit**
Geometry			
Pile length	L_p	27.0	$[m]$
Pile radius	r_p	0.20	$[m]$
Centre to centre distance	ctc	3.00	$[m]$
Stiffness parameters			
Secant stiffness*	E_{50}^{ref}	30.0E3	$[kN/m^2]$
Tangent stiffness**	E_{oed}^{ref}	30.0E3	$[kN/m^2]$
Unloading/reloading stiffness	E_{ur}^{ref}	90.0E3	$[kN/m^2]$
Permeability			
Horizontal permeability	k_x	7.96	$[m/day]$
Vertical permeability	k_y	7.96	$[m/day]$

*In standard drained triaxial test
**For primary oedometer loading

The geometry of the soil layers inside the unit cell are the same as the geometry used in the model validation. In table 7.2 the different soil layers are listed. The tables with the complete sets of material properties of the adjusted FAS layers are listed in Appendix F.

In the sensitivity analysis the soft soil layers are divided into two main types of layers: the top soft soil layers (FAS layers) and the deep clay layers (FAI & FAP layers). This distinction is introduced, because the FAS

Table 7.2: Geometry of the soil layers as modelled in Plaxis 2D for the sensitivity analysis, with respect to the ground surface.

Soil layer	Description	Top	Bottom
Desiccated crust	Remoulded soil	0.00	0.70
FAS A	First top clay layer	0.70	9.60
FAS B	Second top clay layer	9.60	23.40
FAS C	Third top clay layer	23.40	30.20
CD	Silty sand layer	30.20	31.30
FAI	Top deep clay layer	31.30	44.10
SES	Silty sand layer	44.10	50.00
FAP	Bottom deep clay layer	50.00	60.00
FEP	Deep sand layer	60.00	62.00

layers are improved by the sandpile: this sandpile does not reach the FAI & FAP layers. In order to determine the performance of the sandpile, the settlement of both improved and unimproved layers need to be calculated. In figure 7.1 a sketch is provided with the position of both layers and the position of the calculation nodes used for computing the settlements.

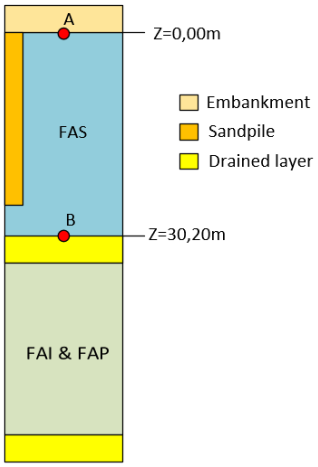

Figure 7.1: Sketch of the improved and unimproved soil layers. Point A and point B are the positions in which the (residual) settlements are calculated.

The loading sequence of the unit cell in the sensitivity analysis is adjusted to match the phased construction of the runways, as described in the UNAM rapport [2]. The construction phases used in the sensitivity analysis are summarised in table 7.3.

Table 7.3: Phased construction of the runways at the NAICM site, conform UNAM [2].

Name	Phase description	Time [days]	Thickness [m]	γ_d/γ_s[kN/m3]
Phase 1	Application of first layer Tezontle	0	1.0	11.0/13.0
Phase 2	Application of second layer Tezontle	30	1.0	11.0/13.0
Phase 3	Application of first layer surcharge	60	1.0	18.0/20.0
Phase 4	Application of second layer surcharge	75	1.0	18.0/20.0
Phase 5	Removal of surcharge	480	-2.0	18.0/20.0
Phase 6	Application of levelling layer Tezontle	525	0.2	11.0/13.0
Phase 7	Application of pavement structure	565	0.8	19.0/19.0
Phase 8	End of construction period	600	-	-
Phase 9	Considered end time	2920	-	-

During the construction of the runways a surcharge load is applied in order to reduce the residual settlements. Applying a surcharge load will increase the over-consolidation ratio in the soft soil layers. After removal of the surcharge load the soil is slightly over-consolidated: when applying the final construction the soil will behave stiffer, as the soil has been subjected to a higher load before. The load applied on top of the unit cell over time is visualised in figure 7.2.

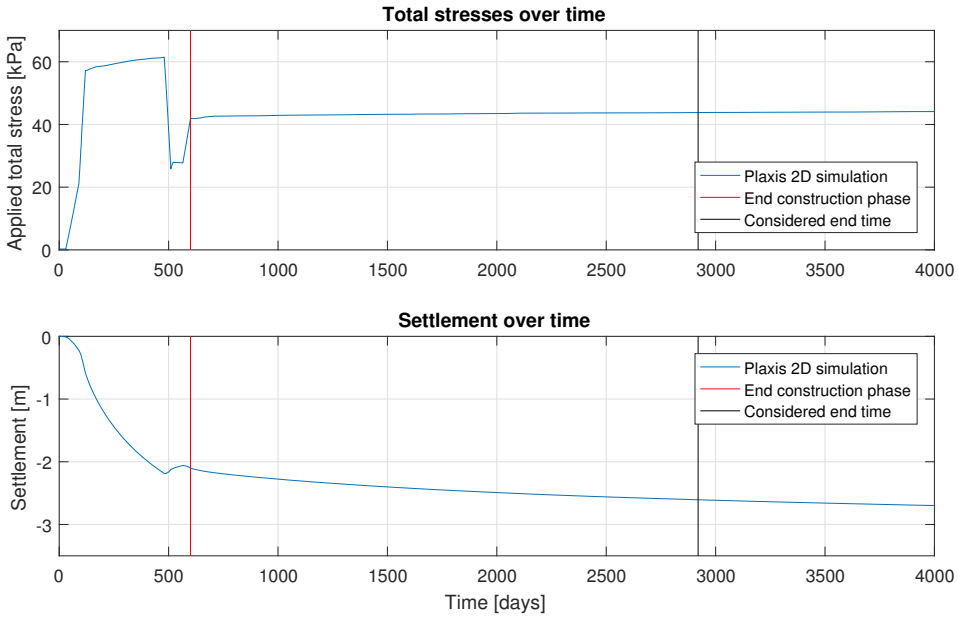

Figure 7.2: Principle of residual settlement visualised, the settlement increase between the end of construction and the end of the time span considered is referred to as residual settlement. In the top graph the increase in total stress over time is visualised, the surcharge load is applied between t=75 and t=480 days. The bottom graph shows the corresponding settlement curve.

In the sensitivity analysis the performance of the sandpiles is quantified with the residual settlement. The aim of the sandpile as soil improvement technique is to reduce the residual settlements after the construction of the runway structure. In the simulations the residual settlement is calculated as the difference in settlement between the end of construction (t=600 days) and the end of the time span considered (t_{end}=2920 days). The aim of the soil improvement methods is to limit the settlements occurring during this time span considered. As can be observed in figure 7.2, the application of the surcharge load during the construction phase results in a reduced rate of settlement during the considered time period of 8 years (between t = 600 and t = 2920 days).

7.2. Sensitivity of single parameters

The first part of the sensitivity analysis considers changes in a single parameters at the time. In this analysis the influence of changing one of the different input parameters can be observed. In the next section the parameters affecting the performance of the sandpile will be adjusted in pairs in order to research the combinations affecting the performance the most.

7.2.1. Stiffness

The first parameter researched in the sensitivity analysis is the stiffness of the sandpile. The default stiffness of the sand is 30.0 MPa, the stiffness has been varied between 15.0 and 250.0 MPa, in figure 7.3 the calculated residual settlements are plotted for changes in stiffness of the sandpile.

As can be observed in figure 7.3, lowering or increasing the stiffness of the sand has minor influence on the residual settlements calculated with the numerical model. A possible explanation is that the support pressure of the clayey soil layers are too weak (there is a lack of support pressure from this layers to the sandpile), resulting in radial deformations of the pile. This 'bulging' behaviour of the sandpile reduces the transfer of stresses from the embankment towards the pile tip. The reduce of residual settlement by increasing the sandpile stiffness is almost negligible.

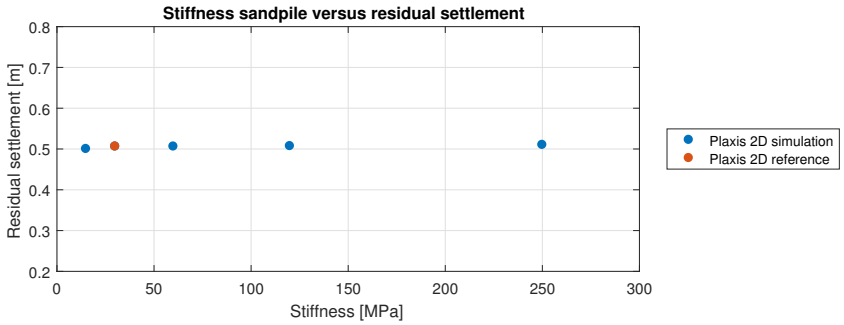

Figure 7.3: Influence of changes in stiffness on the residual settlements, simulated with Plaxis 2D.

7.2.2. Pile length

The sensitivity of pile length on the performance of the sandpile is assessed in this section. In the sensitivity analysis the maximum pile length is 29.0m, just 1.0m above the CD layer. The pile length is shortened in steps of 5.0m. The results of the change in pile length are presented in figure 7.4.

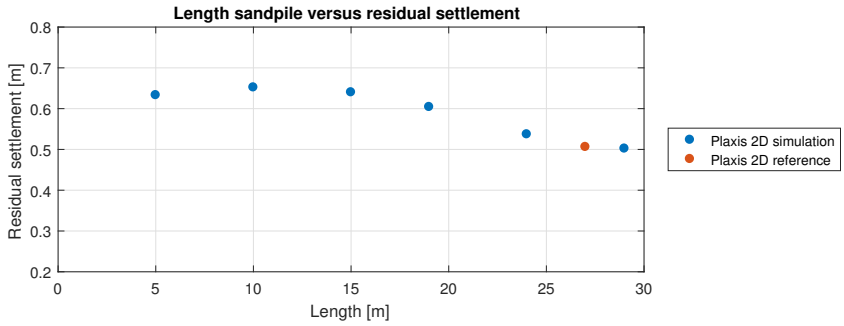

Figure 7.4: Influence of changes in sandpile length on the residual settlements, simulated with Plaxis 2D.

As can be seen in the figure above, the sandpile length does influence the performance of the pile. Shortening the pile is increasing the drainage path of the clay layers the sandpile does not reach. The rate of consolidation of these specific layers will therefore become lower. During the construction phase this lowers the rate of settlement, leaving more settlement to occur during the considered 8 years.

7.2.3. Pile radius

The influence of the radius on the sandpile performance is investigated by varying the radius of the pile in the numerical model. The radius of the sandpile is limited by the technical feasibility. A minimum construction radius is assumed to be 0.10m; the maximum radius assumed to be realistic is set to 0.60m. The results of the sensitivity analysis is presented in figure 7.5.

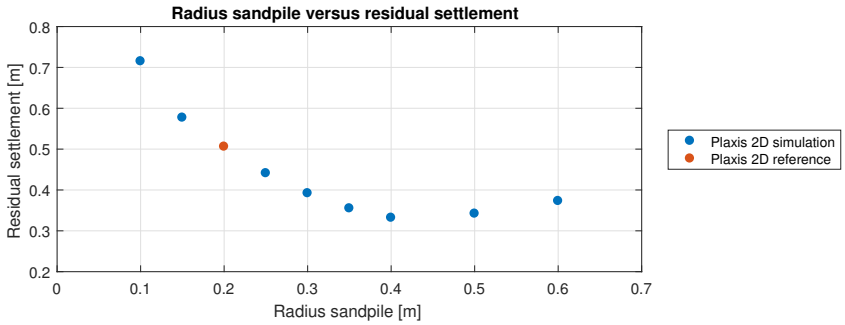

Figure 7.5: Influence of changes in sandpile radius on the residual settlements, simulated with Plaxis 2D.

The trend observed in figure 7.5 is that an increase in pile diameter results in a decrease of residual settlements. However, starting from a radius of 0.40 meter the residual settlements are increasing with an increase

in radius. An explanation for this behaviour is that on one hand the increase in pile diameter reduces the horizontal drainage path of the top clay layers (FAS). This reduction in drainage path causes the consolidation rate to increase, resulting in lower residual settlements.

On the other hand the increase of residual settlement at larger pile diameters is caused by the contribution of the self-weight of the sandpile to the settlement of the deeper clay layers (FAI and FAP). An increase in pile radius and therefore an increase in pile cross-section results in an increment of applied load on the soil layers underneath the sandpile, due to the own-weight of the pile. This causes an increase in settlement of the deep clay layers. In figure 7.6 the settlements of the total unit cell is plotted, together with the separate settlements of the top and bottom clay layers.

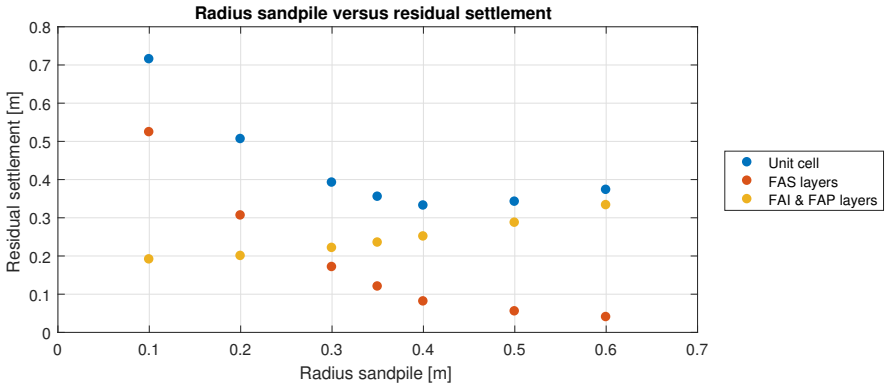

Figure 7.6: Residual settlement of the unit cell, the top clay layers (FAS) and bottom clay layers (FAI & FAP), simulated with Plaxis 2D.

The plot presented in figure 7.6 confirms the positive correlation between the sandpile radius and the settlement of the deeper clay layers. The negative correlation between sandpile radius and settlement of the top layers is also visible.

7.2.4. Centre to centre distance

The centre to centre (ctc) distance between the piles is varied as part of the sensitivity analysis. The reference ctc distance is 3.0m, in this research this distance is varied between the boundary values of 1.5m and 4.0m. Smaller ctc distances are considered not to be valid, as it becomes economic unfeasible. In figure 7.7 the results of the sensitivity analysis are plotted.

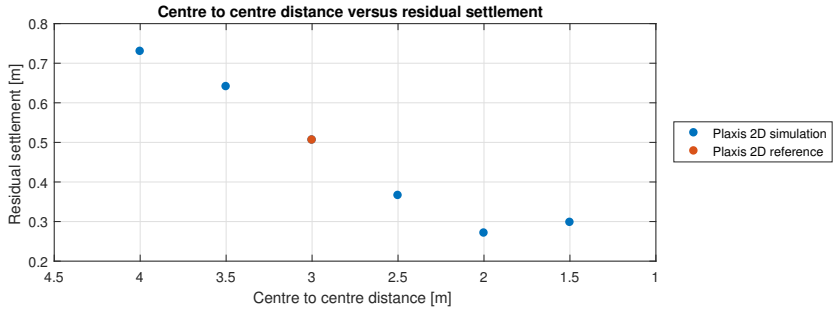

Figure 7.7: Influence of changes in centre to centre distance of the sandpiles on the residual settlements, simulated with Plaxis 2D.

When analysing figure 7.7 it can be observed that increasing the ctc distance results in an increase in residual settlement, while reducing the distance results in an decrease in residual settlements. When the ctc distance is reduced even more, the residual settlements are increasing again. Similar as with the analysis of the radius of the pile, is a reduction in ctc increasing the load applied on the soil layers underneath the sandpiles. This increase of load applied increases the settlements of the deeper layers, hence increasing the residual settlements. This behaviour can be observed in figure 7.8.

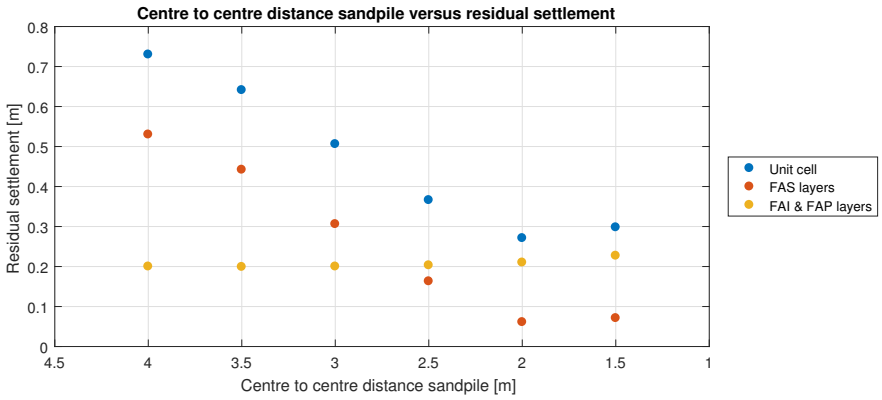

Figure 7.8: Settlement of top- (FAS) and bottom soft soil layers (FAI & FAP) for different ctc distances.

7.2.5. Sandpile permeability

The permeability of the sandpile is varied in this part of the analysis to research the influence on the pile performance. The original horizontal and vertical permeability (k_x and k_y) of the sandpile is assumed to be 7.96 m/day. The permeability is changed in steps of a factor 10 and plotted in figure 7.9.

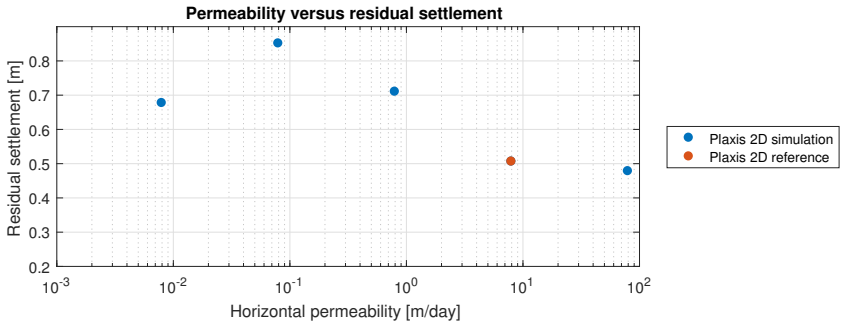

Figure 7.9: Influence of changes in permeability of the sandpile on the residual settlements, simulated with Plaxis 2D.

The plot in figure 7.9 shows that an increase in horizontal permeability results in a decrease in residual settlement. By lowering the permeability of the sandpile, the excess pore water pressure in the clay requires more time to be drained by the sandpile. Therefore, the consolidation rate is lowered and so is the settlement rate. In figure 7.10 the settlement curves for different values of permeability of the sandpile are plotted.

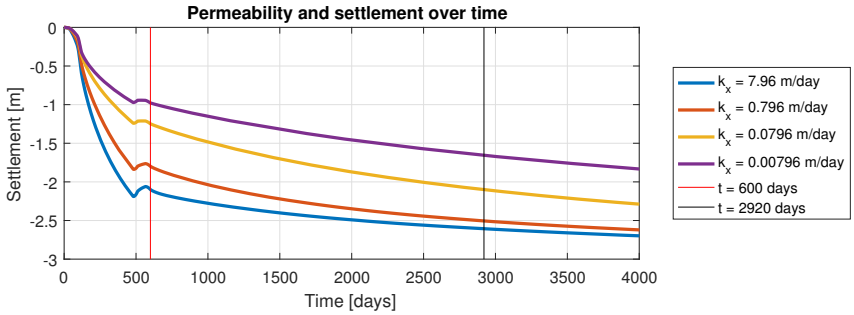

Figure 7.10: Settlement over time of different values of sandpile permeability, simulated with Plaxis 2D.

The settlement curves in figure 7.10 show that the settlement during construction (t=0 until t=600 days) is positive correlated with the sandpile permeability; a higher permeability results in a higher settlement during the construction phase. After the construction phase the increase in settlement between t=600 days and t=2920 days (residual settlement) increases with a decrease in permeability. However, the settlement curve of k_x=0.00796 m/day is showing a different trend.

The observed behaviour of the sandpile at a low permeability can be explained by the degree of consolidation. In figure 7.11 the degree of consolidation is plotted for each case at both the end of construction (t=600 days) and the end of the considered period of 8 years (t=2920 days).

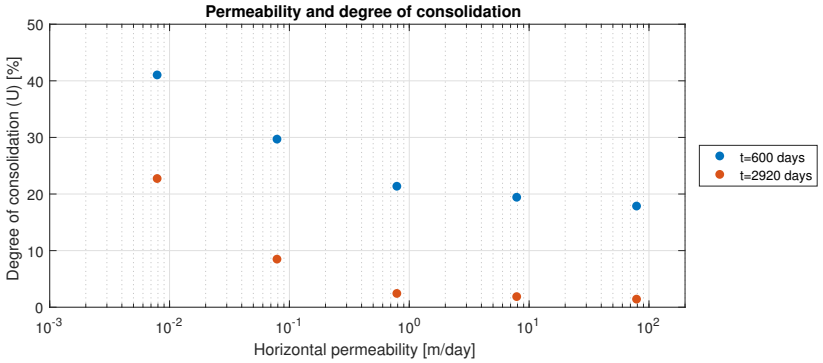

Figure 7.11: Settlement over time of different values of sandpile permeability, simulated with Plaxis 2D.

As can be observed in the figure above, the degree of consolidation in the least permeable sandpile simulation is relatively high (>20%) at the end of the considered 8 years. This indicates that the soft soil layers are still undergoing primary settlement due to pore water dissipating from the pores. With an increase in permeability, the degree of consolidation is close to zero at the end of the time span considered, meaning the primary settlement is nearly completed. The lower residual settlement belonging to the least permeable pile is therefore caused by the still ongoing primary settlement, in contrast with the other model where the primary settlement is nearly completed.

7.3. Multiple variable analysis

In the second phase of the sensitivity analysis multiple parameters are varied in order to quantify the inter-dependency of the parameters. Based upon the results of the first phase of the sensitivity analysis (section 7.2), the sandpile radius and the centre to centre (ctc) distance are used as input parameters. The section concludes with multiple-variable sensitivity analyses in which the properties of PVDs and rigid inclusions are used for simulating the performance of those techniques.

7.3.1. Radius and centre to centre distance

The inter-dependency of the radius and the centre to centre (ctc) distance is researched in this section. In the previous phase of the analysis these parameters, together with the sandpile length, are found to affect the performance of the sandpile the most. However, the sandpile length is constant at the designed length of 27.0m, shorter piles are found to reduce the performance significantly (section 7.2). Varying this length will therefore not result in a feasible alternative. The values of both the ctc distance and the pile radius parameters used in the analysis are listed in table 7.4. All possible combinations of both parameters are researched, the total amount of simulations needed for this analysis is therefore 42. In order to quantify the performance of the sandpiles the residual settlement of each model is plotted together with the pile radius and the ctc distance. The residual settlement is defined as the difference in settlement between the end of the construction phase and the end of the time span of the construction (section 7.1). In table 7.4 the results of the multiple variable analysis are listed.

Table 7.4: Performance measured in residual settlements [m] of the different sandpile configurations, obtained from the multiple variable sensitivity analysis.

Performance [m]	**Centre to centre distance [m]**					
Radius [m]	1.50	2.00	2.50	3.00	3.50	4.00
0.10	0.263	0.371	0.549	0.715	0.787	0.835
0.20	0.298	0.271	0.366	0.506	0.641	0.730
0.30	0.346	0.282	0.298	0.392	0.534	0.652
0.35	0.414	0.312	0.294	0.355	0.487	0.611
0.40	0.493	0.352	0.304	0.332	0.447	0.570
0.50	0.675	0.460	0.362	0.342	0.389	0.502
0.60	0.869	0.593	0.446	0.373	0.368	0.444

The results as listed in table 7.4 are visualised in a 3D plot in figure 7.12. In this figure the x- and y-axis are the different values of radius and ctc distance. The z-axis indicates the performance of the different sandpile configurations.

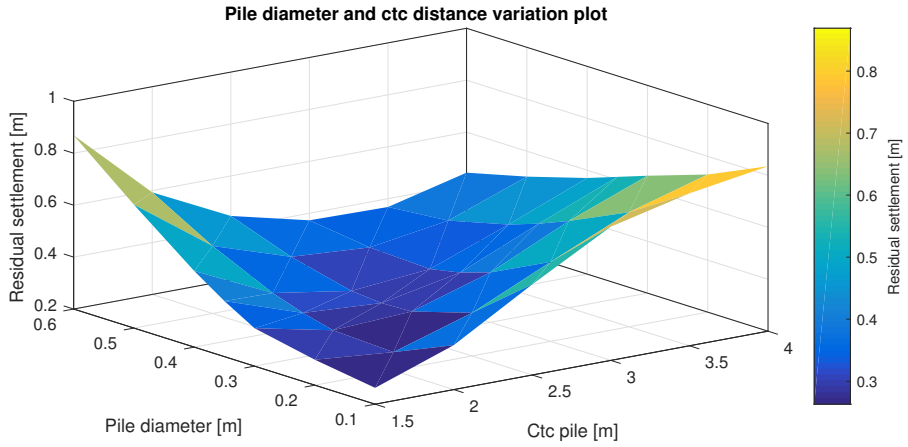

Figure 7.12: Result of multiple-variable sensitivity analysis. The performance of all the possible combinations of sandpile radius and ctc distance is plotted as a 3D surface.

As can be seen in figure 7.12, the performance of the sandpile is increasing when a smaller ctc distance is used in combination with a small pile diameter. As explained in section 7.2.3 and 7.2.4, the self-weight is affecting the performance of the sandpile. The ratio between unit cell surface and sandpile cross section is usually referred to as the area replacement ratio (A_r). In figure 7.13 the performance of the sandpile is plotted for different values of A_r.

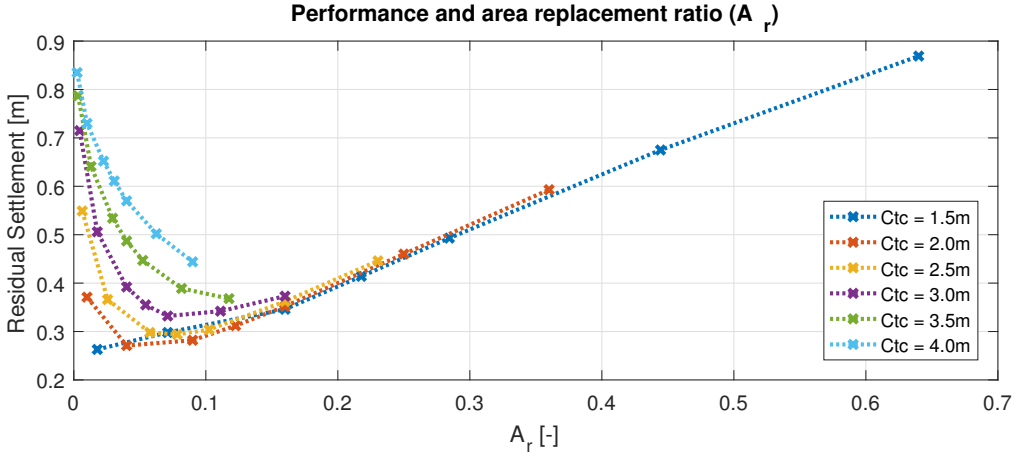

Figure 7.13: Residual settlement versus area replacement ratio, plotted for different ctc distances.

The plot in figure 7.13 shows that for small ctc distances the models with a relative high A_r have a relative high residual settlement compared to the models having a low area replacement ratio. The plots of the larger ctc distances show the opposite trend. The plot also indicates that for a certain area replacement ratio multiple values for the performance are found, depending on the ctc distance. When observing the plots in figure 7.13 it can be noticed that the plots have an optimum A_r in which the residual settlement is the lowest. In order to find a trend in the optimums extra simulations are performed. In the figure below the results of the extra simulations are presented.

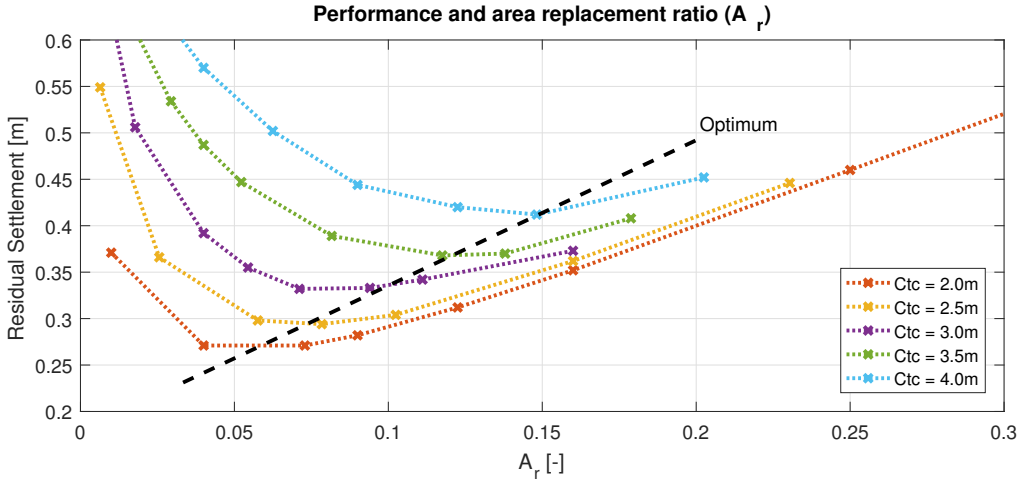

Figure 7.14: Observed trend of optimum in A_r for different ctc distances.

In the figure above the optimal A_r for each ctc distance is indicated with the dotted line. The observed optimum can be found at a lower A_r for smaller ctc distances, increasing with an increase in ctc distance. The requirement regarding the residual settlements do not specify a minimum value; in general the target is to minimise the residual settlements. The graph approaching the optimums in figure 7.14 can therefore be utilised for acquiring the pile geometry resulting in the lowest residual settlements.

7.3.2. Prefabricated vertical drains

The input parameters of the unit cell can be adjusted such that the sandpile has properties similar to a prefabricated vertical drain (PVD). The differences between the two the relative high stiffness and large radius of the sandpiles, while PVDs have no stiffness and a relative small radius. By changing the stiffness, radius and ctc distance, the model can be used to simulate a PVD. In table 7.6 the reference- and updated properties used for simulating the PVD are listed. The radius, ctc distance and length of the PVD match with the PVD design conform UNAM [2]. The settlements calculated with the reference sandpile model and the new PVD model are presented in figure 7.15. As can be observed in the figure, the rate of settlement is lower for the PVD simulation than the sandpile simulation. This is against the expectation, as earlier results (section 7.2.4) show that a lower ctc distance is increasing the consolidation rate.

The Plaxis 2D simulation shows an increase in excess pore pressure at the location of the PVDs during loading, which indicates that the drain is not functioning well. In order to make sure that the drain is fully functional, a numerical drain is placed at the boundary over the full depth of the PVD (r =0.05m). This drain ensures that the PVD is able to drain water during the construction and consolidation phases. The Plaxis 2D model with the drain installed at the border of the PVD is referred to as the 'PVD adjusted' simulation, as shown in figure 7.15.

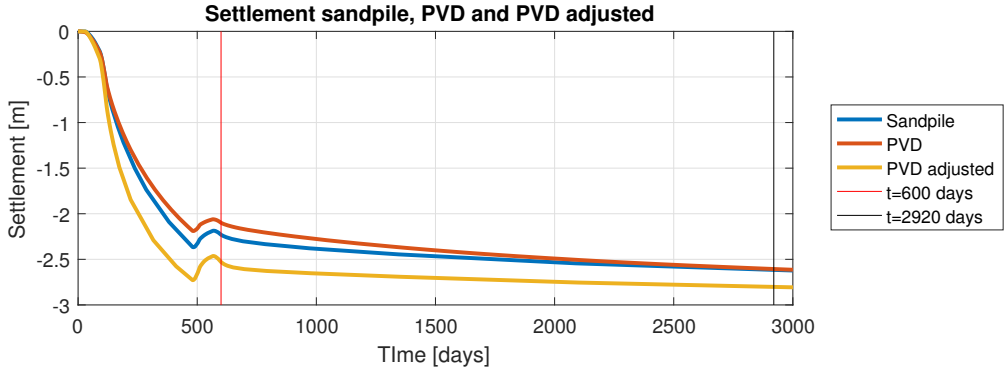

Figure 7.15: Settlement over time for reference sandpile and the model adjusted to match the PVD properties. The adjusted PVD model has a drain installed at the border of the 'PVD'.

The PVD adjusted model shows an increase in settlement during the first 600 days and a reduction in residual settlements afterwards. In table 7.5 the obtained values for the residual settlements are listed. Note that the installation procedure of PVDs differs from the installation procedure of sandpiles. The permeability of the soft soil layers in the direct surrounding of the PVDs is likely to be remoulded, creating a smear- and transition zone (section 3.5.1). As described by TASANA the influence of smear is taken into account by lowering the permeability of the adjacent soil layers with a smear factor (s_f), in case of a ctc distance of 1.5m this factor is 0.92 [34].

The results of the multiple variable analysis taking no drain stiffness and a small radius into account are presented in both table 7.5 and figure 7.15. The difference in performance compared to the original sandpile design is caused by the smaller ctc distance of both techniques. The reduced stiffness of the sandpile in order to model the drain is not influencing the performance of the pile, as described in section 7.2.1.

Table 7.5: Results of simulations PVD models together with reference sandpile performance.

Performance	**Settlements**			
Model	**t=600 days**	**t=2920 days**	**Residual**	**Unit**
Sandpile	2.102	2.608	0.506	[m]
PVD	2.230	2.620	0.390	[m]
PVD adjusted	2.529	2.802	0.271	[m]

Table 7.6: Adjusted input parameters for simulating the behaviour of the PVD and rigid inclusion, together with the reference values used for simulating the behaviour of the sandpile.

Parameter	**Name**	**Sandpile**	**PVD**	**Rigid inclusion**	**Unit**
Material model	Model	HS	HS	Linear Elastic	-
Geometry					
Pile length	L_p	27.0	27.0	27.0	$[m]$
Pile radius	r_p	0.20	0.05	0.15	$[m]$
Centre to centre distance	ctc	3.00	1.50	3.00	$[m]$
General					
Unit Weight (dry)	γ_{unsat}	17.00	12.10	24.00	$[kN/m^3]$
Unit Weight (wet)	γ_{sat}	18.00	12.80	24.00	$[kN/m^3]$
Parameters					
Young's Modulus	E'	-	-	10.00E7	$[kN/m^2]$
Poisson's ratio	ν'	-	-	0.00	[-]
Secant stiffness*	E_{50}^{ref}	30.0E3	3.00E3	-	$[kN/m^2]$
Tangent stiffness**	E_{oed}^{ref}	30.0E3	3.00E3	-	$[kN/m^2]$
Unloading/reloading stiffness	E_{ur}^{ref}	90.0E3	3.00E3	-	$[kN/m^2]$
Groundwater					
Horizontal permeability	k_x	7.96	7.96	Non porous	$[m/day]$
Vertical permeability	k_y	7.96	7.96	Non porous	$[m/day]$
Extra					
Smear factor	s_f	1.00	0.92	1.00	[-]

*In standard drained triaxial test
**For primary oedometer loading

7.3.3. Rigid Inclusions

In this section rigid inclusions as soil improvement method are compared with the sandpiles. The aim of installing rigid inclusions into the subsoil is to reduce the load applied on the top soil layers by transferring them towards the deeper stiffer soil layers. In the most ideal case, the rigid inclusions transfer all the load from the surface level towards a stiff sand layer, which has limited settlements. The main difference in properties between both methods is the high stiffness and non porosity of the inclusions, compared to the lower stiffness and high permeability of the sandpiles. In order to model the rigid inclusion, a linear elastic material model is used. In table 7.6 the properties of the reference sandpile are presented, together with the properties of the rigid inclusions. The settlement of the improved soil by both rigid inclusions and sandpiles are plotted in figure 7.16.

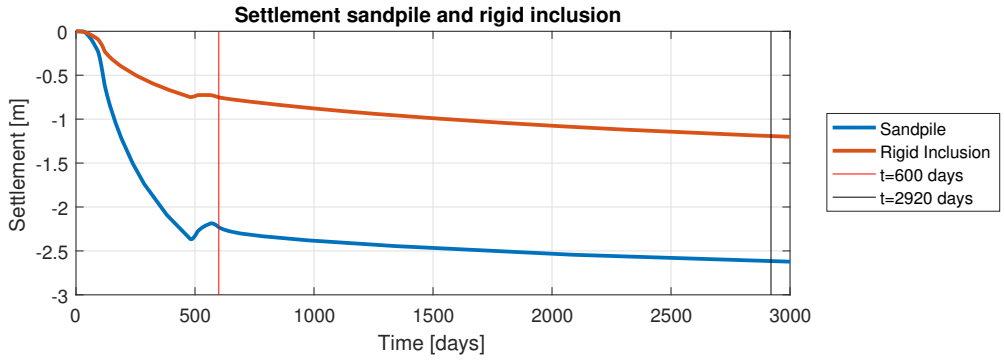

Figure 7.16: Settlement of sandpile and rigid as soil improvement method, simulated with Plaxis 2D.

The plot in figure 7.16 shows a large difference in settlements between the two methods. In section 7.2 it

was investigated that the effect of pile stiffness is not contributing to a change in performance, while changing the permeability will only reduce the rate of consolidation, not lower the total settlement. However, the analysis performed in section 7.2 was based on the HS material model, in this analysis an linear elastic (LE) model is used. The LE material model is chosen because the HS model is not capable of modelling a material with zero permeability and a very high stiffness. The stress nodes in the Plaxis 2D simulation all reached plastic failure due to the very low effective stresses of the material inside the inclusion.

The effect of changing the material model of the rigid inclusion from HS to LE is visible in the settlement of the column itself. Where the sandpile is limited in the stress transfer from the top load towards the deeper soil layers, is the rigid inclusion providing this transfer of stresses. The pile itself does not bulge upon loading, therefore not losing any stiffness over time. The performance of the pile is quantified in table 7.7.

Table 7.7: Results of simulation rigid inclusion model together with reference sandpile performance.

Performance	**Settlements**			
Model	**t=600 days**	**t=2920 days**	**Residual**	**Unit**
Sandpile	2.102	2.608	0.506	[m]
Rigid inclusion	0.752	1.193	0.441	[m]

Note that the consolidation process is still ongoing in the rigid inclusion simulation, the residual settlements become larger when the considered time span increases. The rigid inclusions as soil improvement method transfer the loads applied at the surface level to deeper, often stiffer, soil layers. As the inclusions are non porous, these piles are not providing any drainage to the soft soil layers surrounding the piles. When looking at the settlement of the subsoil presented in figure 7.16, it can be observed that the main settlement and therefore the primary consolidation is still ongoing during the considered time span. Therefore, the total settlements might be lower compared to the sandpile, but the residual settlements will be high, especially when longer time periods are evaluated.

7.3.4. Stress transfer

The transfer of stresses from soil towards rigid inclusion is

7.4. Comparing results

The performance of the sandpiles, PVDs and rigid inclusions as soil improvement techniques are analysed in the previous subsections. In addition the performance of the unimproved 'reference' soil is presented, in order to compare the effectiveness of the methods with the unimproved soil response. The performance of the three improvement methods together with the results of the unimproved reference simulation are listed in table 7.8.

Table 7.8: Result of reference model, compared with the performance of the sandpile, PVD and rigid rigid inclusion, simulated in Plaxis 2D.

Performance	**Settlements**			
Model	**t=600 days**	**t=2920 days**	**Residual**	**Unit**
Reference	0.864	1.414	0.550	[m]
Sandpile	2.230	2.615	0.385	[m]
PVD	2.520	2.800	0.280	[m]
Rigid inclusion	0.752	1.193	0.441	[m]

The material models and properties used in the simulations are listed in table 7.6. The performance of the different methods indicate that the soil improved with the PVD results is the most effective in reducing the residual settlements during the considered time period. The sandpiles are less effective, in section 7.2 it is explained that the self-weight of the sandpile is causing additional settlements of the deeper clay layers, resulting in an increase in residual settlements. Finally, the rigid inclusions are the least efficient in reducing the residual settlements. The rigid inclusion is not capable of transferring the majority of the surface loads to

the deeper, stiffer soil layers, therefore the total effect of the improvement method on the residual settlements is limited. The performance of both the natural 'reference' soil and the soils improved with the three different techniques are visualised in figure 7.17.

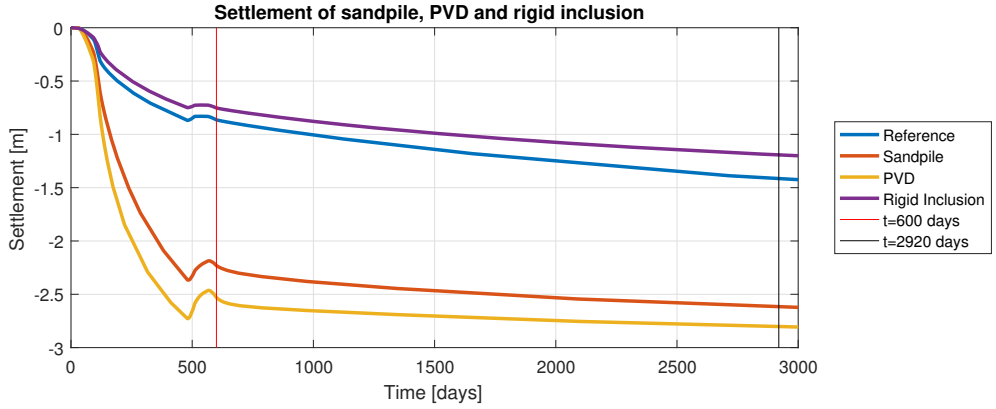

Figure 7.17: Settlement of sandpile and rigid inclusions as soil improvement method, simulated with Plaxis 2D.

Figure 7.17 shows the performance of the reference case, in which the runway structure is constructed on top of the natural unimproved soil. It can be noted that the main settlements of both the reference simulation and rigid inclusion are still ongoing after a period of 8 years. When considering the application of rigid inclusions as soil improvement technique it is important to take into account that the final settlements will be close to those of the other improvement methods. When the time period considered increases, the performance of the rigid inclusions will therefore decrease significant.

The settlement curves of both the sandpile and PVD indicate that the majority of the settlements take place during the construction of the runway structure, as can be observed in figure 7.17. Both the improvement methods ensure that the majority of the primary settlements take place in during the construction phase, limiting the residual settlements. Therefore, when only the performance is taken into account, it can be concluded that both sandpile and PVD increase the performance of the soil significantly. Based upon the results of the simulations and the analysis performed in section 7.2, it is proved that the PVD is the most efficient method for reducing the residual settlements of the runways at the NAICM site.

8

Discussion and Limitations

The approach used for the numerical modelling of the sandpiles is based on several assumptions and is subjected to numerical limitations affecting the results of this research. In this chapter the assumptions and simplifications of the modelling approach are listed and explained. Additionally, the findings and limitations of this research are discussed.

8.1. Assumptions, simplifications and limitations

In this section the assumptions and simplifications which this research is based on are listed. Furthermore, the limitations of this research are discussed.

Assumption and simplifications

The subsoil at the trial embankment site is simplified by a set of homogeneous soil layers. The heterogeneity of the subsoil in both the geometry and the material properties of the soils are not taken into account. During the modelling of the sandpile behaviour multiple simplifications have been applied. The area of influence of the sandpile is modelled as a circle around the pile, while in reality this area could be a square or hexagonal. The groundwater table in the models remains constant over time, the effects of precipitation and seepage are not taken into account.

The sandpiles are 'wished in place', the installation effects of the sandpiles on the surrounding soft soil are not known and neglected in the numerical models. It is possible to take the installation effects into account by adjusting the material properties and stresses in the subsoil, but as no information regarding the installation procedure and measured data was available, the changes in the subsoil could not be modelled or verified. In the model verification chapter the numerical model has been adjusted to fit the measured field data, the installation effects regarding the permeability of the surrounding soft soil are incorporated in the model by adjusting the material properties.

In the numerical models the behaviour of the sandpile and soft soil are simulated by using a set of material models. The models used, both the basic Mohr Coulomb (MC) and the more advanced hardening soil (HS) and soft soil creep (SSC), are not capable of simulating the exact behaviour of the materials. Material behaviour including softening and small strain stiffness are not considered in this study. The properties of the sandpile material are tested in the trials, therefore a set of material properties is taken from literature. This set of properties is not validated.

The material properties of the soft soil layers are validated based upon limited data retrieved from the trial embankments. During the trials only the response of the top soft soil layers upon loading is measured, the response of the deeper clay layers is not analysed. The subsidence of the region caused by deep water extraction is not included in the models, a constant rate of subsidence over time is assumed in the analysis.

The analysis performed considers static loading due to the construction of a runway structure. Dynamic loading due to earthquakes or traffic passing the structure is not taken into consideration. Failure of the sandpile due to horizontal loading is not taken into consideration

Limitations

Accurate modelling of the stress development in the sandpile was not possible. Stress oscillations are generated during the simulation, which are caused by the large differences in hydraulic conductivity between sandpile and soft soils. The critical time step described the minimum time step required for accurate simulation of the consolidation process. Adjusting the mesh size, tolerated error and initial time step did result in less oscillations in stresses.

8.2. Discussed aspects

In this section the findings of the different stages of the research are discussed.

8.2.1. Theoretical background

In the literature review it is shown that the theorem regarding the consolidation of soft soil and the application of vertical drainage is captured quite well in analytical models. The difficulty in modelling the behaviour of granular columns with an analytical model is the non-linear behaviour of these columns. The column in terms of behaviour is not only time dependent, but also stress dependent. The models reviewed in the theoretical background are based upon many assumptions which enable the simulation of one or two aspects regarding the column behaviour. An accurate analytical model capable of simulating accurately the behaviour of a granular column is not available yet. Most of the literature considering the behaviour of granular columns are using the unit cell approach. Therefore the analysis preformed in this research is also considering the unit cell approach.

8.2.2. Site conditions

The installation depth of the soil improvement methods is limited due to the differences in hydraulic head of the different soil layers. The maximum installation depth is located at -27.0m below surface level, 3.0m above the drained Capa Dura (CD) layer. This design requirement prevents a hydraulic shortcut between two aquifers. The sandpiles are therefore designed as 'floating' piles, the pile tip is not connected to the underlaying stiff layer and is therefore not 'end-bearing'. The limitation in installation depth has a large influence on the performance of the sandpiles, as the deeper clay layers positioned underneath the sandpiles remain unimproved. The self-weight of the sandpiles is causing additional settlements at these layers, which reduce the performance of the sandpile significantly.

8.2.3. Analytical modelling

The research started with the use of analytical models in order to increase the knowledge about the sandpile behaviour.

Unit cell

As most of the analytical models provide an approximation of the sandpile behaviour based upon an unit cell, this type of model was used throughout the whole research. By using an unit cell, an cylindrical representation of the sandpile and surrounding soil, some approximations have been made. First the area of influence of the sandpile modelled is an equivalent of the real area of influence, which shape depends on the grid in which the piles are installed. By using the equivalent area the soil influenced by the sandpile can be modelled as an unit cell.

Simplifications

The use of analytical models enables a relative quick first estimate on the behaviour of the sandpile and surrounding soil. However, the analytical models used in this research are based upon many simplifications. These simplifications are crucial as the behaviour of the sandpile is both non-linear and time dependent. The analytical models in the analytical approach are therefore used as a first assumption, taking the simplifications into account.

8.2.4. Numerical modelling

The transition from analytical model to advanced realistic model for simulating the behaviour of the sandpile is done using three model stages, Model 1, Model 2 and Model 3.

Model axisymmetry
The numerical finite element (FE) software Plaxis 2D is used for simulating the behaviour of the sandpile. The model type used is the axisymmetrical model, which is similar to the unit cell approach used in the analytical models. A 2D cross section over the radius of the cell is modelled and rotated along the $y-axis$. The simplification made in the axisymmetric model is the assumption of an embankment with infinite width and length on top of the subsoil, resulting in an over-estimation of stresses in the deeper soil layers. Furthermore, the axisymmetric model assumes homogeneous horizontal stresses and geometry in the subsoil. The numerical models are therefore not able to simulate failure of the sandpile due to horizontal loading.

Mesh size and quality
The software used enables the user to automatically generate a mesh in the geometry of the soil created. The mesh size used in this research is set to very fine, but even with this refined mesh the simulation initially proved to be of a low quality, especially in the areas with large differences in settlement. The mesh size in these areas have been manually refined in order to improve the quality of the mesh.

Tolerated error
The tolerated error in the Plaxis 2D software governs the allowed error in each calculation step. The default value of this error is 0.01. In order to speed up the calculation procedure this value can be increased, so less iterations are needed to reach this maximum error. During the sensitivity analysis many simulations were required, in order to limit the time consumed by running the simulations the tolerated error has been set to 0.05. The deviations in the simulated settlement for the default- and adjusted tolerated error have been researched and proved to be negligible.

Model stability
The stresses generated in the sandpile during the consolidation analysis are oscillating. Due to the large differences in permeability of both the sandpile and soft soils adjacent to the pile, the stresses are not calculated precisely. Further refinement of the mesh, lowering the tolerated error or changing the first time step did not influence the accuracy of the stresses simulated. As the magnitude of stress oscillation remains within reasonable boundaries, the effect on the performance of the sandpile is minor. The oscillations are believed to be caused by the large difference in hydraulic conductivity between the sandpile and surrounding soft soils, the critical time step calculated is not suitable to model the stresses correctly in both materials.

8.2.5. Model verification
The numerical model is verified by measurements obtained from trial embankments constructed on the NAICM site. The input of the soil material properties in the Plaxis 2D model is adjusted in order to match the measured data. The data available for the model verification was limited, the measured data of two piezometers, one pressure cell and the monitored settlement of the trial embankment was available. The adjusted material properties enable the numerical model to simulate behaviour which is considered to be more similar to the measured behaviour than the default material properties. Note that the fit obtained is not the only possible set of material properties providing a close fit to the measured results. There is a range of properties which could provide a close fit to the measured results. The field data provided is not complete enough to determine to reduce this range. However, it is assumed that the set of material properties used in the numerical models generate reliable results, based on the close match between simulated results and the trial results.

In order to increase the validity of the simulated behaviour, more data from the trial embankments is needed. The development of excess pore pressures in all clay layers could improve the validity. Furthermore, the use of extensometers for measuring the deformations of the sandpile could contribute to the reliability of the model verification. The heterogeneity present in the natural soil layers is not represented in the modelling of the subsoil.

8.2.6. Sandpile sensitivity analysis
The main findings of the sandpile sensitivity analysis are discussed in this section.

Single variable analysis
In the sandpile sensitivity analysis the sensitivity of the model to changes in sandpile properties is researched. The properties investigated are the length, radius, centre to centre distance, permeability and stiffness of

the sandpile. The bandwidth of permeability and stiffness are not likely to be very broad. Varying these parameters provides insight in theoretical cases and is performed for academic purpose. The pile length, centre to centre distance and pile radius are realistic properties which can be varied in order to optimise a ground improvement design.

Multiple-variable analysis

The centre to centre distance and pile radius proved to be the most dominant sandpile properties influencing the sandpile performance. In the multiple variable analysis these parameters have been varied together in order to investigate the performance of each combination. The performance of the pile was largely influenced by the self-weight of the pile. Simulations in which the pile has a combination of a relative high area replacement ratio the simulation resulted in large residual settlements. The increase in load due to the higher area replacement ratio is resulting in a higher stress increase in the deeper clay layers, which generate more settlement over time. The performance of different area replacement ratios has been plotted and a trend is found in optima for different ctc distances. These optima depend on both the length of the drainage path between two drains and the self-weight on the pile itself.

Performance of PVDs and rigid inclusions

The performance of the most optimal sandpile configuration is compared with the performance of two alternative soil improvement methods, namely PVDs and rigid inclusions. The main difference between using PVDs and sandpiles is the additional stiffness that the sandpile adds to the improved soil, unlike PVDs. The performance of the PVDs is analysed by using the same numerical model but with adjusted values for the pile radius and stiffness, in order to match the properties of the PVDs. The length, radius and centre to centre distance of the drain are chosen conform the design of TASANA [34]. The low-self weight of the PVD is causing almost no additional load to the soft soil layers underneath the drain, in contrast to the sandpile. This difference in self-weight is the main cause of the difference in performance, in which the PVD shows less residual settlement over a time span of 8 years. With an increase in time period it is expected that the difference in performance will increase, as long as the deeper clay layers consolidate.

The rigid inclusions as soil improvement method do not contribute to a reduction of the drainage path for pore water trapped in the soft soil layers. The main function of the concrete piles is to transfer the load applied on top of the subsoil towards the stiffer deeper soil layers. These stiffer soil layers have often a lower settlement potential, therefore reducing the total settlement of the improved soil. The rigid inclusion is modelled with the numerical model, conform the geometry of the inclusions as listed in the UNAM report [2]. The material model for the pile was set to a linear elastic (LE) model, in order to model the non-porous and pure elastic behaviour of the concrete pile. The rigid inclusion proved to be less effective in reducing the residual settlement compared with the PVD and Sandpile. The non-porous behaviour of the pile resulted in an unimproved consolidation rate of the soft soil layers. The consolidation occurring during the construction of the runway was limited, the primary consolidation is still ongoing after completion. Thus, the total settlement occurring during the considered 8 years is less compared to the other improvement methods, but the performance is significant lower compared to the PVD and sandpile.

9

Conclusions and Recommendations

In this chapter the conclusions of the research questions are listed, after which the general conclusion is presented.

9.1. Answers to research questions

Research questions 1-5, provided in the introduction to this study, are answered as part of the conclusion.

1. What is the expected behaviour of the sandpiles at the NAICM site?

The new airport of Mexico City (NAICM) is positioned on thick layers of Mexico clay soils, which are characterised by their high water content and impressibility. In order to built on the NAICM site, the subsoil needs to be improved. In this research, the improvement of the subsoil at the NAICM site by sandpiles is researched. In order to study the expected behaviour, analytical models are have been used. Upon installation, the relative high stiffness and permeability of the sandpile improve the engineering properties of soft soils. The engineering properties considered are the stiffness and the permeability of the soft soils. The sandpile inside a soft clay layer was modelled by using the unit cell approach. Different analytical models have then been used for estimating different aspects regarding the behaviour of the sandpile and surrounding soil, including the horizontal and vertical deformations, the rate of consolidation and the stress developments.

The expected behaviour of the sandpile in the soft clay layers is the increase in consolidation rate, as the pile provides a reduction in drainage path for the excess pore water trapped in the soft soil. As a result, the settlement rate of the improved soil is increased. In order to reduce the settlements taking place during the operation of the runways (residual settlements), a consolidation period is used as part of the construction phase. During this period the soft soils are allowed to settle, prior to the construction of the runways. A surcharge load is applied during this period to increase the effective stress in the soils. As a result, the soft soil will have an increased over-consolidation ratio (OCR) after removal of the surcharge load. When the final structure is applied on the soils, the increased OCR causes smaller residual settlements and a reduced creep rate during operation.

The settlements over the radius of the unit cell are expected to increase, starting with limited settlements at the edge of the sandpile and increasing towards the outer boundary of the unit cell. Upon loading, the stresses inside the sandpile will increase more compared to those inside the clay layer. The relative high stiffness of the sandpile attracts more of the applied load than the surrounding soft soil. At the moment of yielding, after which the sandpile behaves elastic-plastic, the effective stresses in the sandpile reduce over time until an equilibrium in stress distribution is obtained between the sandpile and surrounding soil. As the vertical stresses inside the sandpile remain higher compared to those in the soft soils during the whole consolidation process, the total settlement of the unit cell is reduced.

2. What material models can be used for modelling sandpiles in a FEM program?

The material models used in the analyses are the Mohr-Coulomb (MC) model and the advanced Hardening Soil (HS) and Soft Soil Creep (SSC) models. The simulated behaviour of both the sandpile and soft soil with use of the Mohr-Coulomb model is similar to those simulated by the analytical models. However, these analytical models simplify the actual sandpile behaviour. The stiffness used in the MC model is constant and the material behaves linear elastic perfectly plastic.

The accuracy of the simulated behaviour can be improved by implementing advanced material models. The Hardening Soil (HS) model and the Soft Soil Creep (SSC) model are used for simulating the behaviour of the sandpile and soft soil, respectively. The advanced material models introduce the stress dependent stiffness of the soil and sandpile and the non-linearity of the material behaviour upon loading. The former changes the constant horizontal deformations of the sandpile towards a 'bulging' type of behaviour, in which the horizontal deformations of the pile are large at the top of the pile and decrease with pile depth. Furthermore, the advanced models are able to take the loading history into account, preventing the simulations from overestimating the plastic deformations of the materials.

3. How do the sandpile design parameters affect the behaviour of the pile?

The influence of the sandpile design parameters have been investigated in the sensitivity analysis. The performance of the sandpiles has been quantified as the magnitude of residual settlements. The lower the residual settlements, the better the sandpile performs. The radius and the centre to centre (ctc) distance are the sandpile properties affecting the performance of the pile the most, while the influence of the pile stiffness on the performance is only minor. The shortening of the ctc distance and the increase in pile radius both improve the performance of the sandpile. The drainage path for the excess pore water is reduced, accelerating the consolidation process. However, an optimum was found for both parameters. The self-weight of the sandpiles induces an additional load to the deeper soft soil layers, resulting in an increase in settlements.

A reduction in sandpile length results in a decrease in pile performance, the soft soil layer positioned underneath the sandpile tip is not improved. In order to prevent a shortcut between aquifers, a minimum distance between pile tip and underlaying drained layer of 3.0m is required. The influence of shortening the sandpile on the settlement rate and total settlement is minor. The layers underneath the sandpile remain unimproved, the consolidation rate in these layers remains low. This results in a reduction in pile performance.

4. What sandpile configuration results in the best performance?

In the multiple variable analysis the ctc distance and the radius of the sandpile are varied together, in order to investigate which design geometry results in the best performance. The performance is quantified by the difference in settlement at the end of the construction period of the runway structure, compared to the settlement at the end of the lifespan of the structure. The best performances were found at a low ctc distance and a low pile radius, from the analysis a ctc distance of 1.5m and a pile radius of 0.10m resulted in the least settlements during the considered period. A sandpile radius of 0.10m is a practical size, therefore a minimum radius of 0.20m is used as the optimum pile radius.

The ratio of soil replaced by sandpiles versus the total soil area is referred to as the area replacement ratio (A_r). A trend is observed in the performance of different combination of ctc distance and sandpile radius. At lower area replacement ratios the performance is increasing by a reduction in ctc distance. At higher values of A_r, starting around 0.10, a decrease in performance is found for lower ctc distances. The optimum ratio between A_r and performance is influenced by both the self-weight of the pile and the length of the drainage path. The length of the sandpile is not varied, a constant installation depth of 27.0m is used in the analysis. A reduction in sandpile length results in thicker unimproved soil layers underneath the pile, resulting in larger residual settlements.

5. How can the numerical model be adjusted to model the PVD behaviour?

The numerical model used for simulating the behaviour of the sandpile is adjusted to simulate the perfor-

mance of a PVD. The geometry of the sandpile is changed to match the geometry of the PVD. The stiffness of the PVD is neglected in this research, a drain stiffness similar to the stiffness of the surrounding soft soils is implemented in the model. At the boundary of the PVD a numerical drain is added, to ensure that water is drained by the PVD.

The last parameter adjusted in the numerical model is the permeability of the soft soils surrounding the pile. The smear- and transition zone due to the installation of the drains is taken into account by introducing a smear factor. This factor represents the reduction of the hydraulic conductivity in the remoulded soil next to the drain. This smear- and transition zones are also present around the sandpiles, but no information was regarding these zones is available. The influence of the smear- and transition zone on the hydraulic conductivity of the surrounding clay is therefore incorporated in the hydraulic conductivity of the soft soils during the model verification.

9.2. General conclusion

The construction of the runways at the NAICM site is challenging, as the soft soils at the site are very compressible. Soil improvement techniques are required to reduce the (differential) settlements of the runways. PVDs are selected as the most efficient method to improve the soil properties and reduce the settlements at the runways. However, the trial embankment with sandpiles as soil improvement technique showed promising results. In this study the applicability of sandpiles as soil improvement method at the NAICM site is researched, as alternative to PVDs. The main research question answered in this study is:

How do sandpiles perform at the NAICM site, with respect to PVDs?

The main difference between PVDs and sandpiles is the high stiffness of the sandpile, while PVDs provide no additional stiffness. The benefits of having an increase in stiffness is the reduction of total settlements of the soft soil layers. However, in this study it is proven that the sandpile installed in the Mexico Clay soils only provides a minor reduction in total settlements. The radial- and vertical deformations of the sandpile prevent shear stress development in the adjacent soft soils, hence limiting the stress transfer towards the pile. The benefit of installing stiff sandpiles over PVDs is therefore negligible. In contrast with PVDs, the installation of sandpiles induces an additional load to the underlaying soft soils caused by the self-weight of the sandpile material. This results in a reduction in pile performance, as higher (residual) settlements are found when improving the soft soil with sandpiles compared to the performance of PVDs. The use of sandpiles over PVDs is therefore not beneficial, even more when costs and installation rates are taken into consideration.

9.3. Recommendations

As discussed in the previous section the sandpiles as soil improvement method at the NAICM site is not a feasible alternative to PVDs. The main difference between the two improvement methods is the high stiffness of the sandpile, which theoretically could increase the total stiffness of the improved soil. However, the stiffness of the sandpile has only a minor affect on the performance, therefore the sandpile provides a very minor reduction to the total settlements of the soft soil. Thus, the main benefit of using sandpiles over PVDs has only little effect on the performance.

The conclusion of this study will not change when more research into the behaviour of sandpiles is conducted, even when extreme scenario's are considered. The sandpiles proved to be less effective than PVDs even when the pile stiffness is increased with a factor 100 (section 7.2.1). There are therefore no recommendations regarding the research into- or the application of sandpiles as alternative for PVDs at the NAICM site.

A

Design of the NAICM

The design of the NAICM site is presented in the figure below.

Figure A.1: Position of the runways, terminals, cargo areas (blue), maintenance facilities (pink), fuel tanks (red) and government facilities (purple) at the future NAICM site [2].

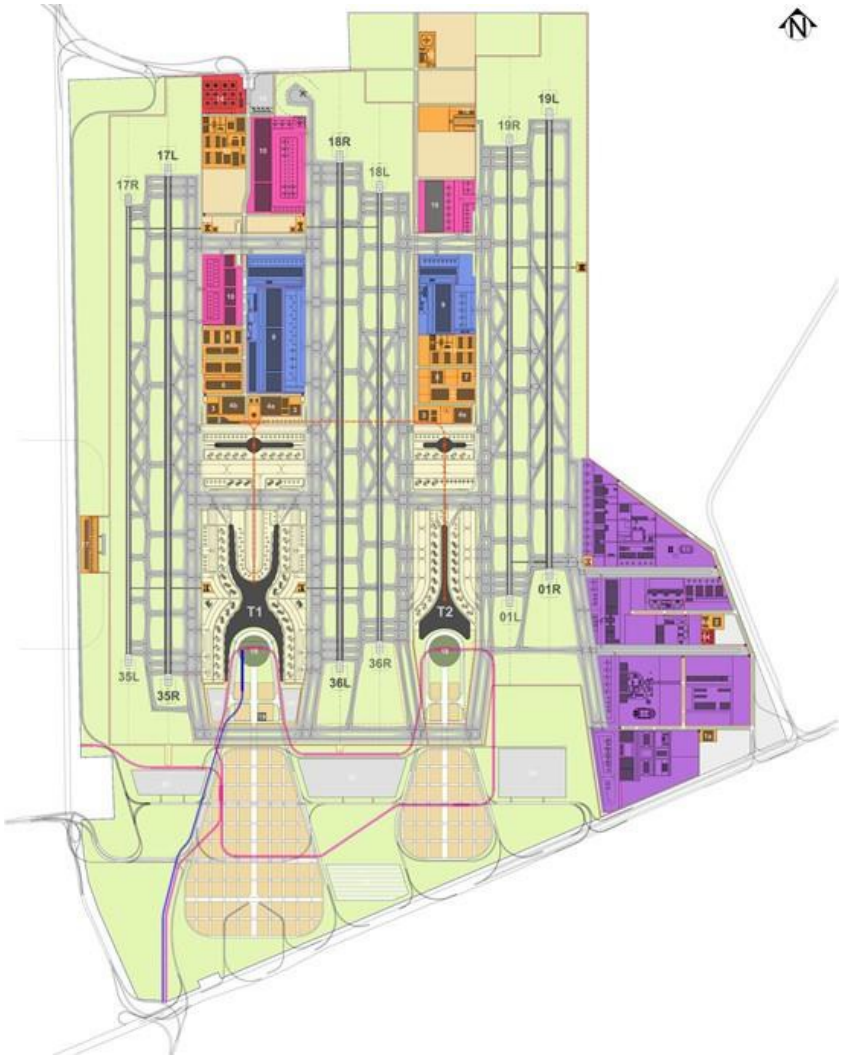

B

Field trial TPDV

In this Appendix one the field tests performed during the NAICM (Nuevo Aeropuerto Internacional de la Ciudad de México) project is discussed. Before the construction of the runways, multiple trial have been performed in order to increase the knowledge about the specific soil conditions and behaviour at the building site. One of the trials used for analysing the soil behaviour is referred to as the TPDV (Terraplén de prueba con Precarga y Drenes Verticales), an trial embankment positioned on top of soil improved with prefabricated vertical drains (PVD) and sandpiles [2]. During the trial the deformations, development of excess pore water pressures and increments in pressure are measured.

B.1. Test location

The NAICM site is located in the North-East direction of Mexico-city, between the highways 57D and 136D. The position of the NAICM site is indicated with the red box in figure B.1.

Figure B.1: Location of the NAICM site (google.maps, 2017).

The area used for experiments is located south of the NAICM zone (Figure B.2), positioned close to the south end of runway 36R.The test area of the TPDV is indicated with the yellow rectangle.

B.2. Soil conditions

The soil at the location of the test embankment has intensively been tested in order to determine the geometry and properties. In section B.2 the geometry of the soil layers is presented, in section B.2 the soil properties of the identified layers are listed.

Geometry of the soil

The soil layers at the embankment test site have been identified by using CPT- and SPT data. The data obtained is translated to a soil profile, which is later checked by using the laboratory tests performed on soil samples taken from the different soil layers. The soil profile as described in the report of UNAM [2] is presented at table B.1.

As can be observed in table B.1 the soil consist of thick clay layers inter bedded by lenses of silty sand. The total thickness of the compressible layers is roughly 50 meters.

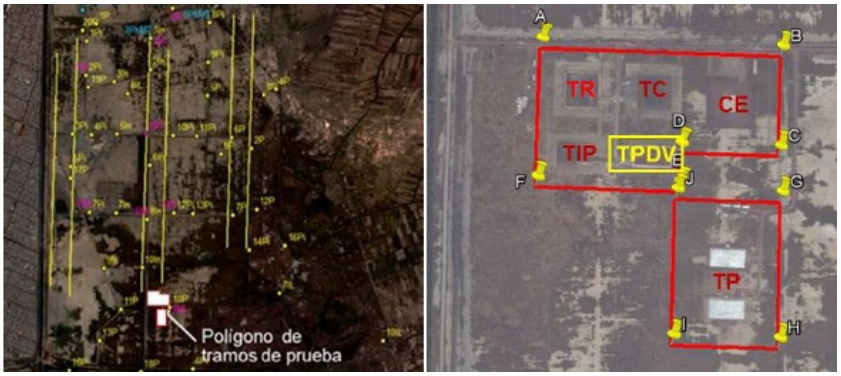

Figure B.2: Location of the TPDV site [2].

Table B.1: Geometry of soil layers at test location [2]

Material	abbr.	Depth top	Depth btm
Surface layer	CS	0.00	0.70
Upper clay layer 1	SAS1	0.70	3.60
Upper clay layer 2	SAS2	3.60	9.00
Sandy silt lens 1	L1	9.00	9.60
Upper clay layer 3	SAS3	9.60	12.60
Upper clay layer 4	SAS4	12.60	22.80
Sandy silt lens 2	L2	22.80	23.40
Upper clay layer 5	SAS5	23.40	24.60
Sandy silt lens 3	L3	24.60	25.20
Upper clay layer 6	SAS6	25.20	30.20
Hard clay layer	CD	30.20	31.30
Deep clay layer 1	SAI 1	31.30	38.40
Deep clay layer 2	SAI 2	38.40	44.10
Deep sand layer 1	DP1	44.10	50.00
Deep clay layer	SAP	50.00	60.00

Soil properties

By performing field permeability tests, undrained unconfined (UU) triaxial testing, SPT's and CPT's, the soil properties of the soil layers as present on the site location have been obtained. The test results can be found in the report of UNAM [2], the soil properties of the different soil layers are listed in table B.2.

Table B.2: Material properties of soil layer at the test site [2]

Material	w	γ	E'	ν'	e0	Cc	Cr	ϕ'	c	Kh	Kv
	%	kN/m3	kPa	-	-	-	-		kPa	-	-
CS	47.78	15.00	10,000	0.33	-	-	-	50.00	35.00	8.10E-02	8.10E-02
SAS1	123.65	12.50	-	0.30	3.28	1.98	0.20	35.00	0.00	1.52E-03	3.03E-04
SAS2	299.04	11.93	-	0.30	6.87	3.07	0.27	36.10	0.00	1.52E-03	3.03E-04
L1	47.89	15.00	15,000	0.33	-	-	-	40.00	20.00	1.07E-03	1.07E-03
SAS3	289.95	12.38	-	0.30	7.41	4.92	0.43	21.86	0.00	1.52E-03	3.03E-04
SAS4	215.34	14.03	-	0.30	7.91	6.51	0.37	36.87	0.00	1.52E-03	3.03E-04
L2	31.82	15.00	15,000	0.33	-	-	-	40.00	20.00	1.07E-03	1.07E-03
SAS5	211.86	12.40	-	0.30	5.61	3.39	0.34	35.00	0.00	1.52E-03	3.03E-04
L3	77.17	15.00	15,000	0.33	-	-	-	40.00	20.00	1.07E-03	1.07E-03
SAS6	223.89	12.46	-	0.30	8.43	8.29	0.45	24.91	0.00	1.52E-03	3.03E-04
CD	47.68	16.00	20,000	0.33	-	-	-	40.00	20.00	2.55E-03	2.55E-03
SAI 1	152.95	12.74	-	0.30	6.69	4.90	0.26	32.29	0.00	2.79E-04	5.59E-05
SAI 2	136.85	13.50	-	0.30	3.63	2.19	0.22	35.00	0.00	2.79E-04	5.59E-05
DP1	38.43	18.00	30,000	0.33	-	-	-	40.00	20.00	3.28E-03	3.28E-03
SAP	87.35	13.56	-	0.30	4.23	0.14	0.05	39.82	0.00	2.79E-04	5.59E-05

B.3. Geometry of test embankment

The geometry in both plan and cross section (over the centre of the embankment) of the TPDV are visualised in figure B.3 and figure, respectively. The rectangular embankment is divided into two parts, the first one is using sand drains (Drenes de Arena, TPDA), in the second part prefabricated drains (Drenes Prefabricados, TPDP) are installed.

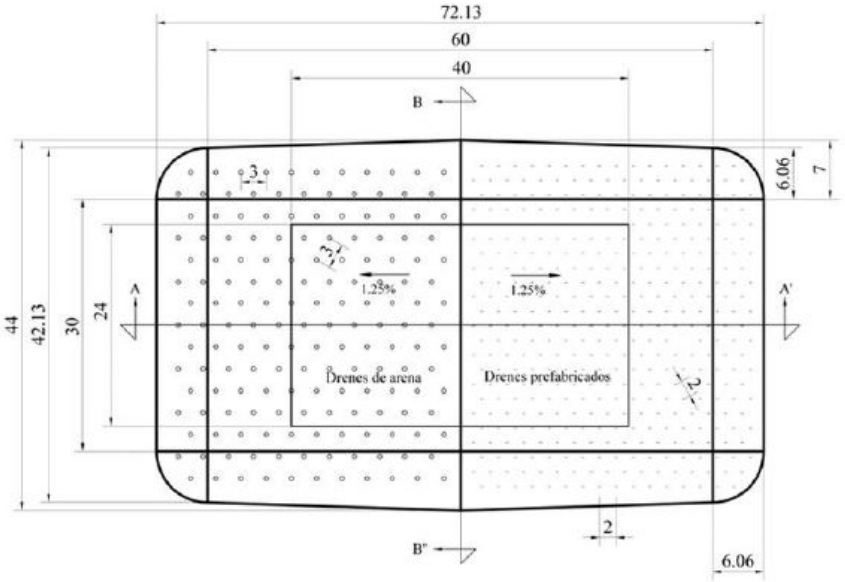

Figure B.3: Plan view of embankment [2].

The total width of the test embankment is 72.13 meter at the toe, at the top of the embankment the width is 60.0. meter. The sand drains are installed with a centre to centre (ctc) distance of 3,0 meter and have a length of 28.3 meter, not penetrating the drained silty sand layer at a depth of 31.3 meter below ground level. The sand drains have a diameter of 0,30 meter. The prefabricated drains are installed with a ctc distance of 2.0 meter, with a length of 31.3 meter penetrating into the strong clay layer. The dimensions of the prefabricated drains in plan view are 100 mm by 3mm.

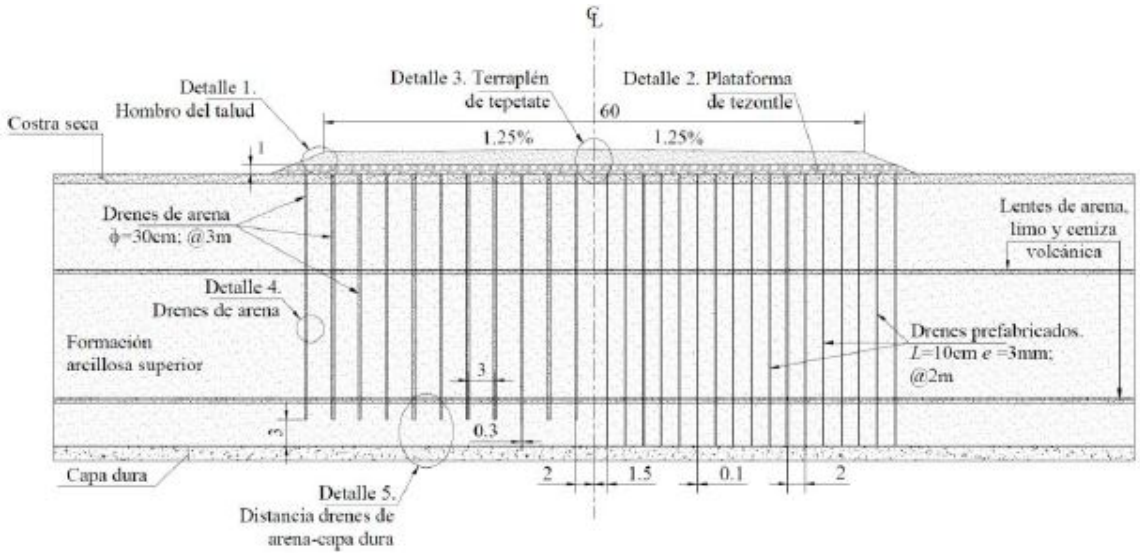

Figure B.4: Cross section of test embankment (A-A') [2].

The geometry of the cross section of the test embankment is visualised in detail in figure B.5. The embankment as constructed on top of the soil consist of a sand layer with a thickness of 1.8 meter on top of a light weight granular layer of Tezontle of 1.0 meter. On the top side of the embankment a talud with steepness 2.5:1 is realised towards the ground level. The sand layer on top of the Tezontle layer has a small gradient of 1.25%.

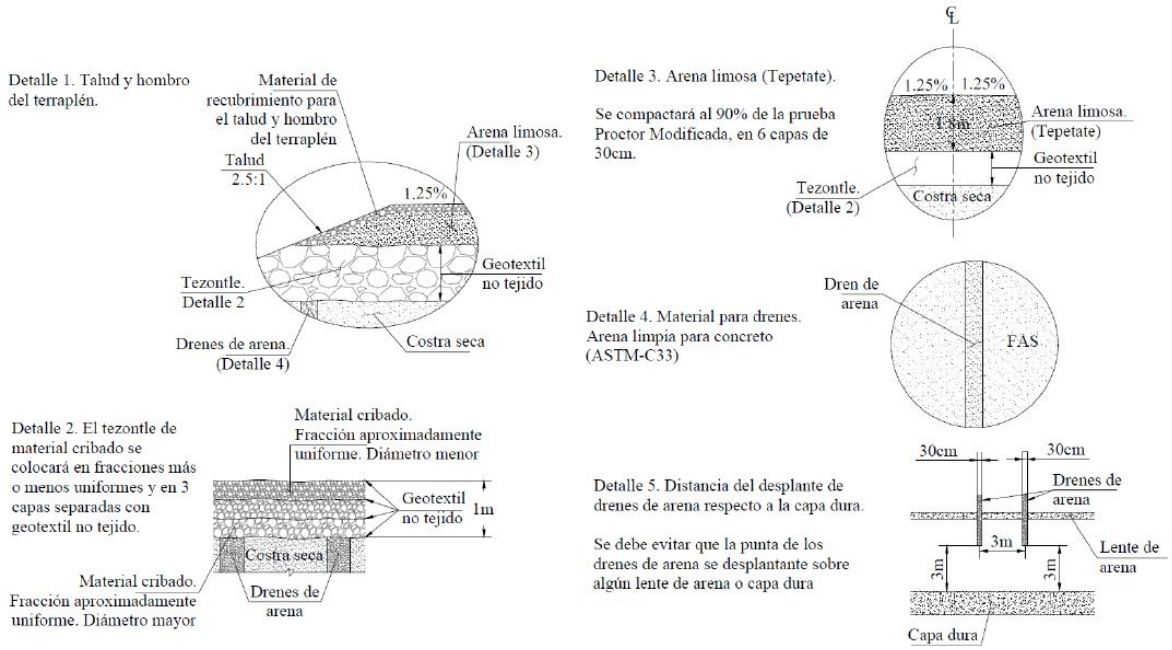

Figure B.5: Details of test embankment [2].

B.4. Measurements devices

In order to measure the behaviour of the embankment and the subsoil, multiple measurement devices have been installed. For the TPDV test the following devices have been installed:

- Pressurecell (7)
- Piezometer (2)
- Horizontal hose (2)
- Inclinometer(8)
- Reference bar under embankment (3)
- Magnetic extensometer (2)

The position of these measurement devices is presented in figure B.6.

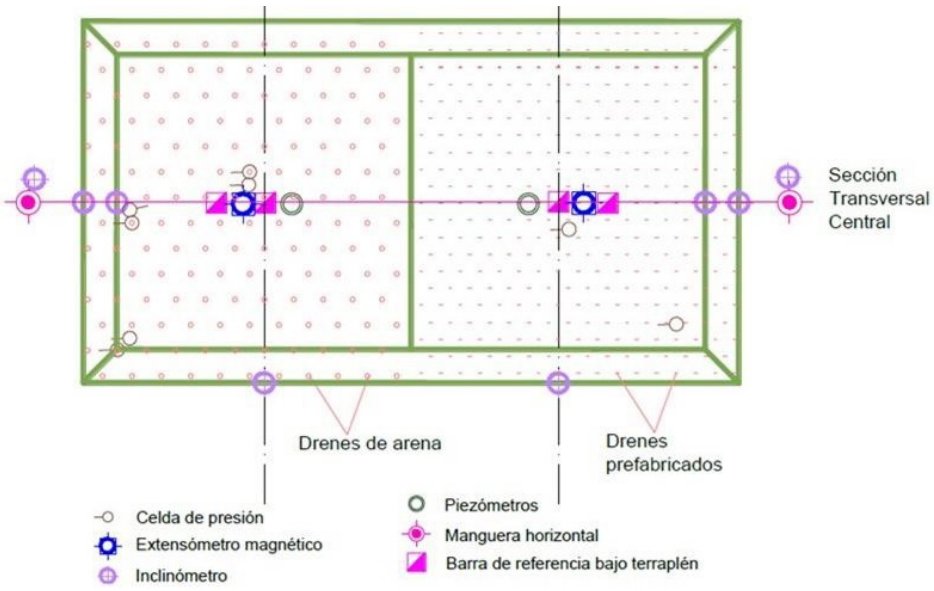

Figure B.6: Position of measurement devices [2].

Pressurecells

The pressurecells are installed to verify the magnitude and distribution of the pressure transmitted to the land and to the sand drains by the embankment. At the embankment with the sand drains, five cells have been installed. The first pair is installed at the centre of the embankment, one positioned at the sandpile and one between the piles. Towards the corner of the embankment, before the last pile, another pair has been installed with the same configuration. The last cell is installed on natural ground between two drains. The embankment with prefabricated drains only two pressure cells have been installed, one at the centre on the natural terrain and another at a corner and on the working platform [2].

Piezometers

The objective of the piezometer is to determine the initial piezometric profile and the excess pore pressure induced in different stages of the construction. The piezometers have been installed in the centre of the embankment with sand drains and one at the centre of the embankment with the prefabricated drains. The meters have been installed at each station at a depth of 4,0m, 9,0m and 18,0m depth [2].

Horizontal Hose

The horizontal hose is installed underneath the Tezontle layer. The hose is used to determine the profile of settlement at the level of natural terrain. The hose is installed at the base of the embankment, passing the central section transverse to the axis of trace. The displacement of the hose is determined by the pressure in the fluid contained inside the hose [2].

Inclinometers

The inclinometers are installed to measure the distribution of the horizontal displacements in the soil with depth, at the shoulders of the slope. A total of 8 tubes were installed of inclinometers at 31m depth, four for the TPDA and four for the TPDP. The distribution in each sub-section is as follows: in the central cross-section, an inclinometer was installed at the shoulder of the embankment, one at the foot of the slope and one more at 5 m distance from the foot of the slope. The fourth inclinometer was installed in an orthogonal section at the foot of the slope [2].

Reference bar under embankment

The reference bar is installed in order to have a control point to the flexible horizontal hose to define the settlement profile. A total of three benches have been installed in the central section transverse to the axis of the trace, one bank to the centre and two more at the ends of the paved area [2].

Magnetic extensometer

The objective of the magnetic extensometers is to evaluate the contribution of sub-strata to the total settlement and the corresponding vertical deformations. Two tubes are installed at 44m depth, one at the centre of the TPDA and another at the centre of the TPDV. Magnetic "plates and spiders" have been installed at a depth of 0m, 2.5m, 5.0m, 7.5m, 11.0m, 13.5m, 16.0m, 20.0m, 24.0m, 31.0m and at the bottom of the boreholes [2].

B.5. Phased construction

Prior to the construction of the test embankment, the site had to be cleaned and the land had to be levelled. Subsequent to the cleaning and the tracing were constructed the perimeter and internal drainage trenches of 0.6 by 0.6m were constructed. Simultaneously to these works the instrumentation system was placed [2].

Start of construction

On September 23, 2014 the construction of the TPDV was initiated with the construction of the work platform of 1m in thickness, which was realised by placing granular material (Tezontle) in three beds inter-bedded by non woven geotextile. An additional geotextile was placed between the natural soil and the first layer of Tezontle. The position of each drain was located with wooden stakes. The prefabricated drains were installed from the surface of the work platform to a depth of 30m, that is 29m below the level of natural terrain (NTN).

The drains were installed with kneading mandrels which protects the drains from landslides, cuts or abrasion during installation. Once placed, the drain was cut leaving a clearance from the top of the platform. When all the prefabricated drains were installed, a first layer of tepetate to place the sand drains was installed. This layer allowed efficient cleaning of the extracted material.

Subsequently the equipment that performed the drilling was placed in the position of each drain. A piece of steel with a diameter of 0.40m was placed up to the indicated depth. Sand placement was performed by free fall through the pipe until it reached the lower level of the working platform. It was necessary to apply vibration to the hopper and air at the end of the pipe.

Once the construction of the drains was completed, the tepetate was placed in layers, of thickness not specified by the contractor. The date at the end of construction was November 26, 2014 [2].

Changes during work

The construction method of the TPDV has a great relevance in its response and behaviour. Initially a procedure was defined to carry out its construction. However, in the field there were some unforeseen events that forces to modify the following aspects:

1. The diameter of the sand drains was prescribed as 0.30m based upon modelling that verified the system was optimal; however the machine of the contractor made holes of 0.40m. This caused an over-volume of sand of approximately 78%.

2. The placement of sand in the tubes. International literature mentions the construction of sand drains with perforator helical with hollow shank, the contractor could not place the sand into the perforation through said shank. The argument was that a arc effect was created which prevented the sand from being deposited. As a result, the contractor had to place a pipe in the drilled hole and deposit the sand through it. This did not solve the problem since the arching effect still occurred. Eventually it was necessary to use an air pump and generate vibration in order to break the arching effect. The consequences are a big overhaul on the drilling walls and major delays.

3. The type of sand used was Tezontle sand which contained up to 6% of fines. Prescribed was concrete clean sand (ASTM-C33), which did not exist in the banks that had been contemplated for the extraction of building materials.

4. The replacement material in the thickness of the dried crust. Clean sandy gravel (Sand> 15% and Fine <5%) were specified. The same type of sand was placed in the drain.

5. The depth of the prefabricated drains. It was specified that these drains should the depth of the hard layer. The installed drains reach a depth of 29m, while the hard layer is found at a depth of 32m.

B.6. Observed behaviour of the TPDV

Pressure cells

The location of the pressure cells (CP) installed at the TPDV are presented in figure B.7. On the left side is the embankment with preload and sand drains (TPDA) and on the right there is the embankment with preload and prefabricated drains (TPDP).

In the TPDA, the TDA-CP-01, 03 and 04 cells measure the stresses in the ground contact. The TDA-CP-02 and 05 cells measure the stresses in the drain contact of the sand-work platform. In the TPDP the sell TDP-CP-01 measures the contact forces on the ground-work platform and the cell TDP-CP-02 measure the stresses of the working platform contact with the tepetate.

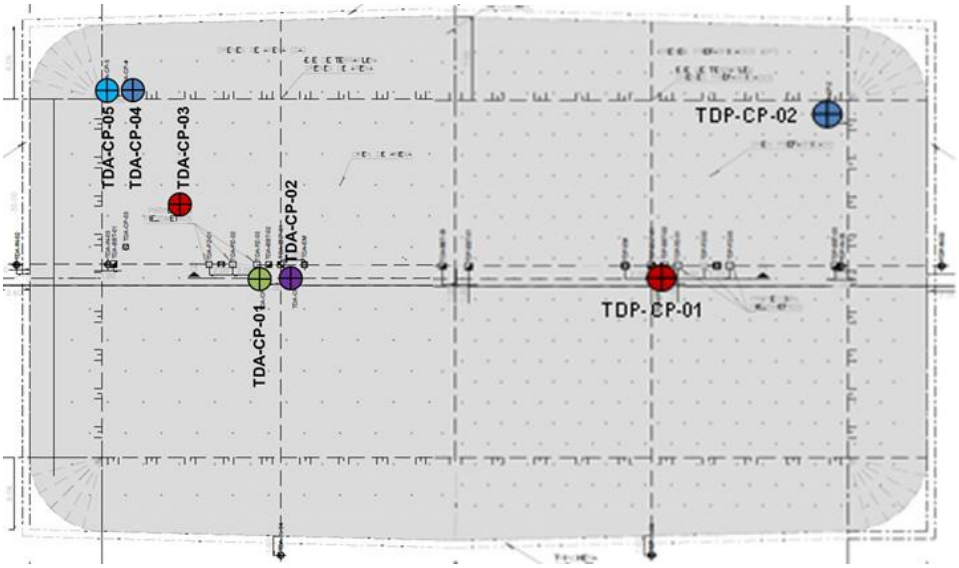

Figure B.7: Position of pressure cells (CP) in the TPDV [2].

In figure @@ and @@ the pressure versus time graphs are shown of each of the CP's installed in the TPDV. With vertical and horizontal lines, the following in indicated;

- The red vertical line indicated the end date of the construction of the platform work.
- The horizontal red line indicates the theoretical pressure corresponding to the weight of the work platform.
- The yellow horizontal line indicates the theoretical pressure corresponding to the weight of the embankment (tezontle and tepetate).

In both figures it is observed that the measured forces with the cells TDA-Cp-01, 03 and 04 and TDP-CP-01, in the dates corresponding to the end of the construction of the work platform and embankment are generally larger than those calculated from the thicknesses and volumetric weights of the tezontle and tepetate embankments. This indicated that there may be over-volumes in the construction of the embankment.

The TDA-CP-02 and 05 cells measure pressure in the sand-platform drain contact, so the start dates of registration are after the start of the construction of the embankment (figure B.8). The pressures recorded in these cells depend on their position and interaction with the drains, terrain and embankment. The cell TDP-CP-02 measure pressures in the tepetate's deflection but registers values lower than the weight of the same (figure B.9), reason why is that it is possible damaged.

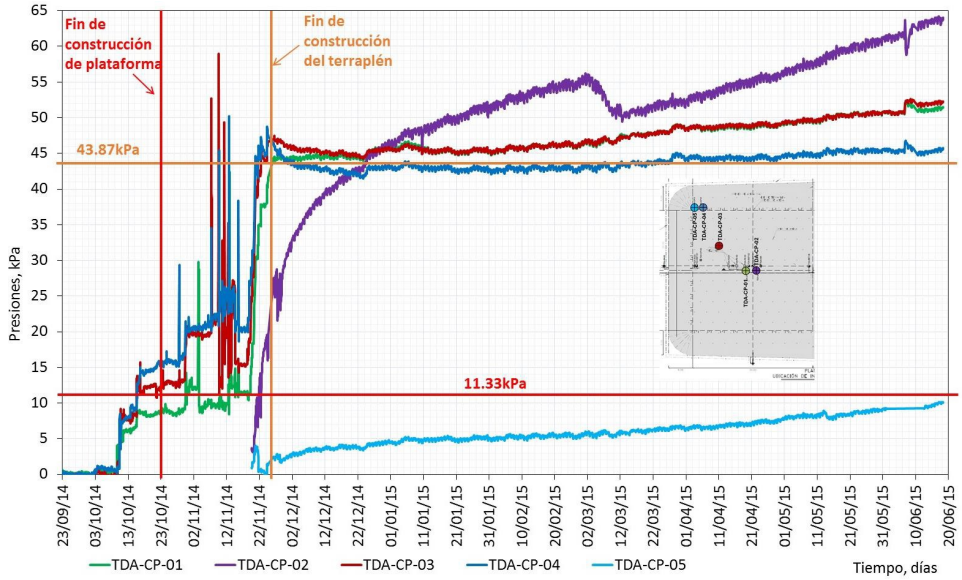

Figure B.8: Pressures over time measured at the TPDA (sand drains) [2].

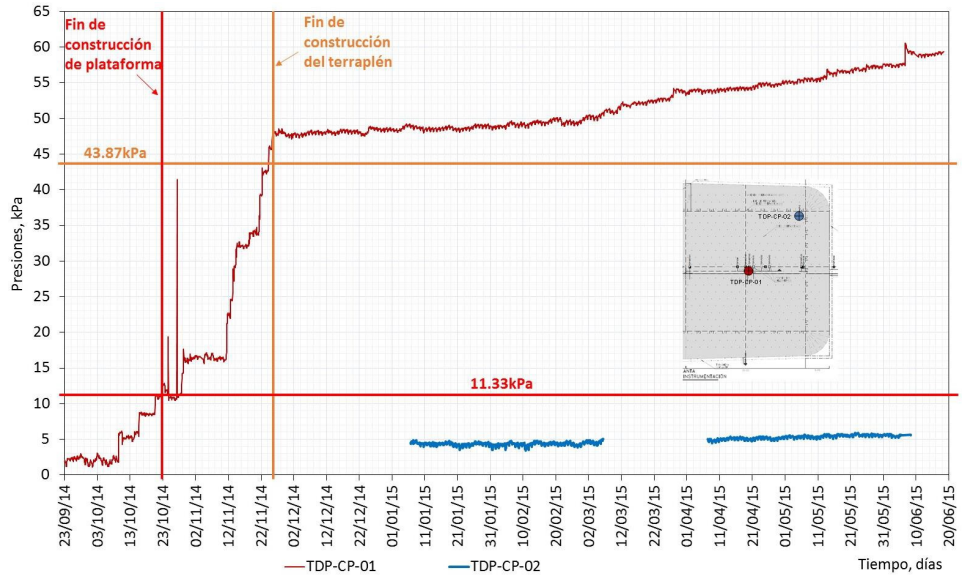

Figure B.9: Pressures over time measured at the TPDP (prefabricated drains) [2].

All CP's are installed in the TPDV, except for the TDP-CP-02, registering pressures that increase with time, after the date corresponding to the end of the construction. This may be due to a process of consolidation of the materials from the body of the embankment, mainly the tepetate. The TDA-CP-01, 03 and 04 and TDP-CP-01 cells were built before the embankment and have been under pressure since the start of construction. Therefore, it is possible to identify with some precision the constructive stages of the TPDV.

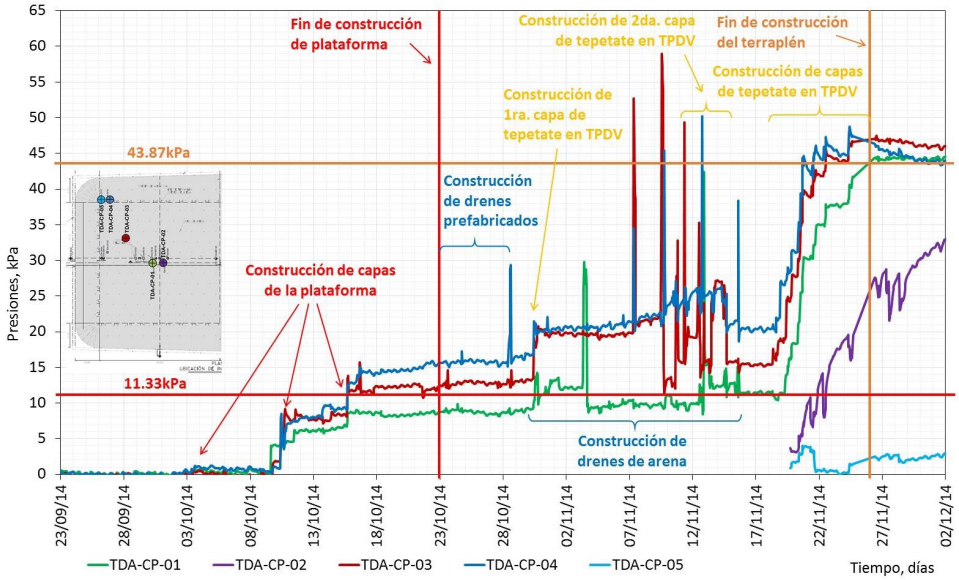

Figure B.10: Pressures over time measured at the TPDA (sand drains) [2].

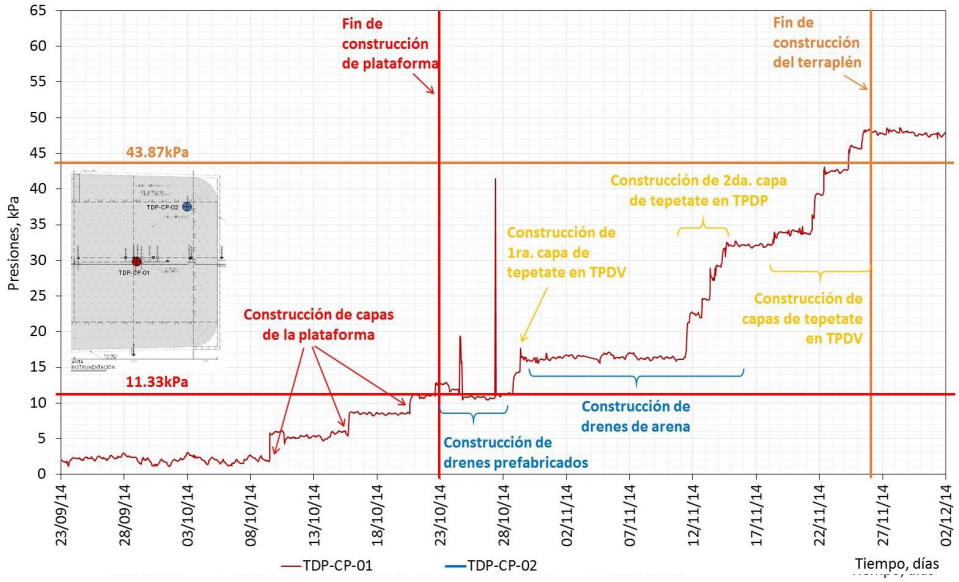

Figure B.11: Pressures over time measured at the TPDP (prefabricated drains) [2].

Piezometric stations

The position of the installed piezometer stations in the TPDV are presented in figure B.12. On the left and right sides the piezometers are installed in the TPDA and the TPDP, respectively. In both embankments, the depth of the piezometers are 4, 9 and 18m.

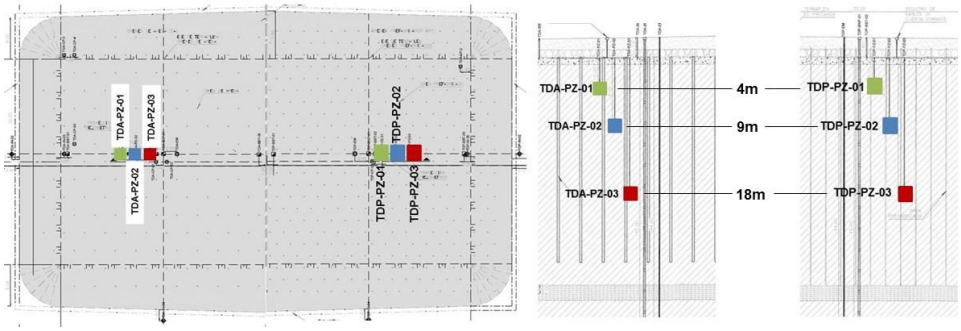

Figure B.12: Position of piezometer stations in the TPDP [2].

In figure B.13 and B.14 the graphs are presented with excess pore pressure versus time of each of the piezometers installed in the TPDV. The vertical and horizontal line indicate the same as in figures B.8 and B.9. In the more superficial piezometers of the TPDA (TDA-PZ-01 and 02) it is observed that the theoretical efforts are approximately equal to those measured. The same is not true for piezometers TPDP (TDP-PZ-01 and 02) where the measurements are significantly lower. This indicates a greater dissipation of excess pore pressure in the TPDP during construction. The TDA-PZ-03 and TDP-PZ-03 piezometers are positioned deeper, so the influence of the embankment is lower. In all piezometers, an increase in excess pore pressure is seen in the last measurement (June).

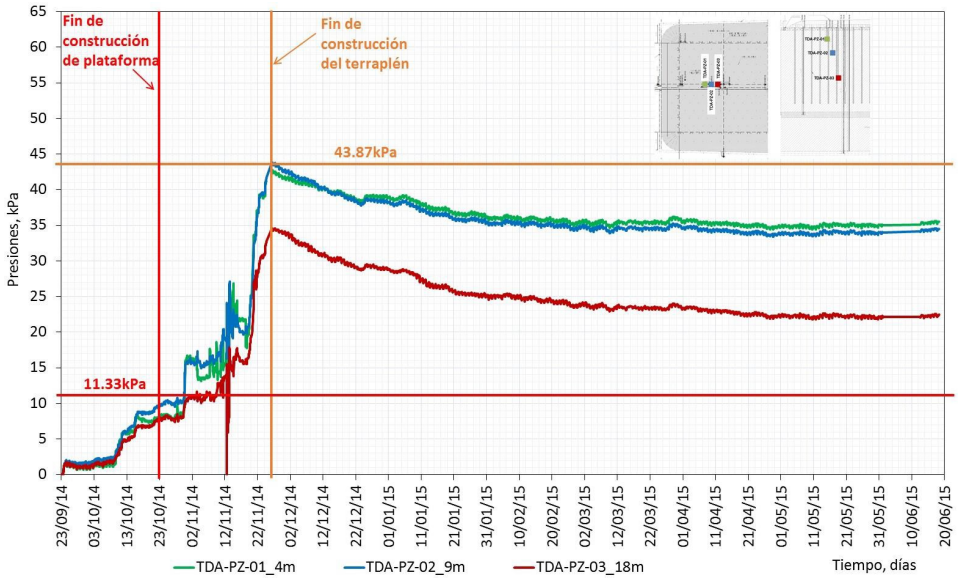

Figure B.13: Pressures measured with the Piezometers in the TPDA [2].

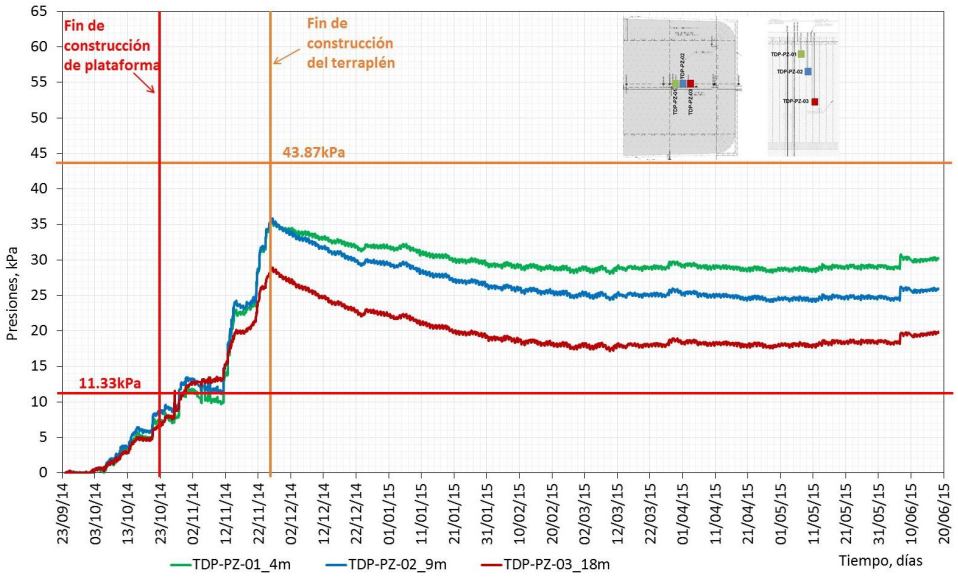

Figure B.14: Pressures measured with the Piezometers in the TPDA [2].

Horizontal transverse hose

The flexible horizontal hose which is positioned transverse at the base of the embankment and is alligned over the width of the embankment is used for measuring the settlement of the soil over time. In figure B.15 the settlement distribution over time is presented. In this figure the color of the graphs corresponding to the following dates is highlighted:

1. October 23, 2014; End construction of tezontle platform (red)
2. November 26, 2014; End of tepetate embankment construction (yellow)
3. June 3, 2015; Final reading (black)

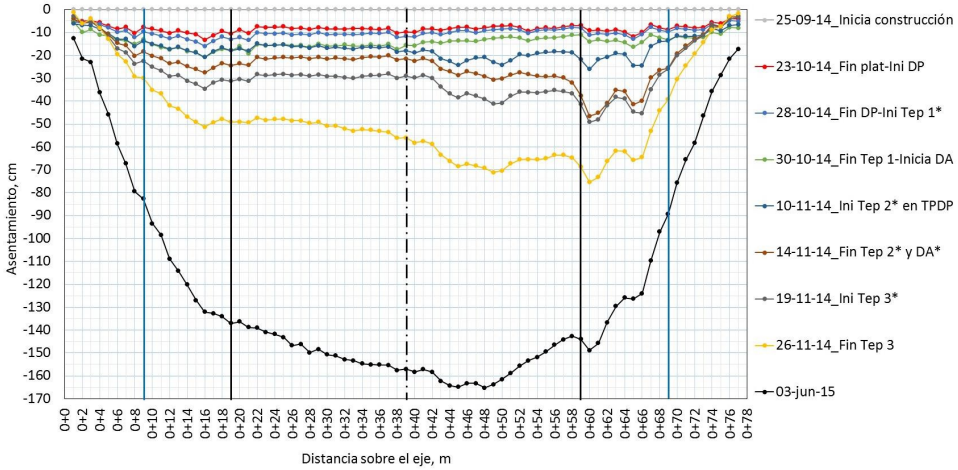

Figure B.15: Pressures measured with the Piezometers in the TPDP [2].

By looking at figure B.15, the following can be observed:

1. Similar settings are observed on both sides of the TPDV until the beginning of the construction of the sand drains (October 30, 2014), due to the symmetry of the construction stages.
2. Minor settlements on the side of the TPDA during the construction of the DAs and before the construction of the second layer of tepetate on the side of the TPDP (November 10, 2014). To date, more than

half of the project DAs have been installed. The above indicates that the DAs begin to work as a massive improvement of the terrain.

3. Larger settlements in the TPDP due to the construction of the second layer of tepetate (November 14, 2014), on the same side of the TPDV. In figures B.13 and B.14 it is observed that during the loading stages the DPs dissipate more pore pressure than the DAs. It should be noted that during this stage the construction of the AD.

4. Larger settlements on the TDPA side before the last stage of tepetate construction. This indicates that in the times in which the load did not increase there was greater dissipation of pore pressure in the DA.

5. Small settlements on the side of the TPDA during the construction of the last stage of constructing the tepetate.

6. The above corroborates that during the stages (load increments), the sand drains reduce the settlements in the TPDA and the prefabricated ones dissipate more pore pressure.

7. Slightly larger settlements on the TPDA side during observation time. In this stage effects are added: DAs dissipate more excess pore pressure in rest stages, but their greater rigidity decreases settlements. The DPs dissipate less pore pressure but the terrain does not have any type of improvement.

Surface settlement of embankment

The surface references are installed at the surface of the TPDV. By using a grid of references, the settlement over the whole surface can be measured. in figures B.16 and B.17 the level curves are presented corresponding to the following readings: Initial (December 23, 20140 and final 9June 9, 2015). The change of the slopes and the lower areas in the surface of the TPDV is observed.

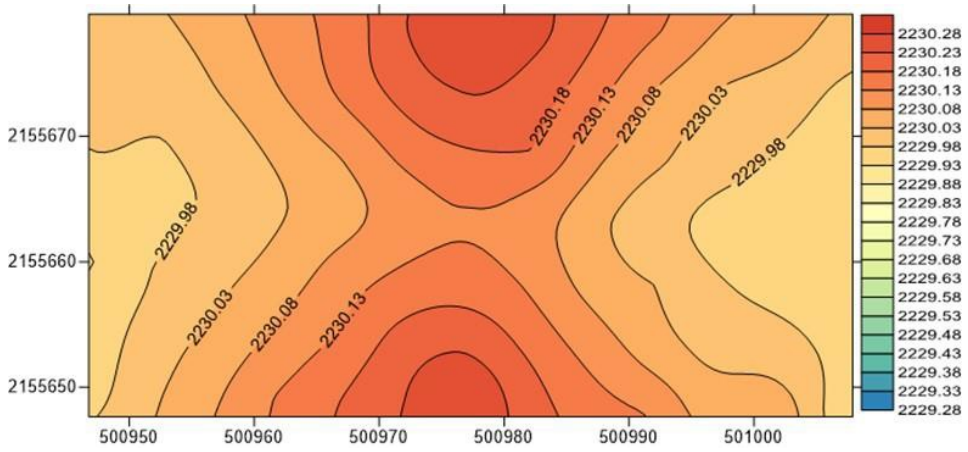

Figure B.16: Height levels prior to construction of the TPDV (23 December, 2014) [2].

In figure B.18 a graph is presented in which the settlements prior (23 December, 2014) and after the construction (09 June, 2015) are presented.

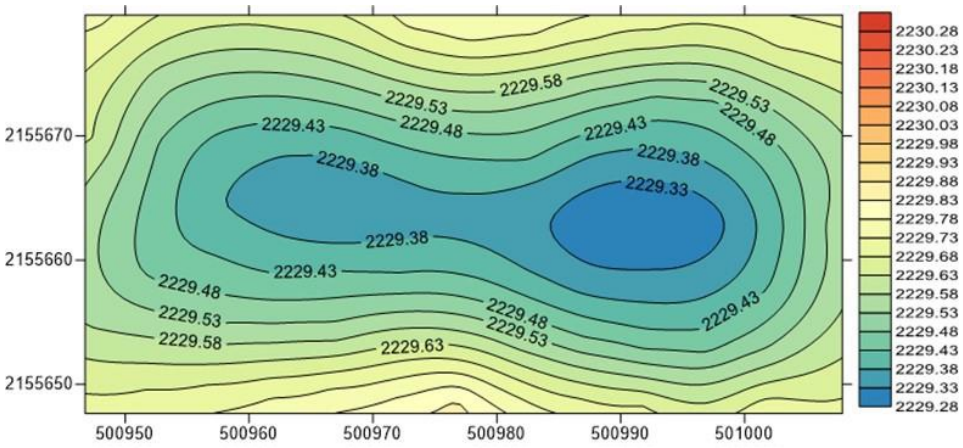

Figure B.17: Final height level after construction of the TPDV (09 June, 2015) [2].

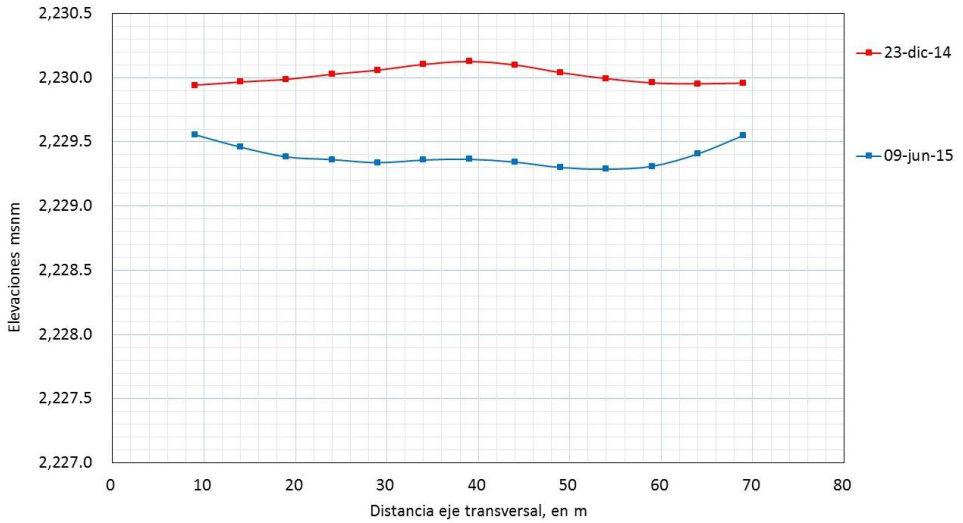

Figure B.18: Settlement before and after construction of the TPDV [2].

Inclinometers

The position of the inclinometers installed is presented in figure B.19. In figures B.20 and B.21 the horizontal displacements measured at the foot of the slope on the transverse axes of the TPDV(TDA-IN-02 and TDP-IN-02) and longitudinal of the TPDA (TDA-IN-04) and TPDP (TDP-IN-04) respectively.

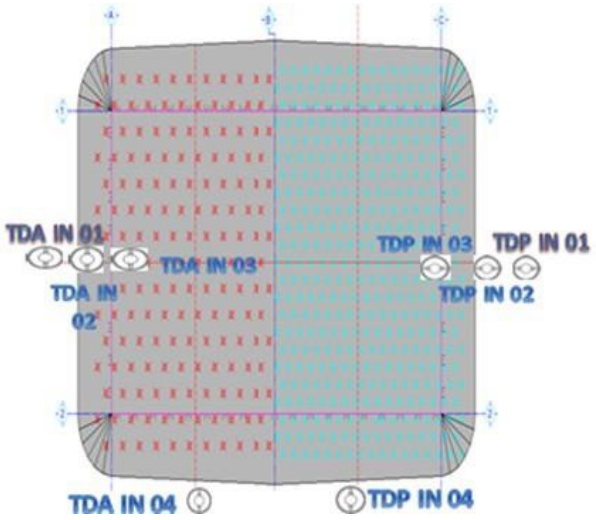

Figure B.19: Position of the inclinometers installed at the TPDV [2].

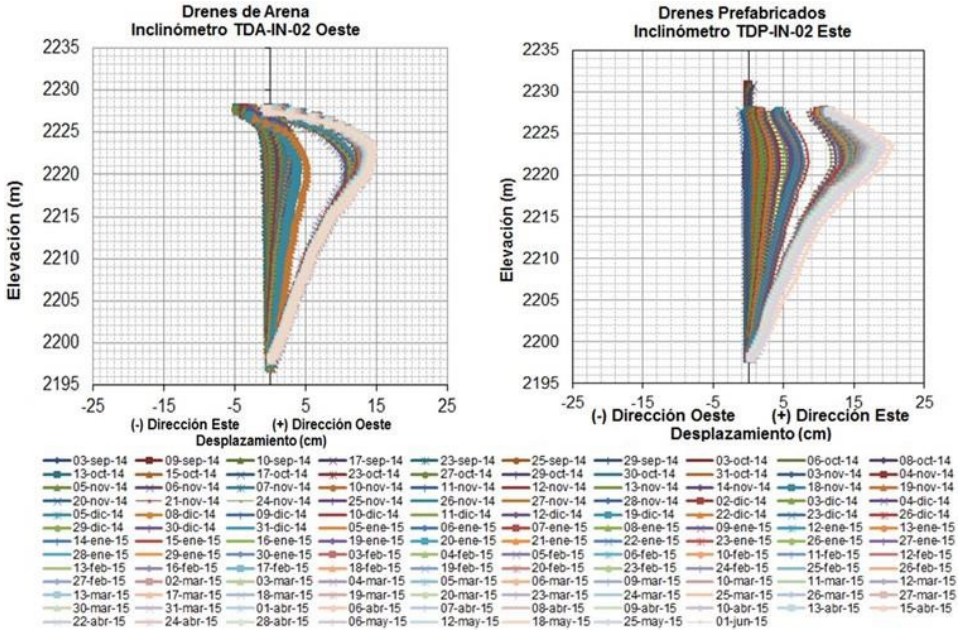

Figure B.20: Horizontal displacements at the foot of the slope at the transverse axis of the TPDV (TDA-IN-02 and TDP-IN-02) [2].

Figures B.22 and B.23 show the time distribution of maximum horizontal displacements, measured in the inclinometers installed in the TPDA and TPDP, respectively. It is observed that these displacements have not been completely established, so that some settlements associated with lateral displacements of the soil will continue to be present.

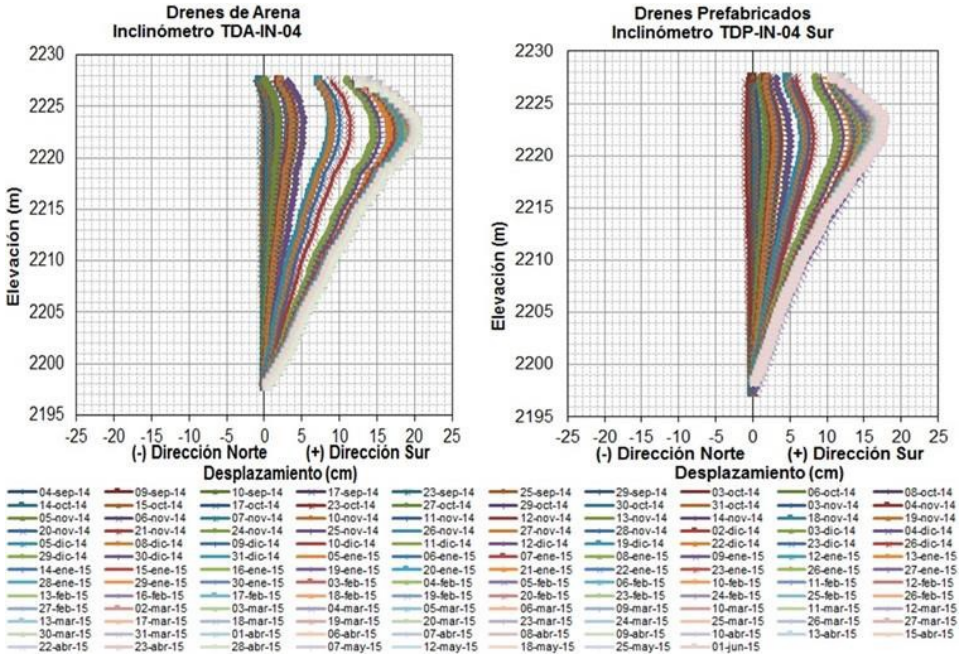

Figure B.21: Horizontal displacements at the foot of the slope at the longitudinal axis of the TPDV (TDA-IN-04 and TDP-IN-04) [2].

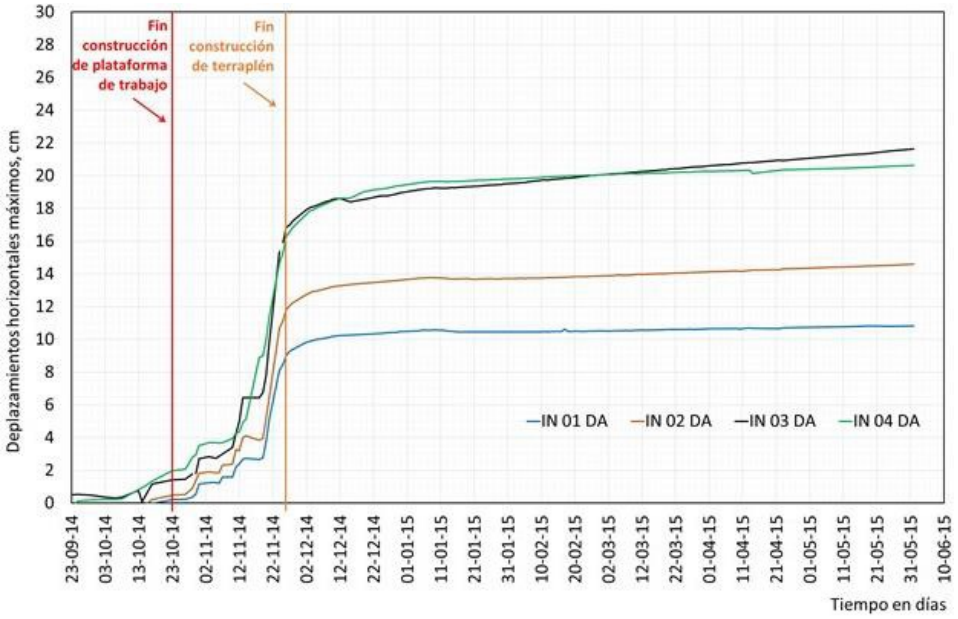

Figure B.22: Distributions of maximum horizontal displacements, measured in inclinometers installed in the TPDA [2].

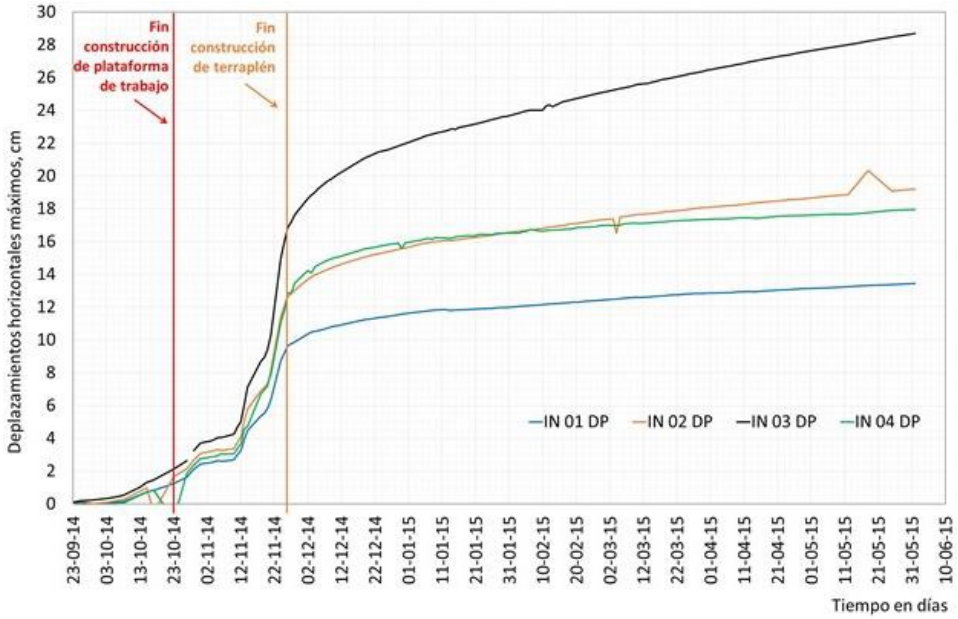

Figure B.23: Distributions of maximum horizontal displacements, measured in inclinometers installed in the TPDP [2].

C

Stress oscillations and tolerated error

In the plots below the development of stresses and settlement inside the sandpile are visualised, taken at a depth of -5.0m and a radius of 0.19m (node K). As can be observed is a decrease in tolerated error not resulting in a decrease in stress oscillations.

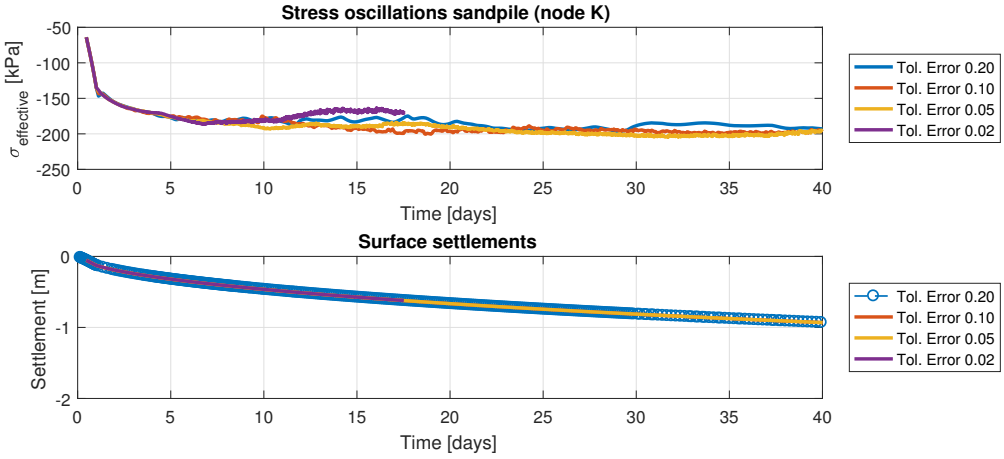

Figure C.1: Development of stresses and settlements inside the sandpile (node K) over a reduced time span.

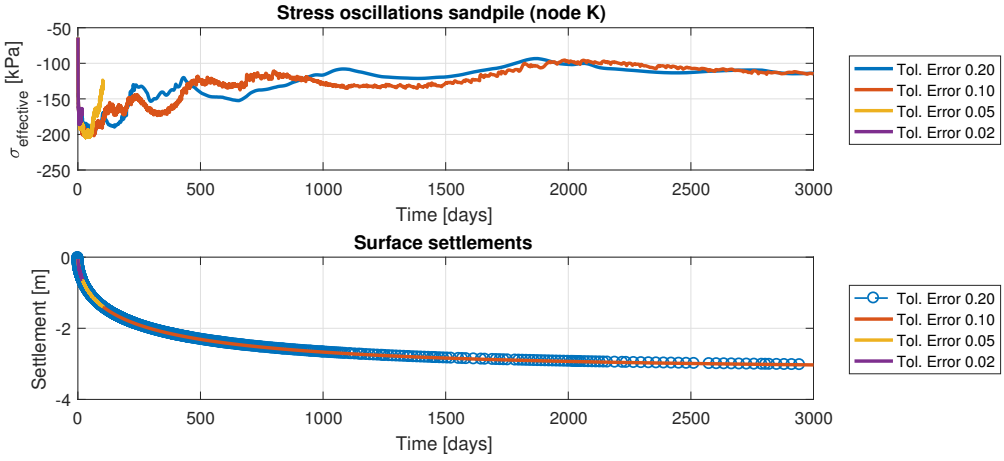

Figure C.2: Development of stresses and settlements inside the sandpile (node K).

D

Sensitivity of input parameters

In this appendix the sensitivity analysis of the input parameters is presented. In the plots below the different input parameters are varied with respect to the reference simulation. The high and low values are +20% and -20% of the reference value, respectively.

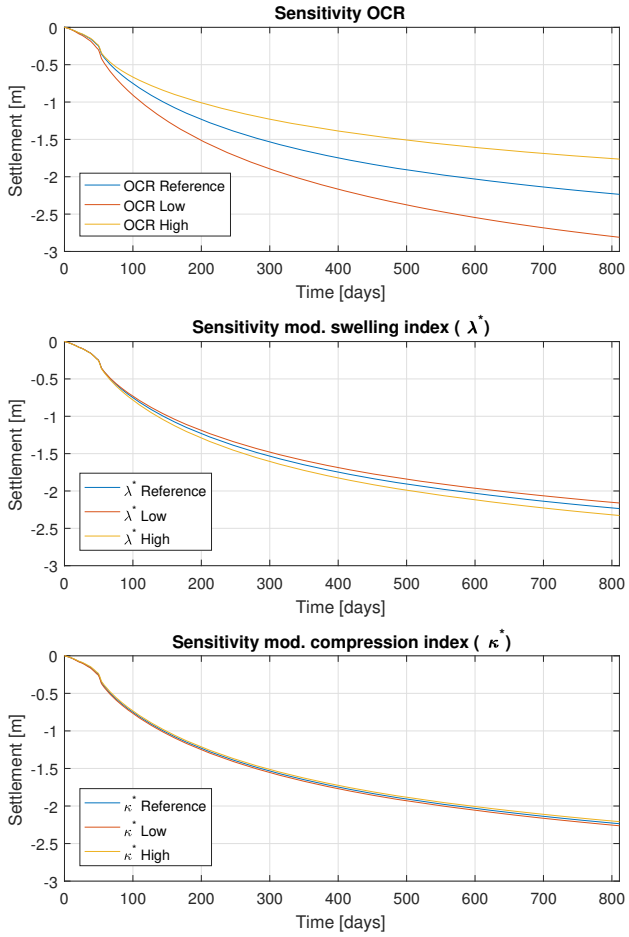

Figure D.1: Sensitivity of the first input parameters, used for the model verification.

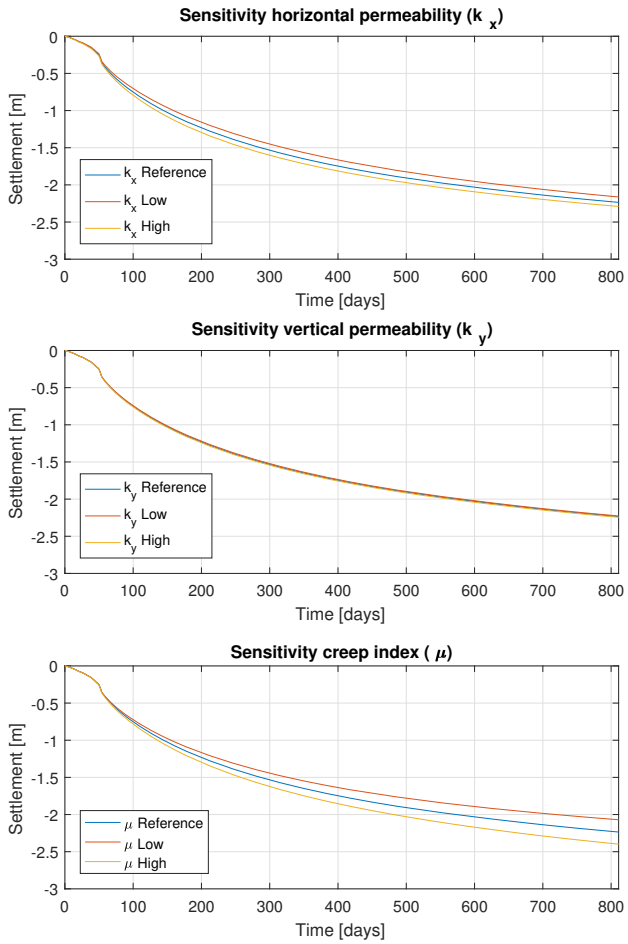

Figure D.2: Sensitivity of the second input parameters, used for the model verification.

E

Soil Properties TASANA

The soil properties used in the realistic numerical model are listed in the tables below.

Table E.1: Geometry and head distribution of the soil layers.

Soil layer	**Description**	**Top [m]**	**Bottom [m]**	**Head top**	**Head Bottom**
Desiccated crust	Remoulded soil	0.00	-0.70	Phreatic	Phreatic
FAS A	First top clay layer	-0.70	-9.60	Phreatic	Phreatic
FAS B	Second top clay layer	-9.60	-23.40	Phreatic	Phreatic
FAS C	Third top clay layer	-23.40	-30.20	Phreatic	-4m
CD	Silty sand layer	-30.20	-31.30	-4m	-4m
FAI	Top deep clay layer	-31.30	-44.10	-4m	-9m
SES	Silty sand layer	-44.10	-50.00	-9m	-9m
FAP	Bottom deep clay layer	-50.00	-60.00	-9m	Linear
FEP	Deep sand layer	-60.00	-62.00	-50m	-50m

Table E.2: Model phases used in model 3.

Phase	**Calculation type**	**Loading type**	**Description**
Initial phase	K_0 procedure	Staged construction	Initial stage
Phase 1	Plastic	Staged construction	Placement of sandpile
Phase 2	Plastic	Staged construction	Apply line loads on top of unit cell
Phase 3	Consolidation	Degree of consolidation	Consolidation analysis

Table E.3: Material properties of the FAS layers [34].

Parameter	**Name**	**FAS A**	**FAS B**	**FAS C**	**Unit**
General					
Material model	$Model$	SSC	SSC	SSC	-
Material behaviour	$Type$	Undrained (A)	Undrained (A)	Undrained (A)	-
Unit weight (dry)	γ_{unsat}	12.10	12.30	12.80	kN/m^3
Unit weight (sat)	γ_{sat}	12.10	12.30	12.80	kN/m^3
Initial void ratio	e_{init}	7.60	7.30	6.20	-
Parameters					
M. compression index	λ^*	0.31500	0.34000	0.38710	-
M. swelling index	κ^*	0.03529	0.03719	0.03804	-
M. creep index	μ^*	0.01264	0.01383	0.01467	-
Cohesion	c'_{ref}	0.100	0.1000	0.100	kN/m^2
Friction angle	ϕ'	34.00	34.00	34.00	°
Dilatancy angle	ψ'	0.000	0.000	0.000	°
Groundwater					
Data Set	-	Standard	Standard	Standard	-
Model	-	-	-	-	-
Soil type	-	Fine	Fine	Fine	-
Horizontal permeability	k_x	0.2270E-3	0.2270E-3	0.2272E-3	m/day
Vertical permeability	k_y	0.2270E-3	0.2270E-3	0.2272E-3	m/day
Change in permeability	c_k	2.270	2.180	1.850	-
Interfaces					
Interface strength	-	Rigid	Rigid	Rigid	-
Strength reduction factor	R_{inter}	1.000	1.000	1.000	-
Interfaces					
K_0 determination	-	Automatic	Automatic	Automatic	-
Over-consolidation ratio	OCR	1.767	1.767	1.586	-
Pre-overburden pressure	POP	0.000	0.000	0.000	kN/m^2

Table E.4: Material properties of the desiccated crust and the deep clay layers [34].

Parameter	**Name**	**DC**	**FAI**	**FAP**	**Unit**
General					
Material model	$Model$	SS	SSC	SS	-
Material behaviour	$Type$	Undrained (A)	Undrained (A)	Undrained (A)	-
Unit weight (dry)	γ_{unsat}	14.50	13.10	13.50	kN/m^3
Unit weight (sat)	γ_{sat}	14.50	13.10	13.50	kN/m^3
Initial void ratio	e_{init}	3.00	4.20	2.50	-
Parameters					
M. compression index	λ^*	0.24890	0.32360	0.30310	-
M. swelling index	κ^*	0.04239	0.03512	0.03975	-
M. creep index	μ^*	-	0.01346	-	-
Cohesion	c'_{ref}	5.000	0.100	0.100	kN/m^2
Friction angle	ϕ'	25.00	34.00	34.00	°
Dilatancy angle	ψ'	0.000	0.000	0.000	°
Groundwater					
Data Set	-	Standard	User-def.	User-def.	-
Model	-	-	Saturated	Saturated	-
Soil type	-	Fine	-	-	-
Horizontal permeability	k_x	2.8510E-3	0.2246E-3	7.2580E-3	m/day
Vertical permeability	k_y	8.6400E-3	0.2246E-3	7.2580E-3	m/day
Change in permeability	c_k	1.000E15	1.260	0.750	-
Interfaces					
Interface strength	-	Rigid	Rigid	Rigid	-
Strength reduction factor	R_{inter}	1.000	1.000	1.000	-
Interfaces					
K_0 determination	-	Automatic	Automatic	Automatic	-
Over-consolidation ratio	OCR	1.000	1.400	1.150	-
Pre-overburden pressure	POP	30.00	0.000	0.000	kN/m^2

Table E.5: Material properties of drained soil layers 7.

Parameter	**Name**	**CD**	**SES**	**FEP**	**Sandpile**	**Unit**
General						
Material model	$Model$	HS	HS	HS	HS	-
Material behaviour	$Type$	Drained	Drained	Drained	Drained	-
Unit weight (dry)	γ_{unsat}	16.00	16.00	16.00	17.00	kN/m^3
Unit weight (sat)	γ_{sat}	18.00	18.00	18.00	18.00	kN/m^3
Initial void ratio	e_{init}	0.500	0.500	0.500	0.500	-
Parameters						
Secant stiffness*	E_{50}^{ref}	125.0E3	150.0E3	125.0E3	30.0E3	kN/m^2
Tangent stiffness**	E_{oed}^{ref}	125.0E3	150.0E3	125.0E3	30.0E3	kN/m^2
Unloading/reloading stiffness	E_{ur}^{ref}	375.0E3	450.0E3	125.0E3	90.0E3	kN/m^2
Power	m	0.500	0.500	0.500	0.500	-
Cohesion	$c_{ref}^{'}$	1.000	0.100	1.000	0.100	kN/m^2
Friction angle	$\phi^{'}$	38.00	36.00	38.00	33.00	°
Dilatancy angle	ψ	8.000	6.000	8.000	3.000	°
Groundwater						
Data Set	-	User-def.	User-def.	User-def.	Standard	-
Model	-	Saturated	Saturated	Saturated	-	-
Soil type	-	-	-	-	Coarse	-
Horizontal permeability	k_x	5.616	7.690	5.616	7.690	m/day
Vertical permeability	k_y	5.616	7.690	5.616	7.690	m/day
Change in permeability	c_k	1.00E15	1.00E15	1.00E15	1.00E15	-
Interfaces						
Interface strength	-	Rigid	Rigid	Rigid	Rigid	-
Strength reduction factor	R_{inter}	1.000	1.000	1.000	1.000	-
Interfaces						
K_0 determination	-	Automatic	Automatic	Automatic	Manual	-
Over-consolidation ratio	OCR	1.000	1.000	1.000	1.000	-
Pre-overburden pressure	POP	0.000	0.000	0.000	10.00	kN/m^2

*In standard drained triaxial test

**For primary oedometer loading

F

Validated Soil Properties

In the tables below the geometry, loading phasing and validated material properties (chapter 6) of the soil layers are presented.

Table F.1: Geometry and head distribution of the soil layers as used in the sensitivity analysis.

Soil layer	**Description**	**Top [m]**	**Bottom [m]**	**Head top**	**Head Bottom**
Desiccated crust	Remoulded soil	0.00	-0.70	Phreatic	Phreatic
FAS A	First top clay layer	-0.70	-9.60	Phreatic	Phreatic
FAS B	Second top clay layer	-9.60	-23.40	Phreatic	Phreatic
FAS C	Third top clay layer	-23.40	-30.20	Phreatic	-4m
CD	Silty sand layer	-30.20	-31.30	-4m	-4m
FAI	Top deep clay layer	-31.30	-44.10	-4m	-9m
SES	Silty sand layer	-44.10	-50.00	-9m	-9m
FAP	Bottom deep clay layer	-50.00	-60.00	-9m	Linear
FEP	Deep sand layer	-60.00	-62.00	-50m	-50m

Table F.2: Phased construction of the runways at the NAICM site, conform UNAM [2].

Name	**Phase description**	**Time [days]**	**Thickness [m]**	γ_d/γ_s**[kN/m3]**
Phase 1	Application of first layer Tezontle	0	1.0	11.0/13.0
Phase 2	Application of second layer Tezontle	30	1.0	11.0/13.0
Phase 3	Application of first layer surcharge	60	1.0	18.0/20.0
Phase 4	Application of second layer surcharge	75	1.0	18.0/20.0
Phase 5	Removal of surcharge	480	-2.0	18.0/20.0
Phase 6	Application of levelling layer Tezontle	525	0.2	11.0/13.0
Phase 7	Application of pavement structure	565	0.8	19.0/19.0
Phase 8	End of construction period	600	-	-
Phase 9	End life span construction	2920	-	-

Table F.3: Validated material properties of the FAS layers used for the sensitivity analysis in chapter 7.

Parameter	**Name**	**FAS A**	**FAS B**	**FAS C**	**Unit**
General					
Material model	$Model$	SSC	SSC	SSC	-
Material behaviour	$Type$	Undrained (A)	Undrained (A)	Undrained (A)	-
Unit weight (dry)	γ_{unsat}	12.10	12.30	12.80	kN/m^3
Unit weight (sat)	γ_{sat}	12.10	12.30	12.80	kN/m^3
Initial void ratio	e_{init}	7.60	7.30	6.20	-
Parameters					
M. compression index	λ^*	0.31500	0.38000	0.38000	-
M. swelling index	κ^*	0.04000	0.04400	0.04400	-
M. creep index	μ^*	0.01264	0.01383	0.01500	-
Cohesion	c'_{ref}	0.100	0.1000	0.100	kN/m^2
Friction angle	ϕ'	34.00	34.00	34.00	°
Dilatancy angle	ψ'	0.000	0.000	0.000	°
Groundwater					
Data Set	-	Standard	Standard	Standard	-
Model	-	-	-	-	-
Soil type	-	Fine	Fine	Fine	-
Horizontal permeability	k_x	0.2400E-3	0.1700E-3	0.1700E-3	m/day
Vertical permeability	k_y	0.2400E-3	0.1700E-3	0.1700E-3	m/day
Change in permeability	c_k	2.270	2.180	1.850	-
Interfaces					
Interface strength	-	Rigid	Rigid	Rigid	-
Strength reduction factor	R_{inter}	1.000	1.000	1.000	-
Interfaces					
K_0 determination	-	Automatic	Automatic	Automatic	-
Over-consolidation ratio	OCR	1.850	1.650	1.650	-
Pre-overburden pressure	POP	0.000	0.000	0.000	kN/m^2

Bibliography

[1] *Material Models Manual*. Plaxis, Delft, 1e edition, 2017.

[2] N. P. L. Acosta, C. A. G. C. Cortina, and N. P. L. Lópes. "investigaciones y estudios espaciales relacionados con aspectos geotécnicos del nuevo aeropuerto internacional de la ciudad de méxico (naicm) en el vaso del ex-lago de texcoco, zona federal". Technical Report GACM/DCI/SJ/CI/013-2015, UNAM Geotecnia, Ciudad Universitaria, D.F., 2015.

[3] M. Alamgir, N. Miura, H. B. Poorooshasb, and M. R. Madhav. Deformation analysis of soft ground reinforced by columnar inclusions. *Computers and Geotechnics*, 18:267–290, 1995.

[4] R. A. Barron. Consolidation of fine-grained soil using vertical drains. *Geotechnique*, 31:718–742, 1948.

[5] D. Basu, P. Basu, and M. Prezzi. Analytical solutions for consolidation aided by vertical drains. *Geomechanics and Geoengineering: An International Journal*, 1:63–71, 2006.

[6] N. Carrilo. Simple two and three dimensional cases in the theory of consolidation of soils. *J. Math. Phys.*, 21:1–5, 1942.

[7] J. Castro and C. Sagaseta. Consolidation around stone columns. influence of column deformation. *Int. J. Numer. Anal. Meth. Geomech.*, 33:851–877, 2009.

[8] B. Chevalier, P. Villard, and G. Combe. Investigation of load-transder mechanisms in geotechnical earth structures with thin fill platforms reinforced by rigid inclusions. *American Society of Civil Engineers*, 1: 35–43, 2011.

[9] E. Conte and A. Troncone. Radial consolidation with vertical drains and general time dependent loading. *Can. Geotech. J.*, 46:25–36, 2009.

[10] A. F. Di Milli. "design and construction of stone columns". Technical Report FHWA/RD-83/026, School of Civil Engineering Georgia Institute of Technology, Georgia Institute of Technology, Atlanta, Georgia 30332, 1983.

[11] ESA. Mexico city subsidence. `http://www.esa.int/spaceinimages/Images/2014/12/Mexico_City_subsidence`, 2014.

[12] M. Etezad, A. M. Hanna, and T. Ayadat. Bearing capacity of a group of stone columns in soft soils. *Int. J. Geomech*, 15:1–14, 2015.

[13] M. Y. Fattah, M. A. Al-Neami, and A. S. Al-Suhaily. Estimation of bearing capacity of floating group of stone columns. *Eng. Sci. Tech. Int. J.*, 1:1–7, 2017.

[14] Foster. Artist impression of the naicm terminal. `www.fosterandpartners.com`, 2014.

[15] Google.com. Location naicm site. `https://www.google.com/maps`, 2017.

[16] J. Han and S.-L. Ye. Simplified method for consolidation rate of stone column reinforcement foundations. *Journal of Geotechnical and Geoenvironmental engineering*, pages 597–603, 2001.

[17] I. Hosseinpour, M. S. S. Almeida, and M. Riccio. Full-scale load test and finite-element analysis of soft ground improved by geotextile-encased granular columns. *Geosynthetics International*, 22:428–438, 2015.

[18] J. M. O. Hughes and N. J. Withers. Reinforcing of soft cohesive soils with stone columns. *Ground Eng*, pages 42–49, 1974.

[19] B. Indraratna, C. Bamunawita, W. I. Redana, and G. McIntosh. Modelling of prefabricated vertical drains in soft clay and evaluation of their effectiveness in practise. *Ground Improvement*, 3:127–137, 2003.

[20] M. de Kant. "construction and postconstruction soil displacements at comercial apron - terminal interface area". Technical Report ITP-SRO-DCAGI-SC-015/2015, Tasana Ingenieria Aeroportuaria, Edificio Moncavo, Piso 14, Col. Juarez, Del. Cuauhtémoc (MX), 2017.

[21] W. Kjellman. Consolidation of clay by band-shaped prefabricated drains. *Ground Engineering*, 12:16–25, 1948.

[22] A. M. Krishna, M. R. Madhav, and G. M. Letha. Liquefaction mitigation of ground treated with granular piles: Densification effect. *ISET Journal of Earthquake Technology*, 43:105–120, 2006.

[23] M. R. Madhav and P. A. Khan. Consolidation of soft ground with drains with no (pvds) and finite stiffness (granular piles). *Proceedings of Indian Geotechnical Conference*, 1:33–40, 2011.

[24] B. A. McCabe and J. A. McNeill. Vibro techniques for ground improvement in ireland. *The Engineers Journal*, 60:181–182, 2006.

[25] R. Melnikov, J. Zazulya, M. Stepanov, O. Ashikhmin, and T. Maltseva. Ocr and pop parameters in plaxis-based numerical analysis of loaded over consolidated soils. *Procedia Engineering*, 165:845–852, 2016.

[26] R. Morales, R. Murillo-Fernandez, and A. Hernandez-Rubio. Subsidence of the former texcoco lake. *Land Subsidence, Proceeding of the Fourth International Symposium on Land Subsidence*, 200:35–43, 1991.

[27] S. S. Najjar. A state-of-the-art review of stone/sand-column reinforced clay systems. *Geotech Geol Eng*, 31:355–386, 2013.

[28] Joint Academies Committee on the Mexico City Water Supply. *Mexico City's Water Supply: Improving the Outlook for Sustainability*. National Academies, Washington, DC, 1e edition, 1995.

[29] E. Ovando-Shelley, A. Ossa, and M. P. Romo. The sinking of mexico city: Its effects on soil properties and seismic response. *Soil Dynamics and Earthquake Engineering*, 11:239–250, 2007.

[30] J. L. Rangel-Núñez, A. Gómez-Bernal, J. Aguirre-González, E. Sordo-Zabay, and E. Ibarra-Raza. Dynamic response of soft soil deposits improved with rigid inclusions. *The 14th World Conference on Earthquake Engineering*, 1:2–8, 2008.

[31] I. Sathananthan, B. Indraratna, and C. Rujikiatkamjorn. Evaluation of smear zone extent surrounding mandrel driven vertical drains using the cavity expansion theory. *International Journal Of Geomechanics*, 8:355–365, 2008.

[32] K. Terzaghi. *Theoretical Soil Mechanics*. John Wiley & Sons, New York, 1 edition, 1943.

[33] A. Verruijt and W. Broere. *Grondmechanica*. Vereniging voor Studie- an Studentenbelangen te Delft, Leeghwaterstraat 42, Delft, 1e edition, 2012.

[34] A. Verweij. "reporte de diseno cuarta fase - general - estudios de subsuelo - geotecnia". Technical Report TSN/GACM/REP/317, Tasana Ingenieria Aeroportuaria, Edificio Moncavo, Piso 14, Col. Juarez, Del. Cuauhtémoc (MX), 2016.

[35] K. S. Watts, D. Johnson, L. A. Wood, and A. Saadi. Instrumental trial of vibro ground treatment supporting strip foundations in a variable fill. *Geotechnique*, 50:699–709, 2000.